Dissertation

Submitted to the

Combined Faculties for the Natural Sciences and for Mathematics

of the Ruperto-Carola University of Heidelberg, Germany

for the degree of

Doctor of Natural Sciences

presented by

Maike Reith, Diploma in Biology

born in: Bühl, Germany

Oral-examination: 09.10.2015

Role of RAGE in melanoma development, growth, and progression

Referees: Prof. Dr. Viktor Umansky

Prof. Dr. Jochen Utikal

Declarations according to § 8 (3) b) and c) of the doctoral degree regulations:

b) I hereby declare that I have written the submitted dissertation myself and in this process have used no other sources or materials than those expressly indicated,

c) I hereby declare that I have not applied to be examined at any other institution, nor have I used the dissertation in this or any other form at any other institution as an examination paper, nor submitted it to any other faculty as a dissertation.

Heidelberg, Date

Name

This thesis is dedicated to my parents.

Families are the compass that guide us.
They are the inspiration to reach great heights,
and our comfort when we occasionally falter.

Parts of this thesis have been published in:

Conferences and workshop presentations:

Reith, M., Tarnanidis, K., Wagner, N. B., Ikenberg, K., Kehrel, C., Utikal, J., Gebhardt, C.

Poster presentation: “The role of RAGE in melanoma development, growth, and progression”

DKFZ PhD Retreat, July 2013, Weil der Stadt, Germany

Reith, M., Gebhardt, W.H., Tarnanidis, K., Wagner, N. B., Ikenberg, K., Kehrel, C., Utikal, J., Gebhardt, C.

Poster presentation: “The pattern recognition receptor RAGE regulates growth and progression of malignant melanoma”

DKFZ PhD poster session, November 2014, Heidelberg, Germany

Reith, M., Gebhardt, W.H., Tarnanidis, K., Wagner, N. B., Ikenberg, K., Kehrel, C., Utikal, J., Gebhardt, C.

Poster presentation: “Subcellular distribution of RAGE affects its functions in melanoma growth and progression”

Annual Meeting 2015 of the American Association for Cancer Research (AACR), April 2015, Philadelphia, PE, United States of America

Within the thesis, work from the following publications was included:

Wagner, N. B., Weide, B., **Reith, M.**, Tarnanidis, K., Kehrel, C., Lichtenberger, R., Pflugfelder, A., Herpel, E., Ikenberg, K., Busch, C., Holland-Letz, T., Naeher, H., Garbe, C., Umansky, V., Enk, A., Utikal, J., Gebhardt, C. Diminished levels of the soluble form of RAGE are related to poor survival in malignant melanoma. Int J Cancer, 2015.

Table of Content

I. List of figures

II. List of tables

III. Abstract

The receptor for advanced glycation end-products (RAGE) was identified as cell membrane-bound pattern recognition receptor sensing endogenous alarming signals. Previous work revealed the existence of a plethora of RAGE isoforms and of a complex regulatory machinery enabling their controlled expression. While mainly expressed at low levels in healthy tissues, pathological disorders are often connected with increased RAGE expression. Indeed, besides providing evidence for an upregulation of RAGE in melanoma, we demonstrated recently that diminished sRAGE and esRAGE levels serve as prognostic markers, suggesting a differential expression of distinct RAGE variants in malignant melanoma. To date, the functional role of RAGE in melanoma has not been systematically investigated so far.

This study demonstrated an upregulation of *AGER* transcripts in benign melanocytic nevi in line with a sufficiency of RAGE overexpression in establishing melanoma hallmarks in a melanocytic cell line. In addition, combining gain- and loss-of-function studies with gene expression analysis led to the identification of RAGE as negative regulator of *in trans* molecules, such as DNA repair proteins, and consequently of genomic integrity in human and mouse. These findings illustrate that the early occurrence of melanoma-associated mutations found in benign melanocytic nevi and the high genomic instability of melanoma cells might be a consequence of dysregulated RAGE expression. Furthermore, the study provided evidence that the observed benefits of a high RAGE expression on melanoma cells, including sustained proliferation, deregulation of cellular energetics, and prolonged survival, also come along with negative effects such as higher vulnerability to exogenous genotoxic insults. Such negative consequences, which might be another issue of the impact of RAGE on genomic integrity, implicate the existence of strategies regulating RAGE functionality in melanoma. As demonstrated in this study, these might not only comprise the control of gene expression but also alternative splicing and subcellular translocation. Indeed, this work showed for the first time that RAGE protein in melanocytes can also be translocated to the nucleus *via* active cargo transport, and indicated a loss of nuclear RAGE as characteristic of human malignant melanoma. The study further indicated a pathological upregulation of nuclear export proteins as well as a differential expression of RAGE splicing factors as potential mechanisms behind the aberrant compartmentalization of RAGE upon malignant transformation.

IV. Zusammenfassung

Der Mustererkennungsrezeptor RAGE (engl. '*receptor for advanced glycation end-products*') wurde als Zellmembran-ständiges Molekül beschrieben, dessen Rezeptorbindungsprofil Moleküle der sogenannten DAMP (engl. '*damage-associated molecular pattern*') - Familie umfasst. Frühere Studien konnten neben der Existenz einer Vielzahl von RAGE-Proteinvarianten, komplexe Regulationsmaschinerien nachweisen, die eine gezielte Steuerung deren Expression ermöglichen. Dies deutet daraufhin, dass die Funktionen von RAGE durch eine größere Komplexität gekennzeichnet sind als ursprünglich angenommen. Während in gesundem Gewebe eine meist geringe RAGE-Expression zu finden ist, sind pathologische Zustände häufig mit einer erhöhten RAGE-Proteinexpression verbunden. In einer bereits eingereichten Studie konnten wir in Patienten mit malignem Melanom neben einem erhöhtem RAGE Gesamtprotein eine verminderte Menge zweier sezernierter RAGE-Varianten nachweisen und damit die differenzielle Expression verschiedener RAGE-Proteinvarianten auch im Melanom bestätigen. Ungeachtet des großen Interesses, ist die funktionelle Rolle von RAGE im malignen Melanom bisher weitgehend unbekannt.

In der vorliegenden Arbeit konnte die Induktion der *AGER*-spezifischen Expression im benignen, melanozytären *Naevus* demonstriert, wie auch der Nachweis tumorspezifischer Merkmale in einer melanozytären Zelllinie durch die Überexpression von RAGE erbracht werden. Dies weist auf eine mögliche Rolle von RAGE in der frühen Melanomentstehung hin. Überexpressions- und Knockdown-Studien zusammen mit Genexpressionsanalysen ermöglichten zudem die Charakterisierung von RAGE als negativem Regulator sogenannter *in trans* Moleküle, zu denen unter anderem DNA Reparaturproteine gezählt werden, mit Auswirkungen auf die Genomintegrität im humanen System als auch in der Maus. Darausfolgernd, könnte eine gesteigerte genomische Instabilität aufgrund erhöhter RAGE-Expression einer der Faktoren sein, die die bereits in melanozytären *Naevi* auftauchenden Melanom-spezifischen Mutationen und die hohe Mutationsrate im Melanom selbst bedingen. Ferner konnte gezeigt werden, dass eine erhöhte Expression von RAGE neben primär tumor-promovierenden Auswirkungen, die eine kontinuierliche Proliferation, als auch die Aneignung eines tumorspezifischen Stoffwechsels und eines gesteigerten Zellüberlebens umfassen, auch anti-tumorigene Effekte zur Folge hat. Zu letzteren zählt die gesteigerte Sensibilität von RAGE-überexprimierenden Melanomzellen gegenüber exogen-induzierten DNA Schäden. Basierend auf der hohen Adaptionsmöglichkeit von Melanomzellen wurden Regulationsmechanismen vermutet, die eine Umgehung solcher Effekte ermöglichen. Diese Arbeit zeigt, dass diese nicht nur eine Genexpressionskontrolle, sondern auch alternatives Spleißen und subzelluläre Kompartimentierung zu umfassen scheinen. Zudem demonstriert

diese Arbeit erstmalig, dass in Melanozyten RAGE über einen aktiven Cargotransport in den Nukleus transloziert werden kann und diese Eigenschaft bei der malignen Transformation in Melanomzellen verloren geht. Die Ergebnisse weisen darauf hin, dass dieser Effekt zum einen auf der Melanom-spezifischen Hochregulation nukleärer Exportproteine wie auch auf der differenziellen Expression von RAGE Spleißfaktoren und RAGE Spleißvarianten beruhen könnte.

V. Introduction

Despite recent advances in managing malignant melanoma, the progress in developing therapeutic approaches is limited due to remaining questions regarding melanoma growth and progression. Among others the role of pattern recognition receptors, such as the receptor for advanced glycation end-products (RAGE), is unresolved in melanoma biology. In this chapter information on malignant melanoma development, characteristics of the disease, and treatment options will be provided. Furthermore, the receptor RAGE, and its function in physiological and pathophysiological processes, including cancer will be introduced.

V.1. Melanoma

In the next few pages, the development of malignant melanoma, and common characteristics of melanoma cells will be described. In addition, information on diagnosis, treatment options and therapy-associated complications will be provided.

V.1.1. The pathogenesis of melanoma: A general overview

Malignant melanoma can arise in any anatomic region occupied by pigment-producing melanocytes, including the skin, the choroidal layer of the eye, meninges, and mucosal tissues [1]. Accounting for about 75 % of all skin cancer-related deaths, cutaneous melanoma represents the most aggressive and fatal form of skin cancer with persistent increase in incidence and mortality [2]. In 20 to 50 % of all cases, melanomas can be traced back to pre-existing nevi formed by proliferating melanocytes within the basal cell layer of the epidermis [3, 4]. This shows that an aberrant proliferation of melanocytes is not necessarily linked with the development and growth of malignant melanoma. Melanocytic proliferation only occurs in a horizontal pattern, whereas melanoma growth is characterized by a so called vertical growth phase (VGP), either with or without a preceding radial growth phase (RGP). During the vertical growth the tumor adapts, e.g. by deregulation of the expression of distinct adhesion molecules, thereby allowing the formation of metastases [5, 6]. This high plasticity of melanoma cells leads to a significant change regarding the clinical outcome. For localized melanoma, i.e. primary tumor with 1 mm vertical diameter, the five-year survival rate is over 90 %, whereas the progression to a distant metastatic disease is accompanied by drop to 16 % [2].

In order to identify the molecular events propagating malignant transformation of normal human melanocytes, factors associated with melanoma development must be investigated. Besides a familiar predisposition, epidemiologic studies have implicated three closely

associated factors, namely intense intermittent UV light exposure, severe sunburns during childhood, and a “red hair phenotype” (red/blonde hair, blue eyes, fair skin and high sensitivity to UV light), in conferring the highest risk [7-9]. These risk factors, as well as the fact that the signature spectrum of UV mutagenesis accounts for approximately 50 % of driver mutations found in melanoma [10], directly link UV radiation, which negatively influences genomic integrity by introducing DNA damage, and melanocytic transformation. Melanocytes possess features like the production of the photoprotective pigment eumelanin in order to e.g. shield their genomes from UV-induced DNA damage. The Caucasian population, having only impaired attenuation of UV radiation due to low levels of eumelanin, is associated with a ten - fold greater risk to develop melanoma compared to ethnic groups with deeply pigmented skin [11]. The red hair phenotype is characterized by a high ratio of red pheomelanin to black eumelanin and connects UV-dependent and UV-independent risk factors for melanoma development. Pheomelanin does not have the same photoprotective characteristics as eumelanin; instead, it is involved in the generation of reactive oxygen species (ROS), thereby representing an UV-independent mechanism to melanomagenesis [12-15]. Evidence for other UV-independent mechanisms is given by the fact, that sunscreen has shown significant [16] but, nevertheless, incomplete [17] protection against melanoma.

Furthermore, an increased number of nevi (> 50) and familiar predisposition are also ranked among risk factors for melanoma [7, 18, 19]. More precisely, a family history of melanoma is found in approximately 10 % of melanoma patients conferring a two - fold increase in melanoma risk. Hereditary melanoma is often associated with multiple family members affected with melanoma, multiple primary melanomas per individual, and an early onset of the malignancy [19]. Among the genetic loci and variants conferring a high susceptibility to melanoma is the retinoblastoma protein 1 gene (*RB1*) [20-23], *CDK4* [24-26], and the *CKDN2A* locus [27], encoding for the two distinct protein p16INK4a and p14ARF through alternative splicing. Alterations in RB1, p16INK4a, and CDK4 expression mainly result in cell cycle progression, thereby facilitating tumor onset [28-31]. Instead, the net effect of p14ARF loss is the destabilization of the tumor suppressor P53 [32, 33].

In comparison to the rare hereditary genetic alterations, melanoma cells often acquired mutations that are responsible for the malignant transformation and distinct to additional acquired passenger mutations, forming a so-called landscape of driver mutations [10]. In fact, the observed mutation frequency is even higher compared to most other solid tumors [34]. The genes mainly affected by somatic mutations in melanoma, namely *BRAF* (B-rapidly accelerating fibrosarcoma) and *NRAS* (N-rat sarcoma), are belonging to the mitogen-activated protein kinase (MAPK) pathway, thereby leading to its dysregulation [35]. This pathway transduces signals from the extracellular milieu into the cell, and also into the

nucleus, where specific genes are activated in order to induce cell growth, division and differentiation. Accordingly, dysregulation of this pathway is a common event in cancer. *BRAF* mutations, which result mostly in a valine-to-glutamic acid substitution at codon 600 (V600E), have been found in about 60 % of melanomas [10]. It is noteworthy, that many of the melanoma-associated mutations are commonly found in benign nevi, in terms of *BRAF* mutations in 80 %, proving their insufficient capacity to transform melanocytes without cooperating mutations [36-40]. In fact, it is believed that BRAF V600E induces checkpoint mechanisms forcing melanocytes lacking additional driver mutations into a senescence-like state [41]. Interestingly, in cutaneous melanoma *BRAF* and *NRAS* mutations, with the latter being associated with approximately 30 % of melanomas, are in general mutually exclusive [10]. Most *NRAS* mutations in melanoma lead to mutant proteins with glutamine substitutions at codon 61, namely Q61R and Q61K [42]. In melanoma, *BRAF* as well as *NRAS* mutations lead to a continuous downstream signaling of the MAPK pathway with consequent activation of extracellular-signal-regulated kinases (ERK) [35].

Another important pathway, which is aberrantly activated in melanoma, is the phosphatidylinositol– 4,5–bisphosphate 3-kinase (PI3K) pathway. Active PI3K is able to phosphorylate the 3′-OH group on phosphatidylinositols in the plasma membrane, thereby leading to the recruitment and activation of the protein kinase B (PKB), also known as AKT, and to the consequent induction of the transcription factor NF-κB (nuclear factor 'kappa-light-chain-enhancer' of activated B-cell) [43, 44]. 20 to 30% of melanoma cells display a loss of the phosphatase PTEN (phosphatase and tensin homolog) [10], a potent inhibitor of the PI3K pathway, resulting in the hyperactivation of the pathway [45].

The MAPK pathway as well as the PI3K pathway are involved in many molecular networks, including cell-intrinsic networks sensing metabolic stress and DNA damage, as well as cell-extrinsic signaling mediated by cell-cell or cell-matrix interactions [46, 47]. With 17 % *P53* is frequently mutated in melanoma, resulting in aberrant proteins with increased half-life and dominant negative and/or gain of function phenotypes mediating resistance towards apoptosis [10, 48]. Nevertheless, the majority of cancers display even higher frequencies of *P53* mutations, raising the question whether melanoma cells display a distinct mechanism of avoiding apoptosis and other regulatory checkpoints.

The recent progress in the genome-wide mutation analysis unraveled key mutations involved in melanomagenesis leading to the development of novel therapeutics. Nevertheless, the genetic and epigenetic instability giving rise to a remarkable diversity of melanoma cells holds responsible for the complexity of the disease and the high percentage of acquired therapy resistance. Therefore, the investigation of characteristics and functional behaviors of

melanoma cells and their cell states is required. The current level of knowledge regarding this topic will be outlined in the next section.

V.1.2. Hallmarks of melanoma cells

In 2000, Hanahan and Weinberg postulated several hallmarks of cancer cells acquired during transformation, thereby providing an organizing principle for rationalizing the nexus of malignancies [49]. The list of hallmarks was updated in 2011, and comprises genomic instability and mutation, resistance to cell death, deregulation of cellular energetics, sustained proliferative signaling, replicative immortality, growth suppressor evasion, invasion and metastasis formation, prevention of immune destruction, the establishment of a tumor-promoting inflammation, as well as the induction of angiogenesis [50]. These general characteristics of cancer cells can be achieved in a number of different ways; here, methods used by melanoma cells will be described and illustrated (see Figure 1, Hallmarks of melanoma, page 10).

Genomic instability is on the one hand clearly a hallmark of cancer cells, on the other hand it is not well understood by now. Bastian and colleagues demonstrated in 2000, that cutaneous melanomas have specific genomic instability patterns [51] not knowing if these are causative for or effects of the malignant transformation [52]. As already mentioned in the last section, genomic aberrations have also been found in benign nevi suggesting an early role in melanomagenesis [53]. 95 % of melanomas exhibit chromosomal aberrations [54] with non-metastatic tumors being genomically more stable than metastatic ones, indicating genomic instability as an ongoing process with importance not only for development but also for the progression of the disease [52, 53, 55, 56]. Causes for the lack of genomic integrity might be excessive oxidative stress, or failure of cellular functions ensuring the accuracy of DNA transactions like defective DNA repair, and telomere dysfunction [52]. It has been shown that different kinds of cancer, including melanoma, exhibit high levels of ROS [57, 58], thereby being prone for oxidative DNA damage.

In addition, alterations in ***DNA damage repair*** and signaling have been linked to melanoma. For instance, patients with *xeroderma pigmentosum* (XP), a rare disease caused by mutations in DNA repair genes, show a 1000 - fold higher frequency as well as early onset of malignant melanoma [59]. Many of the genes affected by mutations leading to XP are part of the nucleotide excision repair (NER) [60]. Besides NER, also the characterized deregulation of molecules involved in double-strand break (DSB) repair mechanisms like the non-POU domain containing octamer-binding (NONO) protein, significantly influence melanoma cell behavior and progression [61, 62]. Furthermore, Zhang and colleagues demonstrated that SNPs within two DNA damage repair genes, namely *ATR* and *PARP1*, significantly

correlated with an increased susceptibility to melanoma [63]. Although one of the common ways of cancer cells circumventing DNA damage signaling, which is the direct *P53* mutagenesis, is less frequent in melanoma, its inactivation mediated by the loss of p14ARF [32, 33] or amplification of HDM2 [64] leads to comparable effects. The net effect of all these alterations is an increased tolerance towards DNA damage and enhanced ***resistance to cell death***. One indication for a prolonged survival of melanoma cells is the fact, that they often harbor long telomeres [65]. Usually, during the lifespan of a normal somatic cell, mitosis will result in gradual shortening of telomeres. As response to short telomeres, cells undergo destabilization, followed by loss of chromosomes, and induction of senescence and cell death. Therefore, untransformed cells display a kind of 'mitotic clock' restricting their lifespan [66]. Since non-melanoma skin cancers are associated with short telomeres [66], thereby presenting an inverse correlation to melanoma, the latter seem to have different strategies ensuring ***replicative immortality***.

Indeed, melanoma cells found several ways to adjust this 'clock'. One strategy of melanoma is to benefit from intrinsic mechanisms of their cells of origin, namely melanocytes. Melanocytes are characterized by many different intrinsic pro-survival mechanisms counteracting environmental stress, including UV radiation and toxic intermediates of melanogenesis [67, 68]. For instance, the microphthalmia-associated transcription factor (MITF), a master regulator of melanocyte differentiation, is known to be involved in the regulation of pigment synthesis, an important tool of melanocytes to shield their genomes from DNA damage [69, 70]. Besides melanin synthesis, MITF has been demonstrated to have additional pro-survival functions in melanomas. Among MITF targets various anti-apoptotic genes, such as *BCL2* (B-cell leukemia 2) or *BCL2A1* (BCL2 related protein A1), can be found. Whereas BCL2 shows a relatively low expression in melanoma, BCL2A1 seem to have tremendous importance, not only because of its high expression levels in melanoma but since it is also associated with an increased therapy resistance [71-73]. Furthermore, there is evidence for MITF inducing *BIRC7*, a gene encoding for the so-called melanoma inhibitor of apoptosis (ML-IAP). *BIRC7* harbors two predictive MITF binding sites, and the respective transcript levels, which are not detectable in melanocytes, positively correlate with MITF in melanoma [74, 75]. *Via* direct interaction with caspases ML-IAP inhibits intrinsic and extrinsic apoptosis pathways in melanoma; a function which results in diminished patient survival [76, 77]. Although these are only a few examples for the pro-survival effects of MITF, also other features of melanoma cells like the reduction of the apoptotic-protease-activating factor 1 (APAF1) [78], or the aberrant activation states of MAPK and PI3K pathways significantly enhance the viability of melanoma cells. Evidence for the latter has been provided by the study of Koo *et al.* [79], showing that the inhibition of the MAPK pathway induces apoptosis in melanoma cells but not in normal melanocytes. Further studies

revealed that the phosphorylation of pro-apoptotic proteins like BAD and BIM by MAP kinases results in their inactivation, representing one of the MAPK-dependent mechanisms for propagation of survival [80-82]. Since Stambolic and colleagues demonstrated in 1998 that murine embryonic fibroblasts (MEFs) displayed reduced apoptosis upon *PTEN* knockout [83], the finding that loss of *PTEN* is a frequent event in melanoma has soon been connected to the improved survival of melanoma cells. Indeed, ectopic expression of PTEN in melanoma cells lacking the functional protein, led to an impaired activation of AKT3 and downstream mediators, thereby resulting in decreased cell survival [84-86].

The activation state of AKT proteins does not only affect the survival of melanoma cells; it also impacts ***cell energetics and metabolism***. More specifically, changes in AKT activation have been linked to an impaired mitochondrial-dependent glucose oxidation. For energetic compensation melanoma cells induce glycolysis, which results in an immense uptake of glucose and in the generation of high lactate levels [87, 88]. Several studies linked increased lactate dehydrogenase (LDH) levels to metastatic spread of melanoma cells. The establishment of a selective environment might be an intelligent strategy of cancer cells, which seem to easily adapt to acidic conditions in comparison to surrounding cells [89-91].

Melanoma cells seem to have the possibility to pursue different strategies; indeed, they are also capable of switching strategies. Two different states of melanoma cells have been reported: Melanoma cells in the ‘proliferative’ state undergo excessive cell divisions, while enhanced motility and migration are defined as characteristics of ‘invasive’ melanoma cells. The ***high proliferation capacity*** of melanoma cells can be easily demonstrated by comparing doubling times of melanoma cell lines (A375, MeWo, RPMI7951), which lay in between 21 to 36 hours [92], to the doubling time of isolated normal human melanocytes, which has been determined as four to ten days [93]. This is based on hyperactivation of MAPK and PI3K pathways and subsequent activation of transcription factors like NF-κB and ERK [94-96]. Primary melanoma cells as well as melanoma cell lines with a ‘proliferative’ signature are characterized by melanocyte differentiation antigens, including MITF and several of its targets, while cells of the ‘invasive’ state are defined by the expression of negative regulators of the Wnt signaling pathway, like WNT5A (wingless-type MMTV integration site family member 5A), DKK1 (Dickkopf-related protein 1), and CTGF (connective tissue growth factor) [97, 98]. These and additional features discriminating the two phenotypes are well-established characteristics of the ‘epithelial-to-mesenchymal transition’ (EMT) [99, 100], a process involved in ***invasion and metastatic dissemination*** of many epithelial cancers [101]. To acquire the capacity to invade, melanoma cells need to lose cell-cell-contact with keratinocytes. Several groups were able to show that switching between E-cadherin and N-cadherin enables melanoma cells to rather interact with stromal

fibroblasts and endothelial cells. The cadherin switch, a main hallmark of the EMT, is induced by epithelial-mesenchymal transition regulators (EMTRs), such as Snail and Twist [102-104]. Furthermore, melanoma cells need to adhere to extracellular matrices (ECM) and proteolytically degrade ECM proteins. Indeed, invasion and metastasis formation have been linked to the deregulation of different proteolytic enzyme systems, including the family of matrix metalloproteinases (MMP) [105-108]. After migration through the basement membrane into veins and lymphatic vessels potential metastatic cells are then selected for resistance to apoptosis, immunological evasion, adhesion, and migration to a new metastatic site [109].

Melanomas spread in three different ways: locally within the dermis; *via* the lymphatic system, and *via* the bloodstream. Since melanoma tumors acquire rich vascular networks [110] a connection between ***angiogenesis*** and metastasis formation has been long hypothesized. Schietroma and colleagues could demonstrate in 2003 that an increased vascular endothelial growth factor C (VEGF-C) expression significantly correlates with higher frequency of metastasis in sentinel lymph nodes [111].

Beside cell-intrinsic factors affecting the reversible phenotype switch, also microenvironmental components such as nutrients, oxygen, cytokines, and growth factors play an important role. Widmer and colleagues suggested hypoxia as one of the environmental factors influencing the phenotype switch of melanoma cells. They found that tumor regions displaying an ‘invasive’ signature with decreased expression of melanocytic differentiation markers, correlate with hypoxic regions defined by the expression of the glucose transporter 1 (GLUT1) and the hypoxia-inducible factor 1 alpha (HIF1α) [112]. Another environmental influence regulating the two states is the transforming growth factor β (TGF-β). Upon *in vitro* stimulation with TGF-β, cells of the ‘proliferative’ subgroup were inhibited and started to downregulate MITF expression, whereas cells with the ‘invasive’ phenotype responded with increased invasiveness [113, 114]. In order to switch between these two states, melanoma cells need to induce dramatic changes. Therefore, the phenotype switch requires complex molecular regulation and restructuration, illustrating the enormous plasticity of melanoma cells.

The plasticity of melanoma cells is not only useful in the adaption to environmental stress, but also in the ***evasion of growth suppression and immune destruction***. As mentioned earlier, melanoma cells can drive cell cycle progression through mutations or aberrant expression of molecules involved in cell cycle checkpoints like RB1, p16INK4a, or CDK4 [28-31]. It has been shown that MITF, which is upregulated upon switching into the ‘proliferative’ state, induces the cyclin-dependent kinase inhibitor gene *CDKN1A*, thereby regulating the

phosphorylation status of RB1, leading to its activation and consequently to cell cycle progression [28].

Although melanoma cells harbor many genetic as well as epigenetic changes associated with the aberrant expression of multiple molecules, their capacity to up- and downregulate these potential tumor antigens, represents one of the characteristics of melanoma cells making them less vulnerable to host immune responses. In human melanoma various classes of tumor antigens have been identified, including autologous tumor-specific, tissue-specific, and common cancer-specific antigens [115]. Despite the selection of non-immunogenic melanoma cell variants, which belongs to the phenomenon called 'immunoediting', melanoma cells can also conduct 'immunosubversion' by suppressing anti-tumor immune response actively [116].

In 1969, Clark and colleagues first described the lymphocytic infiltration of primary melanomas [117]. The immune system plays an important role in melanomagenesis which has later been proven by the fact that the presence of tumor-infiltrating T lymphocytes (TILs) represents a useful prognostic marker for melanoma [118, 119]. A higher percentage of TILs within primary melanomas has been demonstrated to significantly correlate with lower numbers of lymph node metastases [120], a better prognosis and a higher survival rate [118]. It is noteworthy that these findings are still under discussion since other studies failed to verify the positive correlation of marked TIL infiltrations and improved survival [121-123]. This discrepancy may be partly explained by differences in patient populations, e.g. in terms of clinical stages [124]. Another reason might be the great variance of the tumor microenvironment regarding the immune cell composition between individual patients. For instance, the pattern of infiltrating T cell subsets can range from predominant $CD4^+$ T cell infiltrations to infiltrates with almost 90 % $CD8^+$ T cells [125-127]. In addition, the function of TILs is often impaired by the accumulation of immunosuppressive cells. Accumulations of $CD4^+CD25^+Foxp3^+$ regulatory T cells (Tregs), myeloid-derived suppressor cells (MDSCs), tumor-associated macrophages (TAMs), as well as other immunosuppressive cells are detected in the tumor microenvironment of melanomas [128-134]. Accordingly, the presence of Tregs predicts reduced patient survival [135], as confirmed by the *in vitro* depletion of Tregs from melanoma TIL populations leading to increased tumor cell lysis mediated by NK cells [136].

Beside indirect effects on the tumor stroma, melanoma cells can also directly contribute to immunosuppression. In addition to the already described phenomenon of immunoselection, melanoma cells are able to decrease the expression of co-stimulatory molecules [128], major histocompatibility complex (MHC) class I molecules [137], ligands for natural killer cell receptors [138], and to induce the production and secretion of immunosuppressive factors

such as VEGF, TGF-β, nitric oxide (NO), prostaglandins, or interleukins (IL) [128, 139]. Just recently, Dong and colleagues were able to link loss of PTEN with the induction of immunosuppressive cytokines. In fact, ectopic PTEN expression in a PTEN-defective human melanoma cell line restored the transcriptional repression of IL-10, IL-6 and VEGF in a dose-dependent and STAT-3 (signal transducer and activator of transcription)-driven manner. Furthermore, they were able to demonstrate an inverse correlation of PTEN and programmed death-ligand 1 (PD-L1) expression [140]. Binding of PD-L1 to its receptors, PD-1 (programmed cell death protein 1) and CD80, on T lymphocytes results in the inhibition of proliferation and cytokine production of activated T cells [141]. In fact, T cells found within the melanoma microenvironment are in a so-called state of 'exhaustion', as characterized by functional deficiency, impaired cytokine production, and upregulation of inhibitory receptors like PD-1, cytotoxic T-lymphocyte-associated protein 4 (CTLA-4), and T cell immunoglobulin mucin domain containing molecule-3 (TIM-3) [142-145].

The suppressive environment of cutaneous melanoma is governed by ***chronic inflammatory conditions*** mediated by the activation of several inflammatory signaling pathways resulting in the activation of NF-κB and STAT3 [146-150]. Beside the accumulation of immune suppressor cells, chronic inflammatory processes also involve the production and secretion of pro-inflammatory cytokines, chemokines, growth factors and angiogenesis-inducing molecules. These factors help the tumor to enable the described hallmarks thereby directly linking chronic inflammation with tumor development and progression [151-155]. Chronic inflammation in the melanoma microenvironment can be induced by infection-associated inflammatory responses. Nevertheless, most likely immune activation occurs after traumatic injury and in non-pathogen-associated disease processes. This points towards an existence of other inflammatory signals able to induce inflammations in the absence of infections, i.e. under sterile conditions [156].

In fact, it has been shown that viral infections play a role in the onset and progression of some cancers, including non-melanoma skin cancers [157, 158], whereas data on correlations between the presence of viruses and melanoma progression are rare [159]. Instead, members of the so-called damage-associated molecular pattern (DAMP) family like S100 proteins, known to induce 'sterile inflammations', are not only upregulated in melanoma but at least one S100 family member, S100B, also serves as diagnostic and prognostic marker [160, 161]. Further diagnostic but also therapeutic approaches in melanoma will be described in the next section.

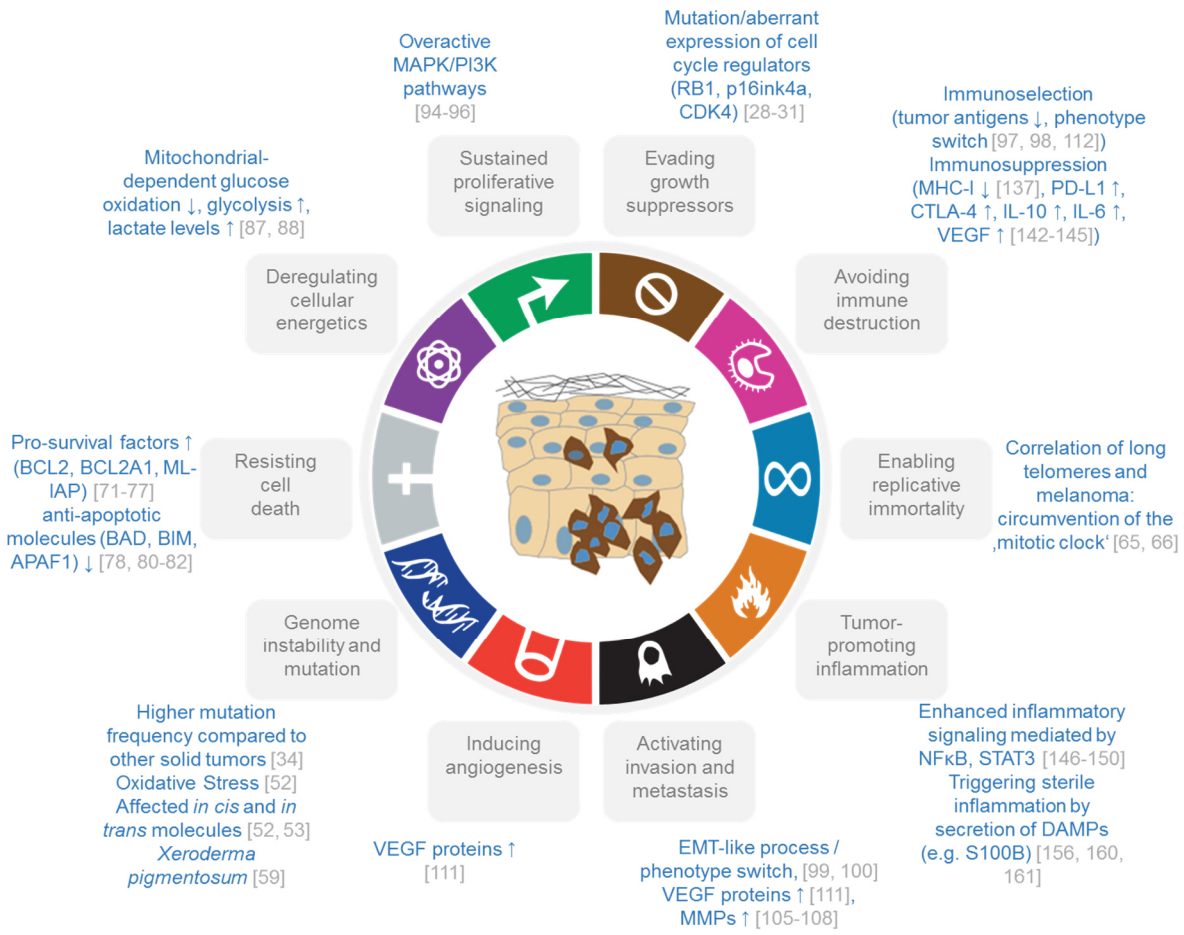

Figure 1 Hallmarks of melanoma cells (adapted from Hanahan and Weinberg [50] with permission from Elsevier). Illustrated are examples of strategies and features displayed by melanoma cells, enabling them to circumvent barriers and regulatory mechanisms of normal, untransformed somatic cells.

V.1.3. Melanoma in the clinic: diagnosis, management, and complications

After introducing the high plasticity of melanoma cells, not only regarding phenotype but also function, it is not surprising that histological diagnosis as well as therapeutic approaches may prove difficult. In this section, the current state of diagnosis, management, and complications of malignant melanoma is described.

V.1.3.1. Diagnostic and prognostic aides for melanoma

As mentioned above, there are difficulties regarding the histological diagnosis of melanoma since it can occur in many different cytomorphological variants. Furthermore, melanomas can also resemble different tumors, such as carcinomas, sarcomas or germ cell tumors [162]. Therefore, immunohistochemical stainings for melanocytic differentiation markers are often applied in the diagnosis of melanoma [163]. The most frequently used marker in clinical

practice is S100B, a member of the DAMP family, and a well-known ligand of the receptor for advanced glycation end-products (RAGE). Since reacting with about 90 % of melanomas, S100B represents a quite sensitive marker. Nevertheless, S100B is also expressed by adipocytes, chondrocytes, Schwann cells, and myoepithelial cells, as well as by some other benign and malignant neoplasms. Therefore, its value as melanocytic marker is limited [164, 165]. In contrast, the melanosome-specific glycoprotein 100 (GP100) shows a higher specificity for melanocytic neoplasms, but a lower sensitivity compared to S100B [13-15]. Furthermore, also markers like MITF, TYR (tyrosinase), and MART-1 (melanoma antigen recognized by T cells 1) are used in routine diagnostic [166-168].

Besides immunohistochemical analyses, biopsy specimens are also used for determining the maximal diameters of lesion penetration, known as Breslow depth [169], as well as the level of invaded tissue layers, referred to as Clark level [117]. Although sharing similarities Breslow depth and Clark level measure two different things: tumor volume and metastatic potential [170]. The system most often used for staging melanoma is the American Joint Commission on Cancer (AJCC) TNM system, which is based on a combination of histologic and clinical characteristics. Histologic features comprise Breslow depth, mitotic rate, defined as number of mitoses per square millimeter, and ulceration. Among clinical features the absence or presence of lymph node metastases, or metastases to distant organs, as well as LDH levels are numbered. The analyzed criteria are then combined and assigned to four main stages (I to IV) that can also be subgrouped. In general, patients with lower stage melanomas have a better outlook regarding cure or long-term survival [171]. Accurate staging does not only provide important prognostic information but also steers the choice of further therapy.

V.1.3.2. Melanoma management

Early diagnosis combined with appropriate surgical removal is currently the best treatment option for melanoma [172, 173]. Whereas the prognosis for patients with small primary melanomas (AJCC stage IA), which have been successfully resected, is similar to healthy individuals, the median overall survival for patients with AJCC stage IV melanoma drops to 7.5 months [174]. As soon as melanomas have spread and formed distant metastases, they become non-removable and difficult to treat. Over a long period, dacarbazine, an alkylating agent interfering with the growth of cancer cells, was the only worldwide-approved drug for stage IV melanoma patients without improving patient overall survival [175]. Although clinical trials using diverse combinations of chemotherapy and immunotherapy managed to increase response rates and alleviate toxic effects, they failed to provide evidence for prolonging survival of these stage IV patients [176, 177]. Important molecular characteristics, such as the role *BRAF* and *NRAS* mutations [35, 42], as well as the role of the immunosuppressive

tumor microenvironment [144, 178] resulted in a better understanding of melanoma pathogenesis. These advances in melanoma research where then rapidly translated into therapeutic approaches like immunomodulation and mutation-targeted therapy providing survival benefits for patients with metastatic melanoma [179, 180].

Between 2011 and 2014 the U.S. Food and Drug Administration (FDA) approved three targeted agents for the treatment of patients with advanced melanoma and mutations in BRAF: the two BRAF inhibitors vemurafenib and dabrafenib, as well as the 'downstream'-acting MEK inhibitor trametinib [176]. In Germany, only BRAF inhibitors vemurafenib and dabrafenib are approved whereas the MEK inhibitors trametinib and cobimetinib are planned for approval by the end of 2015. Since clinical trials comparing vemurafenib with dacarbazine were able to demonstrate significant benefits in median progression-free and overall survival, vemurafenib has been set as first-line treatment of advanced V600E BRAF-mutated melanoma [180]. Comparable results have been recorded in clinical trials with dabrafenib [181]. Also studies using the MEK inhibitors trametinib or cobimetinib were able to register survival benefits, endorsing a dual pathway inhibition strategy [182, 183].

As described before, another member of the MAPK pathway, namely NRAS, is also often affected in melanoma. Until now, there are no targeted therapies against NRAS; however, as studies revealed enhanced MAPK signaling and aberrant cell cycle checkpoints in NRAS-mutated melanomas, patients have been treated with MEK and CDK4/6 inhibitors in the hope to receive off-target effects. Indeed, clinical trials using MEK inhibitors [184], as well as combinations of MEK and CDK4/6 inhibitors resulted in partial responses of patients with NRAS-mutated tumors [185].

For targeting advanced melanoma in a mutation-independent manner, targeted agents interfering with the control of immune checkpoints have been developed. For instance, effects of agonistic antibodies blocking CTLA-4, PD-1, or PD-L1, molecules involved in immunosuppressive signaling, have been investigated. The monoclonal anti-CTLA-4 antibody ipilimumab is able to mediate inhibition of immune tolerance and induction of tumor regression in clinical trials, thereby resulting in a prolonged median overall survival of patients with stage IV melanoma [179, 186]. Ipilimumab was then approved for advanced melanoma in the U.S. and in Europe. Furthermore, antibodies targeting PD-1 and PD-L1 interaction revealed significantly enhanced pro-survival effects and high response rates compared to ipilimumab when tested in clinical trials [187]. Two monoclonal anti-PD-1 antibodies, pembrolizumab and nivolumab, were approved for advanced melanoma in the U.S. in 2014 and will get approval in Europe by mid-2015 [188, 189].

Two cytokine-based immunotherapies have been approved, so far. For instance, interferon alpha-2b (IFNα-2b) is used as adjuvant for therapies aiming to overcome tumor-induced immune suppression. It functions by promoting anti-tumor immune responses *via* recruiting lymphocytes, activating dendritic cells (DC), and switching Th2-biased to Th1-mediated T cell responses resulting in enhanced cytotoxicity [190-195]. Another possibility is the treatment with high doses of IL-2. Although responses are only induced in about 17 % of the patients, the finding that approximately 5 % achieve durable complete responses led to its approval by the FDA [196-198].

Since 2010, the treatment of patients with stage IV melanoma has been continuously shifted from chemotherapy towards targeted immunotherapy. The high adaptation capacity of melanoma cells leading to the development of various resistance mechanisms, as well as drastic side effects limit recent advances of novel therapeutic approaches. An overview on described side effects and resistance mechanisms in melanoma will be provided in the next section.

V.1.3.3. Complications in melanoma management

Although the advances in immunotherapy bring new hope into the melanoma field, the recent therapeutic options still resemble a double-edged sword. In general, patients with advanced melanoma show an initial response to treatment resulting in prolonged overall and progression-free survival; however, the clinical benefits only last for a short period of time, and are often severely limited because of therapy-associated adverse effects.

For instance, high-grade toxicities of BRAF inhibitors have been frequently recorded, here in over 15 % of the treated patients [199], and include dermatologic complications, such as rash, photosensitivity reactions, and hyperkeratosis, as well as arthralgia, fatigue, alopecia, nausea, and diarrhea. Furthermore, up to 26 % of patients treated with either vemurafenib or dabrafenib develop clinically significant cutaneous side effects, such as squamous cell carcinomas [200-202]. A phase III trial with 423 patients randomly assigned to treatment with either combined BRAF and MEK or single BRAF inhibition suggested that the observed skin toxicity is due to the development of a paradoxical MAPK pathway activation despite BRAF inhibition. The combination with MEK inhibitors significantly reduced the incidence of squamous cell carcinomas in this trial [203]. However, clinical trials also showed that MEK inhibitors themselves induce adverse effects at high frequencies, such as cutaneous toxicity, diarrhea and edema [182].

As described above, findings of clinical trials testing combinations of BRAF and MEK inhibitors suggested that some of the adverse effects are mediated by a reactivation of the MAPK pathway. For verification and in order to investigate if such reactivation may be also a

reason for observed relapses, a large phase II clinical trial set up Sanger DNA sequencing and histological examinations of relapse tumor specimens. The analyses demonstrated that nearly all tumors display reactivations of the MAPK pathway with consequent elevation of phosphorylated ERK at time of resistance. A prominent mechanism is the upregulation of redundant paralogs of BRAF, namely CRAF or ARAF [204, 205]. Furthermore, progression of some patients was accompanied with the acquirement of new mutations of molecules within the MAPK pathway, including mutations in NRAS and MEK [206, 207]. Besides MAPK pathway reactivation, alterations in ERK1/2-regulated cell cycle events, activation of alternative signaling pathways, as well as chromatin-regulating events have been suggested as additional mechanisms of melanoma cell resistance against BRAF-targeted therapy [205, 208-210]. For instance, Villanueva and colleagues identified several receptor tyrosine kinases (RTKs) to be differentially phosphorylated between pre-treatment and post-relapse samples. Indeed, pharmacological inhibition of the insulin-like growth factor 1 receptor (IGF-1R) led to decreased viability of melanomas resistant to BRAF inhibitors [205]. Furthermore, enhanced expression of JARID1A, a histone demethylase, has been shown to induce chromatin remodeling, thereby transferring melanoma cells into a drug-tolerant state [211].

Unfortunately, also immunomodulatory therapeutic approaches are associated with high-grade adverse side effects. For instance, the desired function of the anti-CTLA-4 or anti-PD-1 antibodies, which is the activation of T cell-mediated anti-tumor responses, can also negatively affect the melanoma therapy due to adverse side effects. Among the most common clinical manifestations autoimmune disorders leading to entercolitis, hepatitis, dermatitis, neuropathy, and endocrinopathy, are listed. The ipilimumab-induced enterocolitis, which is present in 10 to 20 % of the treated patients, presents a potentially life-threatening disorder due to bowel perforation [212].

Also cytokine-based adjuvant therapies have been demonstrated to result in adverse side effects in most of the patients. A clinical trial with 294 patients with malignant melanoma on high-dose IFNα-2B treatment demonstrated a high frequency of concomitant phenomena, such as influenza-like illness, fatigue, nausea, diarrhea, and neutropenia [213]. Furthermore, although showing low response rates in melanoma patients, treatment with high-dose IL-2 can also be one of the most effective treatments since it can induce complete remissions in some of the patients. Nevertheless, it also belongs to one of the most toxic therapies. For instance, due to the massive inflammation caused by IL-2 patients can develop a capillary leak syndrome, which resembles the clinical picture of a septic shock. Additional adverse effects, such as pulmonary edema, hypotension, cardiac insufficiency, cerebral edema, and renal failure have been described [214, 215].

By targeting tumor-intrinsic aberrations, and immunosuppressive features of melanoma cells great progress has been made in melanoma therapy. Besides improving the clinical benefits of these therapies, a major goal for future melanoma management will be an extended understanding of melanoma pathogenesis, immunosurveillance, and mechanisms leading to therapy resistance. For instance, only little is known about the pathways involved in the induction of a sterile inflammation, which is directly linked to the establishment of an immunosuppressive melanoma microenvironment. One of these pathways with a potential role in melanomagenesis might be regulated by the receptor for advanced glycation end-products (RAGE). In the next main section, some information about characteristics of RAGE, its ligands, and its functions in health and disease is provided.

V.2. The receptor for advanced glycation end-products (RAGE)

The receptor for advanced glycation end-products (RAGE) is a pattern recognition receptor belonging to the immunoglobulin superfamily. Since its discovery in 1992 as a transmembrane receptor for advanced glycation end-products (AGEs), which are generated via non-enzymatic crosslinking of carbohydrates to proteins and other biological molecules, RAGE has not only been identified to bind several other ligands but also to have important functions in physiological processes, and more important as pathogenic factor of several diseases [216-222].

V.2.1. Structure and polymorphism of RAGE

The gene encoding for human RAGE, namely *AGER*, is located on the chromosome six within the major histocompatibility complex (MHC) III locus and contains eleven exons and ten introns. The leader sequence upstream of the coding region of *AGER* contains many functional elements, such as binding sites for transcription factors like NF-κB, specificity protein 1 (SP1), activator protein 1 and 2 (AP1/2), E-twenty-six 1 (ETS1), HIF-1, early growth response gene 1 (EGR-1), and for thyroid transcription factor 1 (TTF-1) [223-226].

Furthermore, several single nucleotide polymorphisms (SNPs) located within the promoter region of *AGER* have been reported. Among those the threonine to alanine substitution at position -374 (-374T/A), threonine to cysteine at -429 (-429T/C), and glycine to serine at +82 (82G/S) have been listed. Additionally a 63 base pair deletion polymorphism has been described for the region encompassing -374. These promoter polymorphisms correlated in most studies with enhanced expression of the *AGER* gene [227-232]. In addition, also the presence of alternative promoters has been demonstrated [233].

In 1999, Malherbe and colleagues successfully identified a secreted splice variant of RAGE, followed by several others [234]. Almost ten years later, in 2008, Hudson *et al.* published a

detailed study on RAGE isoforms showing that *AGER* transcripts are indeed, extensively modulated by alternative splicing. In total, 19 different splicing variants of RAGE have been described and labeled according the HUGO terminology: RAGE_v1 to RAGE_v19 [233].

The most abundant protein form, hereinafter referred to as full-length RAGE (fl-RAGE), consists of 404 amino acids (aa) resulting in a molecular mass of 55 kDa. It contains a N-terminal portion, comprising a signal sequence for secretion (1-22aa), three immunoglobulin domains (Ig domains, 23-317aa), as well as a transmembrane helix (343-363aa), and a short cytoplasmic tail at the C-terminus (364-404aa) [216, 218, 233]. According to the definition of Williams and Barclay from 1988, the Ig-like regions of RAGE are either of a so-called 'variable' (V) type, or of a more 'constant' (C) character. The classification refers to the length of the amino acid sequence between conserved disulfide bonds [216, 235]. Nevertheless, it has been suggested that the V domain (23-116aa) of RAGE forms a structural unit with the connected C1 domain (124-221aa); a formation (VC1) resulting in a large cationic surface area, which is required for at least some of the ligand binding properties. In contrast, it has been reported that the C2 domain (277-317aa) attached to the VC1 unit *via* a flexible linker, is able to function in a fully independent manner [236-238]. Interestingly, the cytoplasmic tail does neither have enzymatic activity nor homology to any known signaling domains, thereby complicating the search for cytosolic interaction partners [216]. The cytoplasmic part of RAGE can be subdivided in three parts: The part laying proximal to the cell membrane is characterized by a high proportion of basic amino acids, the central region by acidic amino acids, whereas the C-terminal part is less conserved [239].

Alternative splicing of the *AGER* transcripts can result in proteins that differ tremendously from fl-RAGE, not only regarding their structure but also their function. Beside soluble variants of RAGE lacking both, transmembrane region and cytoplasmic tail, other variants show extensive changes within the extracellular domain. These include changes within the V domain (RAGE_v4, v5) or widespread deletions of the extracellular domain (RAGE_v2 and v13), thereby potentially enhancing the ligand spectrum of the receptor [233]. Recent studies provided evidence of the existence of a complex regulation machinery enabling the selection of alternative *AGER* exons depending on the intracellular concentration or activity of nuclear RNA binding proteins, such as the heterogeneous nuclear ribonucleoprotein H (HNRNP H) and A1 (HNRNP A1), and the transformer2-β1 (TRA2-β1) protein [240, 241]. Indeed, studies were able to demonstrate differentially expressed RAGE splicing forms in Alzheimer's disease and their association with neurodegeneration [241, 242]. This indicates that the regulation of RAGE splicing or of the splicing frequency may affect the functional outcome of total RAGE.

Another way to regulate the function of a protein is posttranslational modification. Fl-RAGE as well as its isoforms can be posttranslationally modified by disulfide bond formation, phosphorylation, proteolysis, and glycosylation. Disulfide bond formation can occur intermolecular between conserved cysteines (C259, C301) of the C2 domain [243], or of the V1 domain [238]. Indeed, fluorescence resonance energy transfer (FRET) could show that RAGE molecules can form homodimers, as well as homooligomers and heterodimers with heparin sulfate proteoglycans (HSPGs) and Toll-like receptors (TLRs) [244]. Proximity ligation assays demonstrated preformed complexes of RAGE and HSPG, which increased in number after stimulation with high-mobility group box 1 protein (HMGB1), possibly as a result of receptor complex stabilization upon ligand binding [245, 246]. Similar results were also found for RAGE and TLR-2 upon stimulation with S100B [247]. Wei and colleagues were able to demonstrate that this multimerization is not only eligible but rather represents a quality control mechanism. Converting the two cysteines to serines significantly reduced RAGE expression on the cell surface in their experiments [243]. If different splicing variants of RAGE can assemble to form multimers remains to be investigated.

Furthermore, RAGE can be posttranslationally modified by phosphorylation as well as by glycosylation within the V domain. For instance, RAGE is phosphorylated by MAP kinases such as ERK1/2 upon HMGB1 binding [248, 249]. Kang and colleagues showed that a phosphorylation at serine 377 enabled the RAGE protein to translocate into the mitochondria, where it influences the bioenergetics of the cell [249].

Proteolysis of membrane-bound RAGE by enzymes like matrix metalloproteinases and γ-secretase can produce soluble ectodomain fragments, fragments containing the transmembrane domain, as well as soluble forms of the cytoplasmic domain. Matrix metalloproteinases, which are known to exert such function are MMP9 and ADAM10 (a disintegrin and metalloproteinase 10). The ectodomain can be either secreted into the extracellular space or localized into intracellular vesicles [250-252] whereas the C-terminal fragment is found in the cytoplasm but has also been demonstrated to be transported into the nucleus [250].

The structure of a protein is closely related to its function. In terms of RAGE, the complexity is extended due to the variety of isoforms and formation of tissue-specific heterocomplexes on the cell surface. In addition, a tissue-specific expression of ligands and modulators allows an individually regulation of RAGE proteins, leading to inconsistent findings regarding its functional role.

V.2.2. RAGE ligands

As mentioned before, RAGE is listed among the pattern recognition receptors. However, RAGE does not recognize a common molecular pattern; instead, it binds to a broad spectrum of mostly negatively charged ligands.

V.2.2.1. Advanced glycation end-products (AGEs)

Advanced glycation end-products (AGEs) are generated by a frequent nonenzymatic glycation and oxidation of proteins and lipids [253]. Increased levels of protein glycosylation have been found to be associated with ageing, diabetes mellitus (DM), active inflammation, as well as malignancies, such as melanoma [254-256]. The generation of AGEs results in the increase of the overall negative surface charge of the substrate, thereby enabling binding to RAGE.

V.2.2.2. Damage-associated molecular pattern molecules (DAMPs)

Damage-associated molecular pattern molecules, from here on referred to as DAMPs, are either actively or passively released cellular molecules, many of them proteins, which induce responses following stress situations like nutrient deprivation, hypoxia, trauma, and chemotherapy treatment. As the endogenous homolog to pathogen-associated molecular patterns (PAMPs), DAMPs can activate the innate immunity, thereby providing a way to induce systemic inflammatory responses in the absence of an infection. DAMPs comprise various molecules such as the HMGB1 protein, S100 family members, heat shock proteins (HSP), uric acid, heparan sulfate (HS), adenosine triphosphate (ATP), and DNA [156, 257].

Since HMGB1 and members of the S100 family are well-described ligands for RAGE, and also known to be involved in melanomagenesis [258-262], they will be used as examples for describing main characteristics of DAMPs, also in regard to their role in malignant melanoma.

V.2.2.2.1. S100 protein family

The S100 protein family contains 21 small EF-hand calcium binding proteins, which have been named according to their solubility in 100 % saturated ammonium sulfate [263-265]. The majority of the S100 proteins all cluster to one region of the chromosome 1 (1q21), which is highly susceptible to deletion and rearrangements, linking S100 proteins and carcinogenesis [266].

Although S100 family members share high similarities in their amino-acid sequence and tri-dimensional structure they are not always functionally redundant [267, 268]. For instance, structural similarities enable S100B and S100A2 to interact with the tumor suppressor P53; however, the interaction with S100B leads to its inhibition, while S100A2 is able to activate

P53 [269, 270]. The sequence and structural homology of S100 family members allows them to form homo- and heterodimers, as well as oligomers [271, 272].

The cytosolic function of S100 proteins, including their role as calcium sensors, is enlarged by the secretion of distinct S100 family members. Individual S100 proteins display cytokine-like functions, involved in a wide range of biological processes such as proliferation, migration, invasion, inflammation and differentiation [273-275]. Since these proteins lack a conventional secretion signal, it is still unclear whether the extracellular S100 dimers or oligomers are actively secreted by living cells or passively released upon cellular disintegration e.g. during necrosis [273, 275]. Recent studies suggested that RAGE might participate in the translocation of S100 proteins, such as S100B [276, 277].

As mentioned earlier, S100B is an established immunohistological as well as serum biomarker for melanoma although its role in melanomagenesis remains unknown [164]. Certainly, extracellular S100B as well as other S100 proteins are able to interact with a variety of cell-surface receptors, including RAGE. Besides S100B, also other S100 family members are suggested to play a role in melanoma. For instance, S100A2, which is believed to function as a tumor suppressor, is downregulated in melanoma, thereby showing a negative correlation to S100B expression [278-280]. Other members, such as S100A4, S100A6, S100A8 and S100A9, are linked to progression and metastasis formation in melanoma, although studies revealed partly conflicting results [279, 281-283]. Despite recent advances in S100 protein biology, there is still a need to understand how each family member contributes to the pathogenesis of malignant melanoma.

V.2.2.2.2. High-mobility group box 1 (HMGB1) protein

The HMGB1 protein has an ambivalent character: On the one hand it has been described as a non-histone DNA-binding nuclear protein [284, 285], on the other hand several cytosolic as well as extracellular functions have been reported for HMGB1 [286-288]. Within the nucleus HMGB1 binds DNA in conformation-dependent, but sequence-independent manner and functions as DNA chaperone, participates in DNA replication and repair, and acts as transcriptional regulator [284, 289]. Active secretion of HMGB1 requires the inhibition of its nuclear import, mediated *via* posttranslational modifications, such as phosphorylation, methylation, and acetylation [290-292]. Similar to the S100 family members HMGB1 lacks conventional secretion signals, thereby depending on non-classical pathways [293].

HMGB1 has not only been demonstrated to be upregulated in several solid tumors, including melanoma, but to be directly associated with increased invasion and metastasis [262]. Secreted HMGB1 is thought to directly promote metastasis formation through its ability to induce cell migration, to modulate the adhesion potential of cells, and to modify extracellular

matrix composition [289, 294]. In addition, Bald and colleagues were able to demonstrate that the UV radiation-induced progression of primary tumors in the genetically engineered melanoma mouse model Hgf-Cdk4^{R24C} could be abolished by pharmacologic inhibition of extracellular HMGB1 [295]. In its function as a transcriptional regulator, and by enhancing the activity of NF-κB it can induce the melanoma inhibitory activity (MIA) protein in an indirect manner. MIA is a secreted protein, which is low expressed in benign nevi but highly in metastatic melanoma, and which has been shown to enhance the migrative and invasive capacity of tumor cells by binding to fibronectin and to integrins [262, 296].

In general, engagement of RAGE by a ligand triggers the activation of key cell signaling pathways. The current knowledge on involved molecules and activated or repressed transcription factors will be outlined in the next section.

V.2.3. RAGE signaling

Engagement of RAGE by its ligands elicits the immediate activation of multiple signaling pathways, dependent on the specific ligand, environmental conditions, and on the cell type. As mentioned before, RAGE is able to form homo- or heteromultimers within the plasma membrane. It is believed that RAGE pre-assembles already in the absence of a ligand, and that receptor engagement by multimeric ligands stabilizes these constitutive complexes, thereby shifting the equilibrium from monomers to higher order oligomerizations [297]. This explains why diverse ligands might have a different outcome regarding pathway activation and subsequent transcription factor induction. If the observed complexes consist only of full-length RAGE molecules, or if different RAGE isoforms contribute has not been described, yet. Also differences in receptor-ligand affinities leading to different dissociation rates might influence receptor activation and consequently signal transduction. RAGE has been shown to bind glycosylated HMGB1 with a higher affinity than the unmodified counterpart [248], thereby probably inducing a prolonged and enhanced receptor activation [298].

As mentioned above, the investigation of mechanisms behind downstream events induced by ligand engagement of RAGE has been impeded by the unique nature of the cytosolic tail of the receptor. Recent studies applying yeast two-hybrid systems as well as immunoprecipitation assays suggested the protein diaphaneous 1 (DIA-1) and the MAP kinases ERK1 and 2 to be direct interactors [239, 299]. Furthermore, it has been shown that the cytosolic tail of RAGE gets phosphorylated at S391 by protein kinase C type ζ (PKCζ) upon ligand binding, then serving as a docking station for TIRAP (toll-interleukin 1 receptor (TIR) domain containing adaptor protein) and MyD88 (myeloid differentiation primary response gene 88) [300]. TIRAP and MyD88 are well-known adaptor proteins for TLR2 and

TLR4, suggesting that the described receptor complexes of RAGE and TLRs at the cell surface represent not the only connection of these pathways.

Molecules interacting with the cytosolic portion of RAGE are able to specifically activate the MAPK cascade, and family members of the RHO (RAS homolog) small G-proteins, such as RAC-1 (Ras-related C3 botulinum toxin substrate 1) and CDC42 (cell division control protein 42), leading to the induction of several transcription factors [301, 302]. The RAGE-dependent activation of the MAPK pathway activates ERK1/2 and leads to an enhanced phosphorylation of the P38 MAP kinase and the stress-activated protein kinase/c-Jun-NH2-terminal kinase (SAPK/JNK) [222]. In neutrophils, RAGE signaling was abolished by application of PI3K inhibitors but not affected by inhibition of ERK or P38 [303], indicating the presence of tissue-specific modulators interacting with RAGE. These cytoplasmic signaling cascades result in the induction of transcription factors like NF-κB, AP-1, SP-1, and CREB [301, 302, 304-306].

Beside the transcription factor-based regulation of gene expression, RAGE has been also implicated to function within epigenetic regulation mechanisms. For instance, RAGE has been shown to induce the thioredoxin interacting protein (TXNIP), which subsequently alters chromatin conformation by histone remodeling, resulting in a higher accessibility for distinct transcription factors [307].

Interestingly, RAGE does not only induce a diverse set of other signaling molecules, but also its own expression *via* a feed-forward loop. In fact, RAGE uses a simple strategy: By activating transcription factors, such as NF-κB, which are able to bind to functional elements within the RAGE promoter, it consequently induces its own expression [308, 309]. This strategy enables the cell to generate fast responses towards stress conditions, but when deregulated, it can also lead to the hyperactivation of important signaling pathways, and consequently to pathological features.

V.2.4. Function of RAGE in health and disease

In normal healthy tissues RAGE is expressed at low to undetectable levels. The only exception is the lung, which demonstrates a high basal expression of RAGE [310, 311]. Pathological disorders are often connected with an upregulation of the RAGE protein, as well as of its ligands. In this section, physiological characteristics, as well as features of pathological RAGE signaling are described that are found in the human system or by applying mouse models (the murine homolog of RAGE will be referred to as Rage).

V.2.4.1. Physiological function of RAGE signaling

Since RAGE is expressed in only minor amounts under physiological conditions, its relevance during pathological processes has been in focus of research. Even in the lung, the

role of RAGE remains unclear although data indicate that it supports the organ's well-functioning [312, 313].

Genetically engineered Rage knockout (Rage$^{-/-}$) mice were viable, displayed normal reproductive fitness, and did not develop spontaneous diseases up to the age of 6 months [314].

A closer examination of Rage$^{-/-}$ mice uncovered a potential role in neuronal signaling, indicated by behavioral abnormalities, such as higher activity in darkness, higher sensitivity to auditory signals, and minimal effects on the animals' spatial learning ability [315]. Other studies observed an osteosclerotic-like phenotype in Rage$^{-/-}$ mice. Analyzing *in vitro* differentiated Rage$^{-/-}$ osteoclasts, Zhou and colleagues were able to demonstrate defects in their cytoskeletal reorganization, adhesion, and function [316]. Furthermore, Rage has been reported to be required for neurite outgrowth in regeneration after nerve injury as pharmacological blockade showed antagonistic effects [317, 318].

Most studies investigating the physiological function of Rage have not considered potential compensatory mechanisms like the upregulation of Toll-like receptors. Small molecule inhibitors targeting RAGE and their application in clinical trials, as for Alzheimer's disease [319], will probably unveil undiscovered tasks of RAGE signaling.

V.2.4.2. Function of RAGE in inflammatory responses

Due to its genetic location within the MHC class III region, a role for RAGE in inflammatory responses has been assumed early. Neighboring genes comprise *TNF-α* as well as several complement components [228, 320]. Further notion came from the analysis of signaling pathways downstream of RAGE that are similarly activated in inflammatory conditions.

Evidence has been provided by comparing Rage$^{-/-}$ and wildtype (wt) mice under different inflammatory settings. Models predominantly inducing adaptive immune responses, such as the induction of enterocolitis or of a delayed type hypersensitivity (DTH), revealed no differences between the two mouse strains. However, settings largely dependent on the innate immunity like the cecal ligation and puncture (CLP) -mediated sepsis showed different patterns. In contrast to wt mice, mice lacking the Rage protein were protected and survived the induced septic challenge [314].

In humans, an increased expression of RAGE has been reported for a diverse set of acute and chronic inflammatory diseases and diseases accompanied with inflammatory conditions, such as psoriasis [321, 322], rheumatoid arthritis [323], atherosclerosis [324], diabetes mellitus [325], Alzheimer's disease (AD) [24], and multiple sclerosis [326]. In general, RAGE

functions *via* inflammation-associated cell recruitment [219], production and secretion of pro-inflammatory cytokines [218, 327], and ROS [328].

The main cause of mortality in late diabetes is its association with sclerotic cardiovascular diseases, leading to heart attacks and strokes [329]. Interestingly, vasculature retrieved from individuals suffering from diabetes showed an enhanced RAGE expression [325]. Indeed, sustained RAGE signaling has been connected with endothelial dysfunction defined by deregulated cytokine secretion and altered membrane composition [330, 331]. In addition, Muhammad and colleagues were able to show that Rage contributes to inflammation and ischemic brain damage as chimeric mice, generated by transplanting Rage$^{-/-}$ bone marrow to wt mice, displayed significantly reduced infarct sizes [332].

Since the major histopathological hallmark of the Alzheimer's disease is the amyloid plaque, consisting of RAGE ligand amyloid-β (Aβ) peptide, a connection between AD pathogenesis and RAGE signaling has been hypothesized [333, 334]. As mentioned above (V.2.1), two independent studies were able to demonstrate a differential expression of RAGE splicing forms in AD. More specifically, higher expression of membrane-bound RAGE and lower levels of soluble forms, which usually impair RAGE signaling due to their function as decoy receptors, were directly associated with neurodegeneration [240, 241]. In fact, sustained RAGE signaling has been demonstrated to mediate blood–brain barrier interruption and neuronal dysfunction by inflammation-associated processes [335, 336].

An elevated AGE and RAGE expression was also found in the hippocampi of multiple sclerosis patients, similar to AD patients [326, 334]. Most interestingly, a recent study was able to demonstrate decreased levels of soluble RAGE in the cerebrospinal fluid of MS patients at clinical onset [337], indicating that alternative splicing is a common mechanism behind the deregulation of RAGE signaling leading to chronic inflammatory processes.

Epidemiologic findings as well as studies on different mouse models have highlighted a strong contribution of chronic inflammation and accompanied tissue remodeling and maladaptation to tumor development [153, 338]. It is now believed that most solid tumors, including melanoma, are surrounded by an inflammatory microenvironment [154]. The role of RAGE in this context as well as other tumor-intrinsic features of RAGE will be described in the next section.

V.2.4.3. Role of RAGE in tumor development, growth, and progression

As described in the last sections, various RAGE isoforms, diverse signaling pathways, as well as differential expression of RAGE modifiers can lead to different cell- and tissue-specific net effects of RAGE signaling. Therefore, findings for one cell type cannot be easily

transferred to another. However, this holds also true for the role of RAGE in tumorigenesis. There are some common patterns, but also cancer-specific differences. In the first part of this section, a general overview will be presented about the role of RAGE in the onset and progression of tumorigenesis, guided by selected examples. In the second part, the impact of RAGE signaling on melanomagenesis will be outlined.

V.2.4.3.1. RAGE: Connecting inflammation and tumorigenesis

The importance of RAGE signaling in tumor development has been recently illustrated by a meta-analysis comprising data of 27 studies. The study by Xia and colleagues revealed that some promoter polymorphisms of RAGE were connected with an either increased or decreased risk of lung cancer. More specifically, the 82G/S polymorphism was associated with significantly increased tumor risk, while the -374T/A polymorphism was linked to reduced lung cancer susceptibility [339]. Another study, investigating oral squamous cell carcinoma (OSCC), correlated the -429T/C polymorphism with increased susceptibility, elevated risk of late-stage and large-size oral tumors [340].

RAGE expression has been detected in a variety of human tumors, such as breast [341], colon [341, 342], gastric [343], lung [344], prostate [345], liver tumors [341], OSCC [346], as well as melanoma [280, 347]. The role of RAGE depends on the different types of tumors and coherent signaling networks. For instance, in some tumors, such as OSCC, RAGE promotes primary tumor growth, but not metastasis formation [346]. In contrast, gastric and prostate cancers upregulate RAGE in terms of invasion to new metastatic sites [343, 345]. In the case of gastric cancer, RAGE expression represents an independent prognostic marker, correlating to histological grade, nodal status, metastasis status, and AJCC stage [348]

Already in the year 2000, Taguchi and colleagues suggested a tumor-promoting role for RAGE. They were able to connect Rage expression with the growth capacity of gliomas and lung carcinomas in xenograft mouse models, as well as in phorbol 12-myristate 13- acetate-inducible papillomas in mice overexpressing *v-Ha-ras* transgene [222].

In 2008, Gebhardt and colleagues provided additional evidence for a role of RAGE in skin carcinogenesis. They were able to demonstrate a higher resistance of Rage$^{-/-}$ mice to chemically-induced skin carcinogenesis compared to wt mice. Besides a lower tumor incidence and lower tumor multiplicities, 12-*O*-tetradecanoylphorbol-13-acetate/7,12-dimethylbenz-[a]-anthracene (TPA/DMBA) treatment revealed hampered inflammatory responses in Rage$^{-/-}$ mice accompanied with decreased levels of pro-inflammatory mediators and epidermal hyperplasia [349], thereby providing evidence for a Rage-driven positive signaling feed-forward loop that creates a tumor-promoting chronic inflammation. In line with the findings for pancreatic cancer [249], and colitis-associated carcinogenesis [342], the

study by Gebhardt *et al.* provided evidence of an impaired infiltration of myeloid precursor cells, implying that Rage signaling also contributes to the recruitment of innate immune cells. Generated bone-marrow chimera proved that Rage expression on immune cells, and not on keratinocytes or endothelial cells, mediated cell recruitment, inflammation, and consequently epidermal hyperplasia [349].

Kang and colleagues investigated the role of RAGE in the pathogenesis of pancreatic tumors and found, that Rage$^{-/-}$ mice were resistant to mutant Kras-induced pancreatic tumorigenesis [350]. Investigating the mechanism behind the RAGE-dependency, they demonstrated that cytosolic RAGE directly induces tumor growth survival by altering bioenergetics of tumor cells. Indeed, HMGB1-induced phosphorylation of RAGE leads to its mitochondrial translocation, where it stimulates ATP production [249]. Furthermore, they observed that RAGE can protect pancreatic tumor cells from ROS-induced cell damage [351], as well as cell damage by chemotherapy-induced genotoxic stress in an autophagy-dependent manner. shRNA-mediated interference was able to abolish the ATP production as well as its pro-survival effects on murine pancreatic tumor cells *in vivo* as demonstrated by the analysis of apoptosis marker. Autophagy-mediated pro-survival effects have not only been demonstrated for pancreatic but also for gastric cancer [352]. Beside these tumor cell-intrinsic effects, a decreased infiltration of CD11b-positive inflammatory cells was observed in the microenvironment of tumors with impaired Hmgb1/Rage axis. Comparing normal tumor growth between wt and Rage$^{-/-}$ mice further demonstrated that also Rage on stroma cells has a tumor-promoting function, as Rage$^{-/-}$ mice displayed significantly decreased tumor growth and ATP production [249]. In line with this finding, Turovskaya and colleagues demonstrated a resistance of Rage$^{-/-}$ mice to colitis-associated carcinogenesis (CAC) partly caused by the inability of Rage$^{-/-}$ mice to sustain a tumor-promoting chronic inflammation. Indeed, they found a decreased number of infiltrating myeloid precursor cells [342].

Most data suggest that RAGE is commonly overexpressed in most types of solid tumors. This is in sharp contrast to the situation found in the lung, where RAGE is highly expressed in healthy tissue but downregulated in non-small cell lung carcinomas (NSCLCs), squamous cell lung carcinomas, adenocarcinomas, as well as in benign lung hamartomas [312, 313]. This opposite direction highly suggests an involvement of RAGE in the well-functioning of lung cells. Comparable results have been reported for rhabdomyosarcoma, which is a highly malignant tumor of skeletal muscle origin, where RAGE expression also resulted in a more benign phenotype with reduced proliferation, migration, and invasiveness [353].

As explained in section V.2.3 there are various possibilities explaining these tissue-specific differences in RAGE signaling. In terms of tumor development, the study by Jules and colleagues highlighted an important explanation. They were able to show that distinct RAGE

isoforms differentially affect tumor cell properties, such as migration, invasion, adhesion and viability in C6 glioma cells [354]. This illustrates the importance of investigating the role of RAGE and its isoforms specifically in the growth and progression of malignant melanoma. Therefore, the next section addresses effects of RAGE on melanomagenesis.

V.2.4.3.2. RAGE signaling and it impacts onto the pathogenesis of malignant melanoma

Already in 1999, Masaki and colleagues suggested that oxidative stress-induced formation of advanced glycation end products (AGE) might be involved in melanomagenesis [355]. Indeed, the administration of AGEs has been shown to successfully induce melanoma growth, migration and invasion *in vitro* [356]. Furthermore, *in vivo* evidence for a role of AGEs has been provided by the fact that administration of a DNA aptamer directed against AGEs (AGE-aptamer) significantly decreased melanoma growth in a xenograft mouse model [357]. As mentioned before (V.2.2), melanoma cells have also been shown to express other RAGE ligands, such as members of the S100 family [164] and HMGB1 [262]. Most importantly, expression of these ligands have been often directly connected to melanoma onset and progression [262, 279].

Not only ligands for RAGE but also the receptor itself might play a role in the pathogenesis of melanoma as indicated by the detection of RAGE in melanoma tissue [347]. In fact, the application of an anti-RAGE blocking antibody has been shown to abolish the tumor-promoting effects of AGE stimulation. Applying xenograft transplantation models, similar effects of anti-RAGE antibodies on melanoma growth have been demonstrated *in vivo*. More specifically, they showed that upon subcutaneous injection of melanoma cells athymic mice showed a two - fold reduction in tumor size by intraperitoneally-administered anti-RAGE antibodies compared to IgG-treatment. Histological analysis of harvested tumor tissues did not reveal any differences in vascularization [356]. In contrast, the impaired tumor growth induced by application of an AGE-aptamer was associated with a significantly reduced angiogenesis [357]. However, if the observed *in vivo* effects have been mediated by tumor cells or by surrounding stroma cells could not be addressed in these settings.

Recent studies tried to get deeper insights into the tumor-cell intrinsic role of RAGE in melanoma. For instance, Meghnani and colleagues overexpressed one human melanoma cell line with RAGE and studied accompanied effects. They found characteristics of an EMT-like process, such as mesenchymal-like morphologies, higher migration abilities and reduced proliferation properties. The morphological and functional alterations have been accompanied with a further upregulation of the RAGE ligand S100B and downregulation of P53, ERK1/2, cyclin E and NF-κB [358]. The fact that melanoma cells usually depend on a

sustained MAPK and NF-κB activation, as well as the experimental set up in this analysis, focusing on a single melanoma cell line, requires additional experiments in order to clarify if these findings are cell-type or melanoma-specific. When implanting the RAGE overexpressing melanoma cells into mice, they reported an increased tumor growth compared to control cells, which could be partly reversed when mice were additionally treated with anti-RAGE antibodies [359]. Another study tried to get more insights into tumor-cell intrinsic functions of RAGE by RNAi-mediated RAGE silencing. Using two different human melanoma cell lines they found conflicting results regarding the influence of RAGE onto cell migration. Since differences regarding the oligomerization state of RAGE on the cell surface between the two cell lines were noted, differential RAGE isoform expression and subcellular localization were claimed to be important determinants for the regulation of its function in tumor progression [360]. Indeed, Leclerc and colleagues could demonstrate a differential expression of fl-RAGE and sRAGE in melanoma. They found fl-RAGE to be upregulated between stage III and stage IV tumors, whereas sRAGE showed an inverse correlation [280]. Recently, our group was able to demonstrate that diminished sRAGE and esRAGE levels are indeed prognostic marker for malignant melanoma [361].

Beside the findings of the few functional studies, the tumor-cell-intrinsic role of RAGE in melanoma and its impact on the ‘melanoma hallmarks’ remains unclear. In this study, different experimental approaches were used, such as RAGE overexpression, RNAi-mediated interference of RAGE in murine and human melanoma cell lines, and induction of genotoxic stress, to clarify unsolved questions. These approaches as well as chosen read-out systems are described in the next section.

VI. Material and Methods

VI.1. Materials

Reagents and kits	Company	Catalog #
20 % sodium dodecyl sulfate (SDS)	G-Biosciences	786016
2- [4 - (2 – hydroxyethyl) piperazin-1- yl] ethanesulfonic acid (HEPES)	Carl Roth	HN78.1
2-(4-aminophenyl)-1H-indole-6-carboxamidine (DAPI)	Roche Diagnostics	10236276001
5-(6)-carboxyfluorescein diacetate succinimidyl ester (CSFE)	affymetrix	650850
7-aminoactinomycin (7-AAD) viability staining solution	affymetrix	699350
AlamarBlue®	Invitrogen	DAL1100
Albumin fraction V	Carl Roth	8076
Amersham ECL prime western blotting detection reagent	GE Healthcare	RPN2232
Ammonium persulfate solution (APS)	Carl Roth	9592
Calcium chloride ($CaCl_2$)	Carl Roth	CN93.1
Complete mini protease inhibitor cocktail	Roche Diagnostics	04693159001
Cultrex® BME cell invasion assay	TREVIGEN	3455096K
Dako antibody diluent	Dako	S0809
Dako fluorescent mounting medium	Dako	S302380-2
Dako peroxidase block solution	Dako	S2023
DCFDA - cellular reactive oxygen species detection assay kit	abcam	ab113851
Endofree plasmid maxi kit	QIAGEN	12362
Ethylene diamine tetraacetic acid (EDTA)	Gerbu	1034
Glycerine	Carl Roth	3783.1

HIER citrate buffer	ZYTOMED SYSTEMS	ZUC028
Hoechst 33342	Thermo Scientific	62249
Immobilion PVDF membrane pore size 0.45 µm	Merck Millipore	IPVH00010
Methanol	Sigma-Aldrich	32213
Phosphate buffered saline (PBS)	Biochrom	L182-50
Pierce BCA protein assay kit	Thermo Scientific	23225
Potassium chloride (KCl)	Carl Roth	6781.3
RevertAid first strand cDNA synthesis kit	Thermo Scientific	K1622
RNase-free DNase set	QIAGEN	79254
RNeasy mini kit	QIAGEN	74106
Rotiphorese® gel 30	Carl Roth	3029
Skim milk powder	Sigma-Aldrich	70166
Sodium chloride (NaCl)	Sigma-Aldrich	31434
SYBR Green PCR master mix	Applied Biosystems	4309155
Tetramethylethylenediamine (TEMED)	Carl Roth	2367
Triton® X 100	Carl Roth	3051
Tween® 20	Applichem	A1389
Vybrant Violet DyeCycle	Invitrogen	V35003

Table 1 Reagents and kits

Cell culture reagents	Company	Catalog #
2-Mercaptoethanol	Gibco® Life Technologies	31350-010
Corning™ cell scraper	Sigma-Aldrich	CLS3010
Dimethylsulfoxide (DMSO)	Carl Roth	A994
DMEM AQmedia™	Sigma-Aldrich	D0819
Dulbecco's phosphate buffered saline	Sigma-Aldrich	D8537
Fetal calf serum (FCS)	Biochrom	S0415

Human melanocyte growth supplement (HMGS) 100x	Gibco® Life Technologies	S0025
Lipofectamine® LTX reagent	Life Technologies	15338100
Lipofectamine® RNAiMAX transfection reagent	Life Technologies	13778075
Medium 254	Gibco® Life Technologies	M254500
Mission® lentiviral transduction particles	Sigma-Aldrich	SHCLNV
Non-essential amino acids (NEAA)	Sigma-Aldrich	M7145
Opti-MEM® I reduced serum medium	Gibco® Life Technologies	31985062
Penicillin-Streptomycin	Sigma-Aldrich	P4333
Stealth RNAi™ siRNA negative control, med GC	Life Technologies	12935300
Stealth RNAi™ siRNA targeting ager mRNA	Life Technologies	1299001
Trypsin-EDTA solution	Sigma-Aldrich	T3924

Table 2 Cell culture reagents

Inhibitors	Company	Catalog #
Doxorubicin	Sigma-Aldrich	D1515
Leptomycin B (LMB)	Cayman	10004976
Mitomycin C	Carl Roth	4150
Z VAD FMK	Invivogen	tlrl-vad

Table 3 Inhibitors

Antibodies	Company	Catalog #
Primary Antibodies		
Alexa Fluor 488 Annexin V	Life Technologies	A13201
Isotype rabbit IgG	Dianova	DLN13124

Mouse-anti-RAGE	abcam	ab54641
Rabbit-anti-Histone 3	New England Biolabs	5192
Rabbit-anti-RAGE	abcam	ab37647
Rabbit-anti-RAGE	SantaCruz	sc5563
Rabbit-anti-βACTIN/βActin	Cell Signaling Technology	mAb5125
Rabbit-anti-βCATENIN	Cell Signaling Technology	mAb9582
Secondary Antibodies		
Goat-anti-rabbit Cy3	Dianova	111165045
Goat-anti-rabbit HRP	New England Biolabs	7074
Anti-mouse EnVision™ HRP AEC+	Dako	K400511-2
Anti-rabbit EnVision™ HRP AEC+	Dako	K400911-2

Table 4 Antibodies

Analysis software	Source
7500 Software v2.0.5	Applied Bioscience
BD FACSDiva™	Biolegend
CELLO	http://cello.life.nctu.edu.tw/; [362]
cNLS Mapper	http://nls-mapper.iab.keio.ac.jp/cgi-bin/NLS_Mapper_form.cgi; [363]
FlowJo 7.2.2.	FlowJo
GraphPad Prism 5	GraphPad Prism
iControl 1.10©2012	TECAN
ImageJ	National Institute of Health (NIH)
NDP.view2	Hamamatsu Photonics K.K.
NetNES	http://www.cbs.dtu.dk/services/NetNES/; [364]
NetNGlyc 1.0	http://www.cbs.dtu.dk/services/NetNGlyc/; [365]

NetOGlyc 3.1	http://www.cbs.dtu.dk/services/NetOGlyc/; [366]
NetPhos 2.0	http://www.cbs.dtu.dk/services/NetPhos/; [367]
NetPhosK 1.0	http://www.cbs.dtu.dk/services/NetPhosK/; [368]
NIS-Elements Viewer	Nikon
NLStradamus	http://www.mosesweb.csb.utoronto.ca/NLStradamus/; [369]
NucPred	http://www.sbc.su.se/~maccallr/nucpred/cgi-bin/single.cgi; [370]
SignalP 3.0	http://www.cbs.dtu.dk/services/SignalP-3.0/; [371]

Table 5 Analysis software

Devices	Company
AB 7500 Real Time PCR machine	Applied Biosciences
ImageQuant LAS biomolecular imager	GE Healthcare
NanoDrop ND-1000 Spectrophotometer	Peqlab Biotechnologie GmbH
Nikon Eclipse Ti Fluorescence microscope	Nikon
TECAN infinite F200 pro microplate reader	TECAN
Stratagene Stratalinker UV Crosslinker 2400	Stratagene
FACS Canto™ II	BD Bioscience

Table 6 Devices

Buffer solutions	
Tris buffered saline (TBS) pH 7.6	Running buffer pH 8.3
137 mM NaCl	25 mM Tris
20 mM Tris	190 mM glycine
	0.1 % SDS

Transfer buffer pH 8.3	Washing buffer (WB) pH 7.6
25 mM Tris	TBS
190 mM glycine	0.02 % Tween® 20
20 % methanol	
Laemmli 4x buffer pH 6.8	Cell lysis buffer for protein isolation
2 % SDS	1x cOmplete mini protease inhibitor cocktail
10 % glycerol	1 % Triton® X 100
1 % 2-mercaptoethanol	in TBS
0.02 % bromophenol blue	
12.5 mM EDTA	
0.05 M Tris HCl	
Washing buffer (IF) pH 7.6	Annexin binding buffer pH 7.4
TBS	10 mM HEPES
0.05 % Tween® 20	140 mM NaCl
	2.5 mM $CaCl_2$

Table 7 Buffer solutions

VI.2. Methods

VI.2.1. Tissue microarray

All analyses involving primary human material were performed in accordance with the Ethics Committee II of the University of Heidelberg. The tissue microarray (TMA) used in this study contained 13, 27 primary melanomas and 37 melanoma metastases samples, and was generated at the Tissue Bank of the National Center for Tumor Diseases (NCT), Department of Pathology, University Hospital Heidelberg. Characteristics and clinical parameters of patients whose samples were enclosed in the TMA analysis are illustrated in Table 8.

		TMA 1		TMA 2	
TMA characteristics		n		n	
TMA Spots	No. of spots	52		90	
Patients	No. of patients	19		20	
Clinicopathological characteristics		n	%	n	%
Age	Mean [years (range)]	62.5 (43-81)		62.1 (50-84)	
Sex	Male	12	63.2		
	Female	7	36.8		
Histology	Melanoma	16	100.0	11	100.0
	SSM	7	43.8	0	0
	NMM	5	31.2	4	36.4
	LMM	0	0	1	9.1
	ALM	1	6.2	1	9.1
	not classifiable	3	18.8	5	45.4
Ulceration	No	11	68.8	8	72.7
	Yes	5	31.2	3	27.3
Histology	Nevi	13	100.0	0	0
	compound	9	69.2		
	junctional	1	7.7		

	lentiginous	0	0		
	Dermal	3	23.1		
	Nevus bleu	0	0		
	not classifiable	0	0		
Histology	Metastases	0	0	37	100.0
	Loco-regional			37	100
	sub-/cutaneous			20	54
	lymph-node			17	46

Abbreviations: SSM, superficial spreading melanoma; NMM, nodular melanoma; LMM, lentigo maligna melanoma; ALM, acro-lentiginous melanoma.

*Tumor classification was performed according to the 2009 AJCC melanoma staging system of the American Joint Committee on Cancer.

Table 8 Characteristics and clinical parameters of melanoma patients enclosed in this study

The TMA slides contain each tissue sample in duplicates and were stained with specific anti-RAGE antibody (ab37647, abcam) overnight at 4 °C according to the immunohistochemistry protocol. The samples were stabilized with mounting medium (Dako), and scanned with the help of the Tissue Bank of the National Center for Tumor Diseases (NCT). Applying the NanoZoomer software NDP.view2 (Hamamatsu Photonics K.K.) two blinded individuals visually scored TMAs according to a quantity/intensity-based IHC scoring system.

Intensity was scored as 0 = negative, 1 = weak, 2 = moderate, and 3 = high; percentage was scored as 0 = 0 %, 1 = 1 – 25 %, 2 = 26 – 50 %, 3 = 51 – 75 %, 4 = 76 – 100 %).

In addition, the intracellular distribution of RAGE protein (nuclear or cytosolic only, as well as predominant nuclear or cytosolic) was analyzed on a percentage basis.

VI.2.2. Cell culture

All cells used in this study were cultivated at 37 °C in a humidified chamber with an atmosphere of 5 % CO_2 and have been routinely tested for mycoplasma. Cells were subcultured before reaching 90 % confluence using a 0.025 % to 0.5 % trypsin solution. Cells and cell lines used in this study are listed in section VI.2.2.1, while their individual culture conditions can be found in the paragraphs VI.2.2.2 and VI.2.2.3.

VI.2.2.1. Cell lines

Cell line	Mutational status		Reference
Human melanoma cell lines	BRAF status	NRAS status	
Skmel 23	wt	wt	[372]
Skmel 173	wt	Q61K	[373]
C32	V600E	wt	[372]
WM2664	wt	wt	[372]
A375	V600E	wt	[372]
HT144	V600E	wt	[372]
MeWo	wt	wt	[374]
Skmel 147	wt	Q61R	[372]
Human melanocytic cell line	Mutational status		
MelSTV	hTERT introduction, disruption of P53 & RB activity by introducing SV40 early region		[375]
Murine melanoma cell line	Background	Notes	
B16F10	C57BL/6	Derived from spontaneous melanoma from DMBA treated backskin of C57BL/6 mice	[376]

Table 9 Cell lines

VI.2.2.2. Cell culture of immortalized melanocytes and tumor cells

Human and murine tumor cell lines as well as the immortalized melanocyte cell line MelSTV were cultivated in Dulbecco's Modified Eagle Medium (DMEM) containing 4,500 mg/l glucose and 4 mM L-alanyl-L-glutamine supplemented with 10 % heat-inactivated fetal bovine serum (FCS), 1 % 100X non-essential amino acids (NEAA), 100 units/ml penicillin, 100 µg/ml streptomycin and 0.1 mM 2-mercaptoethanol, from here on referred as MEF medium.

VI.2.2.3. Cell culture of primary melanocytes

Primary normal human melanocytes (NHM) obtained from foreskins were kindly provided by Dr. Uysal, Mannheim. NHM were cultured in Medium 254 (Gibco® Life Technologies) supplemented with 1 % 100x human melanocyte growth supplement (HMGS) resulting in a final concentration of 0.2 % bovine pituitary extract, 0.5 % fetal bovine serum, 1 µg/ml recombinant human insulin-like growth factor-I, 5 µg/ml bovine transferrin, 3 ng/ml basic fibroblast growth factor (bFGF), 0.18 µg/ml hydrocortisone, 3 µg/ml heparin and 10 ng/ml phorbol 12-myristate 13-acetate.

VI.2.2.4. UV irradiation

UV irradiation of cells was performed applying the Stratagene's Stratalinker UV-Crosslinker. Cell culture plates without lids were irradiated with either 10 or 50 J/m^2.

VI.2.2.5. Inhibitors

Inhibitor	Target	Mechanism of Action	Resolvent
Doxorubicin	DNA topoisomerase type II	Two different mechanisms: (1) Blocking DNA synthesis and transcription by DNA intercalation; (2) Inhibition of topoisomerase type II leading to breaks in the genomic DNA.	DMSO
Leptomycin B (LMB)	CRM-1/XPO	Covalent modification of Cys528 in the central conserved region of CRM-1 preventing the binding to the cargo protein NES	Ethanol
Mitomycin C (MTC)	5′-CpG-3′	Alkylating agent forming crosslinks between complementary strands of DNA leading to the inhibition of DNA replication	H_2O
Z VAD FMK	Caspases	Irreversibly binds to the catalytic site of caspase proteases	DMSO

Table 10 Characteristics of applied inhibitors

Aliquots of the inhibitor (Table 10) solutions were stored at -20 °C and applied in MEF media at the indicated concentrations: Leptomycin B, 4 nM; Mitomycin C, 0.25 µg/ml; Z VAD FMK, 20 µM; Doxorubicin, 100 nM. Control cells were treated with media containing the same amount of resolvent but without compound.

VI.2.3. Transformation and plasmid isolation

To introduce the plasmid of interest into competent Dh5α E.coli cells, plasmid DNA was mixed with chilled cells, incubated on ice for 30 min, and briefly heated to 42 °C (90 s). After a resting phase on ice for 2 minutes 500 µl LB media were added and bacteria were shaked for 60 minutes at 37 °C. Transformed bacteria were plated on pre-warmed LB agar plates with 100 µg/ml ampicillin for selection and incubated overnight at 37 °C. Single colonies were manually picked and transferred to sterile culture tubes containing 5 ml LB media supplemented with 100 µg/ml ampicillin and incubated overnight at 37 °C. Plasmid DNA was isolated using the QIAGEN Plasmid Purification Mini Kit according to the manufacturer's protocol. The amplification of the plasmid of interest was confirmed by restriction digestion and sequencing. Sterile Erlenmeyer flasks containing 200 ml ampicillin-supplemented LB media were inoculated with bacteria containing verified plasmids and were incubated at 37 °C overnight in an orbital shaker. Bacteria were then pelleted, lysed and the plasmid DNA was purified using the EndoFree® QIAGEN Plasmid Purification Maxi Kit according to the manufacturer's protocol. After isopropanol/ethanol precipitation air-dried plasmid DNA was solved in endogen-free water and analyzed using a NanoDrop ND-1000 spectrophotometer for quality and quantity.

VI.2.4. Transfection and transduction

Prior to transfection and transduction cells were seeded at distinct concentrations resulting in a cell density of 60 – 80 % on the day of transfection/transduction.

VI.2.4.1. RAGE overexpression in immortalized human melanocytes and melanoma Cells

Gain-of-function experiments with immortalized human melanocyte and melanoma cell lines were performed using pcDNA3.1., containing a G418 resistance gene as an empty vector control, and, when additionally containing full-length RAGE (HM-310, HMGBiotech), as overexpression construct (RAGE OE). Prior to transfection 5 x 10^4 cells per 24 well were seeded in MEF medium and incubated overnight at 37 °C (5 % CO_2). Using Lipofectamine® LTX cells were transfected with 0.5 µg DNA per well according to the manufacturer's protocol and cultivated for 24 hours.

Cells were then passaged at a one to ten ratio and after 48 hours of incubation with MEF medium at 37 °C (5 % CO_2) selected with MEF medium containing defined G418 concentrations optimized for each cell line. Optimal selection concentrations were defined as the minimal antibiotic concentration sufficient to kill all cells after one week (Table 11). For

long-term culture, the G418 concentration was reduced to 50 % of the optimized selection concentration.

Human melanocytic or melanoma cell line	G418 selection concentration
MelSTV	800 µg/ml
A375	1000 µg/ml
MeWo	1000 µg/ml

Table 11 G418 concentrations for selection

VI.2.4.2. siRNA-mediated reversion of RAGE overexpression effects

For transient knockdown 1 x 10^5 RAGE OE or control cells were seeded in 6 wells and, after proper attachment, transfected with Lipofectamine RNAiMAX and 25 pmol Stealth RNAi™ siRNA targeting RAGE or 25 pmol Stealth RNAi™ siRNA negative control with a medium GC content diluted in Opti-MEM® I Reduced Serum Medium according to manufacturer's protocol. After another 48 hours of incubation at 37 °C (5 % CO_2) cells were validated, and upon successful verification of the knockdown used for functional assays. Due to the transient character of the siRNA-mediated knockdown all functional assays were performed within 5 days after transfection.

VI.2.4.3. shRNA-mediated, stable Rage knockdown in murine B16F10 melanoma cells using lentiviral particles

Murine B16F10 melanoma cells were seeded in MEF medium at a concentration of 1 x 10^4 cells per 96 well and incubated overnight at 37 °C (5 % CO_2). On the day of transduction the medium was exchanged with MEF medium containing hexadimethrine bromide (Polybrene) at a final concentration of 8 µg/ml. MISSION® Lentiviral Transduction Particles containing shRNA targeting the mRNA encoding for RAGE (TRCN0000071743, 1.2 x 10^7 Transducing Units (TU)/ml; TRCN0000071744, 1.1 x 10^7 TU/ml; TRCN0000071745, 8.4 x 10^6 TU/ml; TRCN0000071746, 1 x 10^7 TU/ml; TRCN0000071747, 1.8 x 10^7 TU/ml) as well as MISSION® Lentiviral Transduction Particles containing non-targeting shRNA (2.8 x 10^7 TU/ml) were added to the cells at desired multiplicity of infection (MOI). The plate was gently shaked to ensure proper mixing and incubated for 20 hours at 37 °C (5 % CO_2). The next day medium was exchanged with fresh MEF medium. After another 24 hours of incubation at 37 °C (5 % CO_2) cells were selected with 1 µg puromycin per ml, which was the minimal concentration killing all cells after one week of selection. After the identification of resistant colonies, clones were picked and expanded. For long-term culture, the puromycin

concentration was reduced to 50 % of the optimized selection concentration. Until clones were picked all steps were performed according to the safety class two requirements.

VI.2.5. RNA isolation and reverse transcription

RNA extraction was performed using the RNeasy Mini Kit (QIAGEN) according to manufacturer's instructions. Briefly, pelleted cells were dissolved using RLT lysis buffer containing 1 % 2-mercaptoethanol followed by RNA extraction using a column-based purification. Every sample was DNase I-treated for 15 minutes at room temperature followed by two washing steps and the elution in RNase-free H_2O.

RNA concentration and quality was measured using a NanoDrop ND-1000 spectrophotometer. Samples fulfilling the quality recommendations (260 nm/ 280 nm ratio: 2.0 +/- 0.2; 260 nm/ 230nm ratio: 2.0 + 0.2) were further processed.

500 ng RNA of each sample were then used for cDNA generation. In brief, RNA and non-template controls were incubated with oligo $(dT)_{18}$ primers in a volume of 12 µl for five minutes at 65 °C. Reverse transcription was performed using the RevertAid First Strand cDNA Synthesis Kit according to the manufacturer's protocol. As control for successful removal of genomic DNA within the samples also reactions without reverse transcriptase were performed. Before use cDNA was diluted at a one to five ratio in nuclease-free H_2O resulting in a concentration of 5 ng/µl.

VI.2.6. Quantitative real-time polymerase chain reaction (qPCR)

VI.2.6.1. Standard qPCR Analysis

qPCR was performed using 2x SYBR Green PCR master mix and an Applied Biosystems 7500 Real-Time PCR System. In each qPCR experiment 12.5 ng cDNA per sample were applied and amended by a non-template control as well as minus-reverse-transcriptase controls to monitor the quality of the assay. All primers used in this study show an efficiency within the range of 85 – 110 % as analyzed by cDNA dilution curves.

After testing all samples for low variances of housekeeping gene expression (< 2 cycles) the results of human targets were normalized to *18S*, *βACTIN*, or both, and for murine targets to *Hprt*, *Gapdh*, or both. All samples were analyzed in triplicates and gene quantification was calculated using the Pfaffl method calculating the delta-delta Ct (ΔΔCt) [377]. Statistical analysis was carried out in Excel and visualization of graphs in GraphPad Prism 5. Primers used in this study are listed in Table 12.

	Forward primer	Reverse primer
Human Primer		
Hs_Ager	*CCAGCCCGGGGAGGAGAT*	*GAAGGGGCAAGGGCACACCAT*
Hs_18S	*GAGGATGAGGTGGAAACGTGT*	*TCTTCAGTCGCTCCAGGTCT*
Hs_βACTIN	*GGATGCCACAGGATTCCATACCCA*	*TCACCCACACTGTGCCGATCTACGA*
Hs_HMGB1	*CTAAGAAGTGCTCAGAGAGGTG*	*GGAAGAAGGCCGAAGGAG*
Murine Primer		
Mm_Ager	*TGGGCAGAGATGGCACAGGT*	*AGCTGGCACTTAGATGGGAAACTT*
Mm_Hprt	*CAGCCATTGCAGTACATTGAG*	*TTTTGCCTCTCGGCTTTTTA*
Mm-Gapdh	*AGGTCGGTGTGAACGGATTTG*	*TGTAGACCATGTAGTTGAGGTCA*

Table 12 qPCR primer

VI.2.6.2. Profiling changes in 'in trans' molecules mediated by RAGE overexpression or Rage knockdown

The applied RT² Profiler™ Human and Mouse DNA Damage Signaling Pathway PCR Array allows the simultaneous monitoring of 79 DNA damage signaling-related genes, five house-keeping genes, as well as reverse transcriptase- and positive controls.

Relevant genes out of following signaling pathways were analyzed and normalized to two house-keeping genes (human: *βACTIN*, *RPLO*; mouse: *βActin*, *Hsp90ab1*): ATM/ATR signaling, nucleotide excision repair (NER), base excision repair (BER), mismatch repair (MMR), double-strand break repair (DSB), other DNA repair genes, apoptosis, and cell cycle. Abbreviations for all genes are listed in Table 13.

The average correlation coefficients of these arrays is higher than 0.99, ensuring reliable detection of differences in the expression between biological samples. cDNA from RAGE gain-of-function (A375 pcDNA3.1. vs A375 RAGE OE; human) and loss-of-function studies (B16F10 Ctrl Kd vs. B16F10 RAGE Kd; mouse) served as biological samples in these assays. The arrays were performed using 2x SYBR Green PCR Master Mix and an Applied Biosystems 7500 Real-Time PCR System according manufacturer's protocol.

RT² Profiler™ DNA Damage Signaling Pathway PCR array	
Pathway	Genes
Human Profiler	
ATM / ATR	*ATM, ATR, ATRIP, BARD1, BRCA1, CDC25A, CHEK1, CHEK2, CSNK2A2, FANCD2, H2AFX, HUS1, MDC1, PARP1, RAD1, RAD17, RAD50, RAD9A, RBBP8, RNF168, RNF8, SMC1A, TOPBP1, TP53.*
NER	*CDK7, DDB1, DDB2, ERCC1, ERCC2, LIG1, NTHL1, OGG1, PCNA, PNKP, RPA1, SIRT1, TP53, XPA, XPC.*
BER	*APEX1, FEN1, LIG1, MBD4, MPG, NTHL1, OGG1, PARP1, PCNA, TP53, UNG, XRCC1.*
MMR	*ABL1, EXO1, MLH1, MLH3, MSH2, MSH3, PCNA, PMS1, PMS2, TP73.*
DSB Repair	*ATM, BLM, BRCA1, CHEK1, H2AFX, HUS1, LIG1, MDC1, MLH1, MRE11A, NBN, PRKDC, RAD50, RAD51, RPA1, TP53BP1, XRCC2, XRCC6.*
Other DNA Repair	*ATR, ATRIP, ATRX, BARD1, BRIP1, CHEK2, CIB1, CRY1, FANCA, FANCD2, FANCG, GADD45A, GADD45G, RAD1, RAD17, RAD18, RAD21, RAD51B, RAD9A, RBBP8, REV1, RNF168, RNF8, SMC1A, SUMO1, TOPBP1, XRCC3.*
Apoptosis	*ABL1, ATM, BARD1, BAX, BBC3, BRCA1, CDKN1A, CHEK2 (RAD53), CIB1, CSNK2A2, PPP1R15A, PRKDC, RAD21, RAD9A, SIRT1, TP53, TP73.*
Cell Cycle	*ATM, ATR, ATRIP, CDC25A, CDC25C, CDK7, CDKN1A, CHEK1, CHEK2 (RAD53), DDIT3, MAPK12, MCPH1, MDC1, PPM1D, PPP1R15A (GADD34), TP53, TP73.*

Murine Profiler	
ATM / ATR	*Atm, Atr, Brca1, Cdc25a, Chek1, Chek2, Fancd2, H2afx, Hus1, Mdc1, Parp1, Parp2, Rad1, Rad17, Rad50, Rad9a, Rnf8, Smc1a, Topbp1, Trp53.*
NER	*Brca2, Ddb2, Dclre1a, Ercc1, Ercc2, Fancc, Lig1, Nthl1, Ogg1, Pcna, Pole, Rpa1, Trp53, Xpa, Xpc.*
BER	*Apex1, Fen1, Lig1, Mbd4, Mpg, Nthl1, Ogg1, Parp1, Parp2, Pcna, Pole, Trp53, Ung, Xrcc1, Wrn.*
MMR	*Abl1, Exo1, Mlh1, Mlh3, Msh2, Msh3, Pcna, Pms2.*
DSB Repair	*Atm, Blm, Brca1, Brca2, Chek1, H2afx, Hus1, Lig1, Mdc1, Mlh1, Mre11a, Nbn, Prkdc, Rad50, Rad51, Rad52, Rpa1, Trp53bp1, Xrcc2, Xrcc6.*
Other DNA Repair	*Atr, Atrx, Brip1, Chek2, Fanca, Fancd2, Fancg, Gadd45a, Gadd45g, Mgmt, Polh, Poli, Pttg1, Rad1, Rad17, Rad18, Rad21, Rad51c, Rad51b, Rad9a, Rev1, Rnf8, Smc1a, Smc3, Sumo1, Topbp1, Xrcc3.*
Apoptosis	*Abl1, Atm, Bax, Brca1, Cdkn1a, Chek2, Ppp1r15a, Prkdc, Rad21, Rad9a, Terf1, Trp53.*
Cell Cycle	*Atm, Atr, Cdc25a, Cdc25c, Cdkn1a, Chek1, Chek2, Ddit3, Mcph1, Mdc1, Mif, Ppm1d, Ppp1r15a, Terf1, Trp53.*

Table 13 Genes encoding for *in trans* molecules involved in the regulation of genomic integrity, and analyzed by RT² Profiler™

VI.2.7. Immunoblotting

Cells used for protein extraction were harvested before reaching 90 % confluence using ice-cold PBS and Corning® cell scrapers. For cell fractionation experiments cells were incubated with MEF medium containing Leptomycin B (4 nM), or resolvent only for 24 hours in humidified atmosphere at 37 °C prior to cell lysis.

VI.2.7.1. Generation of total cell lysates

For the extraction of proteins cells were washed twice with ice-cold PBS and lysed with TBS supplemented with 1 % Triton X-100 and Roche cOmplete mini protease inhibitor cocktail. All steps were performed at 4 °C. Protein yield was then measured using the Thermo Scientific™ Pierce™ BCA method.

VI.2.7.2. Generation of cell fractions

For the extraction of proteins from different specific cellular compartments the Thermo Scientific subcellular protein fractionation kit was applied according to the manufacturer's protocol.

Four different extraction buffers supplemented with Thermo Scientific Halt protease inhibitor cocktail enable the extraction of proteins from distinct compartments. Briefly, the first extraction buffer selectively permeabilizes the cell membrane, thereby releasing soluble cytoplasmic contents. The second extraction buffer solubilizes membranes of plasma, mitochondria and ER-golgi but does not affect nuclear membranes. In the next step intact nuclei were isolated *via* centrifugation and treated with the third extraction buffer leading to the release of soluble nuclear extract. Supplementation of the third extraction buffer with micrococcal nuclease in an additional extraction step isolates chromatin-bound nuclear proteins. The remaining insoluble pellet was then treated with the fourth extraction buffer, thereby isolating cytoskeletal proteins. All steps were performed at 4 °C. Protein yield was then measured using the Thermo Scientific™ Pierce™ BCA method.

VI.2.7.3. Western Blot

Under denaturating conditions 30 µg protein were separated on self-made 12 % Tris/glycine SDS-polyacrylamide gels according to the scheme below (Table 14).

Proteins were transferred onto methanol-activated polyvinylidene difluoride (PVDF) membranes with 60 V for 2 hours at 4 °C. Unspecific binding was blocked by incubating the membrane with 5 % non-fat dried milk in TBST (TBS supplemented with 0.02 % Tween-20) for 1 hour at room temperature. Primary antibodies were diluted in TBST containing 5 % BSA or non-fat dried milk according to the manufacturer's protocol: rabbit anti-RAGE (ab37647;

abcam), 1 : 1,000; rabbit anti-RAGE (H300, SantaCruz), 1 : 1,000; rabbit anti-HISTONE 3 (sc-10809, SantaCruz), 1 : 1,000; rabbit anti-β-CATENIN (sc-7199, SantaCruz), 1 : 10,000. After incubation with the primary antibodies overnight at 4 °C, membranes were washed three times in TBST and incubated with secondary antibodies against rabbit IgG labeled with horseradish peroxidase diluted (1 : 10,000) in TBST containing 5 % non-fat dried milk in TBST at room temperature for 2 h. After washing three times with TBST, signals were visualized using ECL™ Western Blotting Detection Reagents (GE Healthcare) and the ImageQuant LAS biomolecular imager. Protein quantification was performed using ImageJ.

Resolving gel		Stacking gel	
3.3 ml	H_2O	3.40 ml	H_2O
3.0 ml	30 % acrylamide/bisacrylamide	0.83 ml	30 % acrylamide/bisacrylamide
2.5 ml	1.5 M Tris pH 8.8	0.63 ml	1 M Tris pH 6.8
100 µl	10 % SDS	50 µl	10 % SDS
100 µl	10 % ammonium persulfate (APS)	50 µl	10 % ammonium persulfate (APS)
20 µl	tetramethylenediamine (TEMED)	5 µl	tetramethylenediamine (TEMED)

Table 14 SDS-Gel preparation

VI.2.8. Immunofluorescence

Human melanocytic and melanoma cell lines were seeded into Lab-Tek® Chamber Slides™. After proper attachment cells were starved in FCS-free MEF medium overnight. Surface and nuclear staining was performed according to the protocol published in Nature Methods [378]. Briefly, cells for nuclear staining were fixed in 4 % paraformaldehyde (PFA) for 5 min on ice and 10 min on room temperature followed by a treatment with 100 % methanol for 2 min at - 20 °C. For surface staining the permeabilization step using methanol was excluded. Blocking was performed with PBS containing 1 % BSA and 0.05 % Tween-20 for 30 min at room temperature. Cells were then incubated overnight at 4 °C with primary antibodies diluted in blocking solution according to the manufacturer's suggestions to indicated concentrations: rabbit anti-RAGE (ab37647, abcam), 1 : 100; rabbit IgG isotype control (DLN13124; Dianova), 1 : 100. After washing, samples were incubated with blocking solution containing DAPI (1 : 50,000) and the secondary antibody goat anti-rabbit Cy3 (1 : 500) for 2 hours at room temperature. Afterwards cells were washed and mounted with Dako Fluorescent Mounting Medium (S3023, Dako). Samples were analyzed with a Nikon ECLIPSE Ti fluorescent microscope. Exposure time was set with isotype control

stained samples to achieve minimal background and further applied for the analysis of all stainings.

VI.2.9. Immunohistochemistry of TMA

For immunohistochemistry TMA slides containing each patient sample in duplicates were deparaffinized and rehydrated by three washes with xylene, 5 min each, followed by a series of 3min washes in 100, 90, 80 and 70 % ethanol, and rinsed distilled water (dH_2O) and Tris-buffered saline (TBS). Antigen retrieval was performed by heating the samples for 60 min at 100 °C in Zytomed HIER Citrate Buffer (pH 6.0). After cooling and additional washing steps with TBS/TBST, blocking of the endogenous peroxidase activity with 0.03% hydrogen peroxide containing sodium azide for 10 min followed. Then, the TMA was again washed with dH_2O, TBS and TBS containing 1 % Tween-20, and then stained with specific anti-RAGE antibodies (ab37647, abcam, 1:200) in Dako antibody diluent overnight at 4 °C. After three washes, 2 min each with PBS, the sections were incubated with Dako EnVision™ anti-rabbit or anti-mouse secondary antibodies conjugated with horse-radish peroxidase (HRP) for 60 min. After two washes with TBS/TBST for 5 min each the samples were developed with AEC (Dako EnVision™) for 15 min, followed by an additional washing step, and counterstaining with haemotoxylin. The samples were then stabilized with mounting medium (Dako) for storage and scanned with the help of the Tissue Bank of the National Center for Tumor Diseases (NCT), Department of Pathology, University Hospital Heidelberg. Applying the NDP.view2 software (Hamamutsu) two blinded individuals visually scored TMAs according to a quantity/intensity-based IHC scoring system.

VI.2.10. Measuring cell metabolic activity as indicator of cell health and proliferation

The alamarBlue® method monitors the metabolic activity of cells *via* measuring their capacity to reduce the non-toxic, cell permeable, and non-fluorescent compound resazurin to resorufin, which produces red fluorescence. Viable cells continuously convert resazurin to resorufin, thereby allowing a quantitative measurement of viability and, as the reduction of resazurin is cell number-dependent, proliferation. 1×10^3 human melanocytic or melanoma cell lines showing empty vector or RAGE OE construct expression, as well as those from the reversion of the overexpression experiment, were resuspended in 150 µl MEF medium containing either DMSO or 10 µM Doxorubicin and plated into black 96-well plates. The same cell number was used for non-treated or UV-radiated (10 J/m^2) murine B16F10 melanoma cells from the RAGE knockdown experiment. Proper attachment of cells was controlled by adding 15 µl alamarBlue on day 1 to the cells while all other plates were incubated for 72 hours in a humidified atmosphere at 37 °C. After administration of

alamarBlue® cells were allowed to reduce the reagent for two to four hours at 37 °C followed by fluorescence measurement using the TECAN infinite F200 pro microplate reader and the TECAN iControl 1.10.©2012 software with a set gain of 30 and the 535 nm (+/- 25 nm) excitation and 590 nm (+/- 20 nm) emission filter. For the human melanocytic and melanoma cells effects were calculated from the resulting change in fluorescent intensity normalized to untreated cells, carrying the empty vector construct. Differences between the murine B16F10 clones were measured *via* normalization to the untransfected B16F10 control cells.

VI.2.11. Cell cycle analysis

Cell cycle analysis was performed using the DNA-selective, cell membrane-permeant, non-fluorescent Vybrant® DyeCycle™ Violet stain. Briefly, cells were seeded and after proper attachment their cell cycle was synchronized by starving overnight in serum-free MEF medium. Afterwards normal MEF medium was added followed by 24 hours incubation in a humidified atmosphere at 37 °C cells were harvested, and resuspended in MEF medium resulting in a cell concentration of 1 x 10^6. To flow cytometry tubes containing 1 ml of cell suspension DAPI (1 : 50,000) and 1 µl of Vybrant® DyeCycle™ Violet stain (5 µM) were added. The Vybrant® DyeCycle™ Violet stain is fluorescent upon binding to double-stranded DNA. Samples were analyzed for differences in the percentages of cells being in different cell cycle stages using FACS Canto 4.0 and FACSDiva provided by the DKFZ Flow Cytometry Core Facility and the FlowJo Single Cell Analysis software 7.2.2.

VI.2.12. Proliferation analysis using CSFE dilution assay

To investigate differences in proliferation, cells were labeled with the fluorescent dye 5,6-carboxyfluorescein diacetate succinimidyl ester (CFSE). Based on the inheritance of the dye from parental to daughter cells resulting in its dilution, cells with an advantage in proliferation show a reduction in CFSE mean fluorescence intensity (MFI) which is measured directly by flow cytometry. Prior to CSFE staining, cells were starved overnight at 37 °C using serum-free MEF medium in a humidified atmosphere to synchronize their cell cycle. After harvesting, cells were washed extensively with PBS to get rid of residual FCS, which would quench CSFE staining. Cells were then resuspended in prewarmed PBS containing 0.1 % BSA resulting in a final cell concentration of 1 x 10^6 cells/ml and then stained with 10 µM CSFE for 10 min at 37 °C. Staining was stopped in ice-cold MEF medium and cells were washed and resuspended in fresh MEF medium. Stained cells were then plated into 24 well plates and treated as indicated in the experiments. To control CSFE stability some cells were additionally treated with 0.25 µg/ml Mitomycin C. After 24 hours cells were harvested using PBS/EDTA and counterstained with DAPI (1 : 50,000). CSFE staining was analyzed by comparing the geometric mean of the fluorescence intensity (MFI) using FACS Canto 4.0

and FACSDiva provided by the DKFZ Flow Cytometry Core Facility and the FlowJo Single Cell Analysis software 7.2.2.

VI.2.13. Apoptosis staining

For Apoptosis staining 2 x 10^4 untreated or UV-irradiated cells were seeded into 48 well plates either using normal MEF medium or MEF medium containing DMSO or 10 µM doxorubicin as indicated in the respective experiments. The cells were incubated for 72 hours in humidified atmosphere at 37 °C. As internal control some cells were also treated with the pan caspase inhibitor Z VAD FMK (20 µM).

Supernatants containing detached, dead cells were collected in the same tubes used to harvest the remaining cells using PBS/EDTA. After centrifugation the cells were washed for two times using Annexin V binding buffer. Cells were then resuspended in 50 µl Annexin V binding buffer (100,000 cells/100 µl) containing 1.25 µl Alexa Fluor 488 Annexin V 488 and 1 µl of Hoechst (0.25 µg/µl). After 10 min incubation in the dark at room temperature 1 µl of 7AAD was added per sample and cells were incubated under the same conditions for 5 more minutes. Then 200 µl Annexin V binding buffer were added and cells were analyzed using FACS Canto 4.0 and FACSDiva provided by the DKFZ Flow Cytometry Core Facility and the FlowJo Single Cell Analysis software 7.2.2.

VI.2.14. DCFDA – cellular reactive oxygen species detection

Reactive oxygen species (ROS) production was determined by the oxidation reaction of the cell-permeant, non-fluorescent compound 2',7'–dichlorofluorescin diacetate (DCFDA) into 2', 7' –dichlorofluorescein (DCF) by ROS within cells. DCF is a highly fluorescent compound which can be detected by fluorescence spectroscopy. The assay was performed after manufacturer's protocol. Briefly, 2.5 x 10^4 cells per well were seeded into a black 96 well plate with transparent bottom and incubated in humidified atmosphere overnight. After staining with 25 µM DCFDA in 1X Buffer for 45 minutes, ROS production was induced by treating the cells for 4 hours with MEF medium containing 50 µM TBHP as positive control, and medium only. The incubations were performed in humidified atmosphere at 37 °C. Fluorescence was measured using the TECAN infinite F200 pro microplate reader and the TECAN iControl 1.10.©2012 software with optimal gain and the 485 nm (+/- 20 nm) excitation and 535 nm (+/- 25 nm) emission filter. After background subtraction the differences were normalized to the untreated empty vector control (for the human melanocytic and melanoma cell lines) or to untransfected B16F10 cells (murine RAGE Kd).

VI.2.15. Invasion assay

Cell invasiveness was determined by the use of the Cultrex® 96 Well BME Cell Invasion Assay (©2008, Trevigen Inc.) according to the manufacturer's protocol. Briefly, transwell chambers were coated with 0.1X basal membrane equivalent (BME) coating solution and cells were starved in serum-free medium overnight. After starvation cells were seeded in 50 µl serum-free MEF medium at a density of 50,000 cells per well into the coated transwell inserts. The bottom chambers were filled with 150 µl normal MEF medium containing FCS. Cells that migrated into the bottom chamber within a 24 h-period were lysed and stained with the fluorescent dye Calcein. Fluorescence was measured using the TECAN infinite F200 pro microplate reader and the TECAN iControl 1.10.©2012 software with optimal gain and the 485 nm (+/- 20 nm) excitation and 535 nm (+/- 25 nm) emission filter. Relative migratory and invasive potential was determined by comparing RFUs.

VI.2.16. *In silico* characterization of RAGE isoforms

In silico analyses of described RAGE isoforms (Uniprot IDs: Q15109-1, Q15109-2, Q15109-3, Q15109-4, Q15109-5, Q15109-6, Q15109-7, Q15109-8, Q15109-9, Q15109-10, Q101R2, Q15109, Q101R5, Q3L1R3, Q3L1R2, Q71BB6, E9LVY7, E9LVY6, E9LVY5) were performed regarding their structural capacity to translocate into the nucleus using the following computational online tools (Table 15):

Prediction Tool	Description	Based on
BindN	predicts DNA- and RNA-binding sites	applies support vector machines based on sequence features, including side chain pKa values, hydrophobicity index and molecular mass of amino acids [379]
CELLO	protein subcellular localization prediction	applies support vector machines based on multiple n-peptide composition [362]
cNLS Mapper	prediction of importin-α-dependent nuclear localization signals	Bayesian network [363]
NetNES	predicts leucine-rich nuclear export signals (NES)	neural networks as well as Hidden Markov Models [364]

NetNGlyc 1.0	predicts N-Glycosylation sites	neural networks [365]
NetOGlyc 3.1	predictions of mucin type GalNAc O-glycosylation sites	neural networks [366]
NetPhos 2.0	predictions for serine, threonine and tyrosine phosphorylation sites	neural networks [367]
NetPhosK highest score	predictions of kinase*- specific eukaryotic protein phosphorylation sites	neural networks [368]
NLStrada-mus	predicts NLSs in nuclear proteins	Hidden Markov Models [369]
NucPred score	predicts if the protein spends at least some time in the nucleus or if it spends no time in the nucleus	ensemble of 100 sequence-based predictors [370]
SignalP 3.0	predicts the presence and location of signal peptide cleavage sites	neural networks as well as Hidden Markov Models [371]

*PKA, PKC, PKG, CKII, CDC2, CaM-II, ATM, DNA PK, CDK5, p38 MAPK, GSK3, CKI, PKB, RSK, INSR, EGFR and SRC

**centromere, chromosome, nucleolus, nuclear envelope, nuclear speckles, telomere, nucleoplasm, nuclear matrix, PML body, and nuclear pore complex

Table 15 Prediction tools for *in silico* characterization of RAGE isoforms

VI.2.17. Statistical analyses

Tests for all data were performed using GraphPad Prism version 5.00 (2007) with the appropriate tests. Significance in two-tailed t-tests and Mann-Whitney U test for non-gaussian distribution was assumed for p-values < 0.05 (*), < 0.01 (**) or < 0.0001 (***).

VII. Aims of the thesis

The identification of driver mutations resulted in a better understanding of melanoma pathogenesis. Nevertheless, the high plasticity of melanoma cells as well as multiple resistance mechanisms to novel therapies demonstrate the existence of complex but flexible regulatory mechanisms beyond genetics.

Recent studies indicated that the receptor for advanced glycation end-products (RAGE) represents a key element within a network of tumor-promoting pathways. The plethora of alternative splicing forms, ways of posttranslational modifications, including protein shedding, phosphorylation and acetylation, represent only a few characteristics of RAGE enabling a fast adaptive response to extrinsic and intrinsic signals. Since RAGE has been found to be upregulated in malignant melanoma, a tumor-promoting role has been hypothesized early. Although first evidence for a tumor-promoting role of RAGE expressed by stroma cells within the melanoma microenvironment, and partially for a melanoma-cell intrinsic function has been provided, mechanisms of action remain completely unknown.

Taken together, within the present thesis the following questions will be addressed:

a) Is there a connection between RAGE expression and melanocyte transformation as well as melanoma pathogenesis? If so, what are the mechanisms behind?

b) Are the enhanced levels of RAGE in melanoma sufficient to explain potential effects on melanoma cell behavior, or are other regulatory mechanisms controlling the activity of the pathway involved?

By investigating the impact of RAGE on melanocyte and melanoma cell behavior as well as possible regulation mechanisms behind, the study may identify new levels of control operating in melanoma pathogenesis and melanoma plasticity, thereby leading to a better understanding of this complex and fatal disease.

VIII. Results

The aforementioned techniques were applied in order to elucidate the functional tumor cell-intrinsic role of RAGE in melanoma. The findings are outlined in this section.

VIII.1. RAGE is overexpressed in malignant melanoma

First, a comparative evaluation of RAGE expression between healthy tissues and malignant melanoma samples was accomplished.

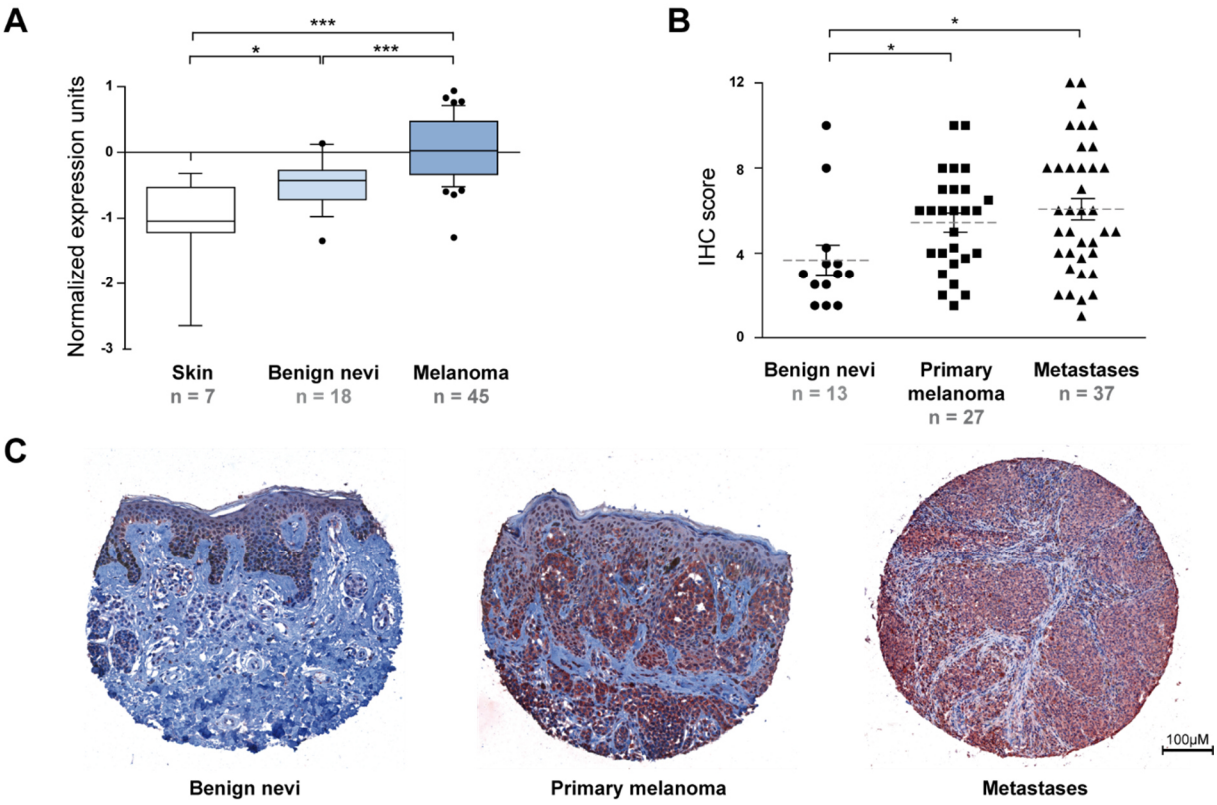

Figure 2 RAGE is overexpressed in human melanoma tissue. Comparative expression analysis of *AGER* transcript levels based on data of a human genome U133A array [388] provided by the Oncomine database. Illustration of *AGER* levels in normal skin (n = 7), benign nevi (n = 18), and melanoma samples (n = 45) with normalized expression units compared to the reporter (**A**). TMAs containing benign nevi (n = 13, circles), primary melanoma (n = 27, squares), and metastases (n = 37, triangles) samples were stained with a rabbit anti-RAGE antibody and scored by two blinded individuals (IHC Score = intensity x percentage of RAGE$^+$ cells; intensity was scored as 0 = negative, 1 = weak, 2 = moderate, and 3 = high; percentage was scored as 0 = 0 %, 1 = 1 – 25 %, 2 = 26 – 50 %, 3 = 51 – 75 %, 4 = 76 - 100 %). All samples were analyzed in duplicates; each symbol represents the respective mean value (**B**). Representative cases of immunohistochemical expression of RAGE for benign nevi, primary melanoma, metastases (**C**). (*$p < 0.05$, ***$p < 0.0001$, unpaired student's t-test)

Differences in *AGER* transcript levels between normal skin (n = 7), benign nevi (n = 18), and melanoma samples (n = 45) were analyzed by the Oncomine database using microarray data provided by Talantov and colleagues [388] (Figure 2A). Levels were found to be significantly increased in benign nevi (*$p < 0.05$), and melanoma samples (***$p < 0.0001$), when compared to normal skin. However, *AGER* expression in melanoma was also significantly higher in comparison to benign nevi (***$p < 0.0001$).

In addition, tissue microarrays (TMA) containing benign nevi (n = 13) as well as primary melanoma (n = 27) and metastases samples (n = 37) were stained with an anti-RAGE antibody and visually scored according to a quantity/intensity-based IHC scoring system by two blinded individuals. The quantity, representing the percentage of positive cells, was scored with numbers ranging from zero to four, whereas the intensity of a staining was scored with numbers from zero to three. Upon scoring the TMA, a significant increase in RAGE expression was found in primary melanomas (IHC score 5.444 ± 0.4462) as well as in associated metastases (IHC score: 6.074 ± 0.4977) compared to melanocytic nevi (IHC score: 3.673 ± 0.7045) (*$p < 0.05$) (Figure 2B). Representative TMA images for benign nevi (left panel), primary melanoma (central panel) and metastases (right panel) are displayed in Figure 2C. However, no significant difference between primary and metastases samples was observed.

VIII.2. RAGE enables melanocytic and melanoma cells to increase their viability, proliferation, and invasion capacity

The described upregulation of RAGE during melanoma development and progression, as well as the lack of evidence of mutations within the protein, implicate gene dosage-effects for RAGE or transactivation of RAGE via hyperactive tumor-related transcription factors [280, 361]. Therefore, overexpression of full-length RAGE provided a powerful tool to decipher the mechanism of action of this protein in melanocytic and melanoma cell lines.

As illustrated in Figure 3A, the human melanocytic cell line MelSTV as well as two conventional, standard human melanoma cell lines, namely A375 and MeWo, were stably transfected with an empty pcDNA3.1. vector or with the respective overexpression construct containing fl-RAGE. All cell lines exhibited a basal endogenous RAGE level, which was relatively low in comparison to other melanoma cell lines (data not shown). Both constructs contained a geneticin-resistance gene allowing the selection of the transfected cells with geneticin (G418). The morphology of the RAGE-overexpressing cells (RAGE OE) in comparison to untransfected (Ø) and control cells (pcDNA3.1.) was assessed but no reliable differences were noted (Figure 3B). The cells were then validated for their *AGER* transcript levels using qPCR (Figure 3C). When normalized to the corresponding untransfected cell

lines, transfection with the RAGE OE construct but not with the empty vector resulted in a marked RAGE overexpression. The RAGE OE cells were characterized by a four - fold increase in *AGER* expression in MelSTV and MeWo, as well as a 28 - fold increase of *AGER* expression in A375 cells.

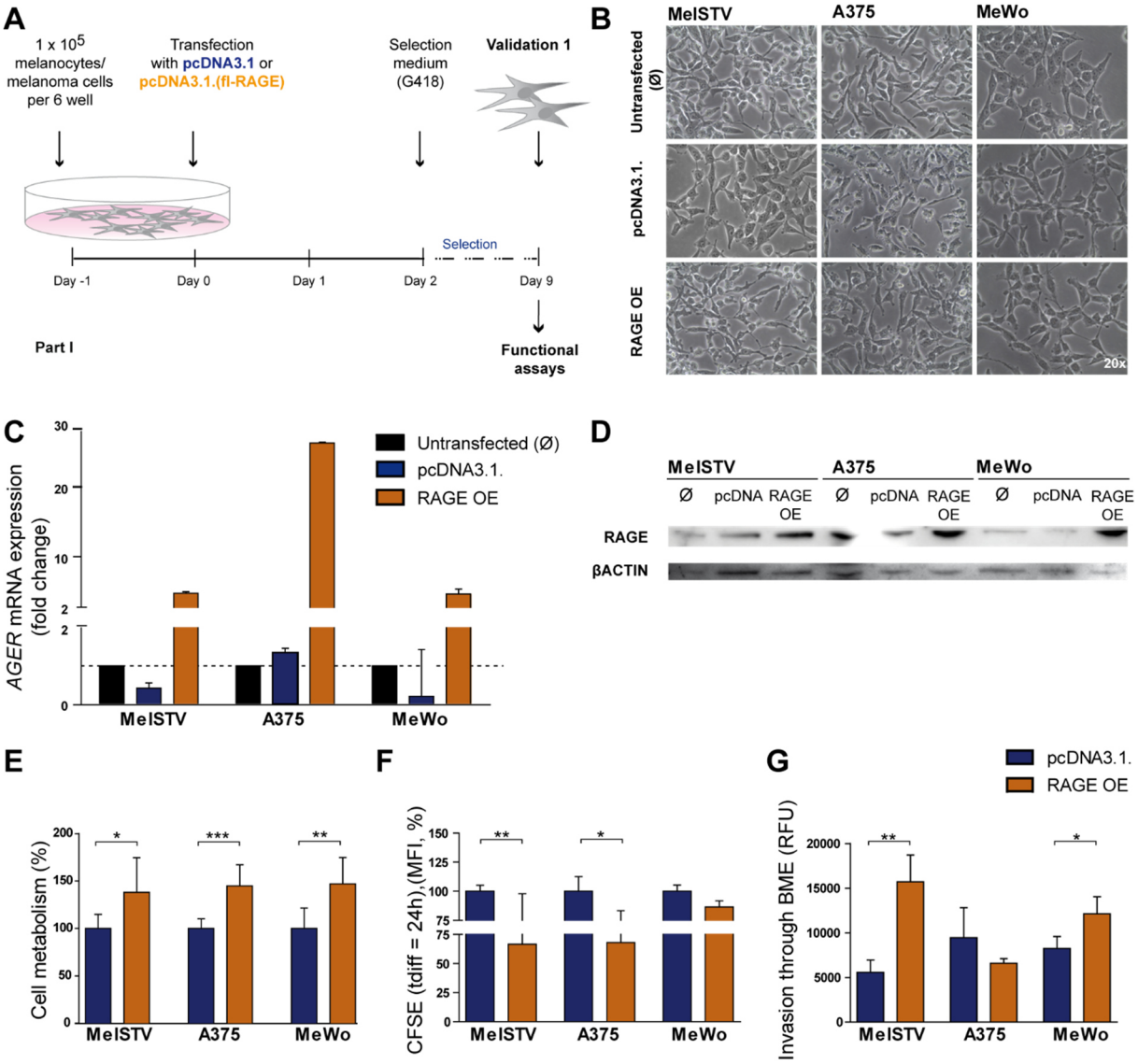

Figure 3 RAGE overexpression (OE) alters human melanocytic (MelSTV) and melanoma (A375, MeWo) cell behavior. Experimental set up (**A**) and morphological appearance of stably transfected control (pcDNA3.1.) and RAGE OE cell lines (**B**). OE was verified via qPCR with *18S* as endogenous control and untransfected cells as reference sample (**C**), and via immunoblotting using a rabbit-anti RAGE antibody and βACTIN as loading control (**D**). RAGE OE and control cells were analyzed 72 hours after seeding for differences in cell metabolic changes using alamarBlue®. 2 hours after alamarBlue® administration fluorescence was measured and the mean value for control cells was used for normalization (**E**). Cells were stained with CSFE and their proliferation was determined by tracing the dilution of the dye via detection of the (geometric) mean fluorescent intensity (MFI) of the cells after 24°hours. Effects on proliferation were determined by normalizing the MFI of RAGE OE cells to the average MFI of control cells (**F**). Invasion through basal membrane extract-coated transwell inserts was compared by fluorescent staining of invaded cells and subsequent measurement of the relative fluorescence units (RFU) (**G**). Graphs display mean ± SD of three (alamarBlue®) and two (invasion) individual experiments with technical triplicates, and four (CSFE) biological replicates with technical duplicates. (*$p < 0.05$, **$p < 0.005$, ***$p < 0.0001$, Mann-Whitney U test (alamarBlue®, CSFE) unpaired student's t-test (invasion))

Furthermore, successful RAGE overexpression in these cells was confirmed by Western Blot. Therefore, samples of untransfected, pcDNA3.1.- and RAGE OE construct-transfected cells were blotted and incubated with an anti-RAGE antibody, and with an antibody against βACTIN as loading control. RAGE protein was detectable in all three cell lines and was increased after the transfection with the overexpression construct (Figure 3D).

After successful verification of RAGE overexpression, cells were functionally characterized for the implementation of melanoma hallmarks such as cell metabolism, sustained proliferation capacity, and invasion capacity.

A potential gain-of-function effect on the survival of melanocytic and melanoma cell lines was found by Kang and colleagues showing that RAGE directly induces tumor survival by enhancing mitochondria function [249]. Based on these findings, experiments to elucidate the role of RAGE in this context were performed. Indeed, alamarBlue® assays demonstrated significantly increased cell metabolic activities upon RAGE overexpression for all three cell lines; melanocytic as well as melanoma cell lines (Figure 3E). In terms of numbers, cell metabolic rates were boosted by approximately 50 % (**$p < 0.005$, ***$p < 0.0001$). Noteworthy, analysis of the obtained raw data for untransfected and pcDNA3.1. transfected cells indicated highest cell metabolic activity in the MeWo cell line, followed by A375, and last MelSTV (data not shown).

Next, the effect of the RAGE overexpression onto the proliferation capacity of the cells was examined. Labeling MelSTV, A375 and MeWo RAGE OE and control cells with the fluorescent dye 5,6-carboxyfluorescein diacetate succinimidyl ester (CFSE) enabled tracing of multiple generations based on dye dilution by cell proliferation. Using flow cytometric analysis, a decrease in the mean fluorescent intensity (MFI) was observed for all three RAGE OE cell lines after 24 hours, with significant differences for MelSTV and A375 when compared to the corresponding controls (Figure 3F, *$p < 0.05$). A lower MFI is equivalent to a higher dilution of the fluorescent dye, and thereby to a higher proliferation rate. Consequently, RAGE OE was associated with an increased proliferation rate in all cell lines tested.

In order to investigate characteristics not only associated with general tumor growth but also with the formation of melanoma metastases, RAGE OE and control cells were analyzed for their capacity to invade extracellular matrices *in vitro.* Therefore, cells were seeded in transwell chamber inserts coated with basement membrane extracts (BME). The amounts of cells that were able to proteolytically degrade the BME components, including laminin, collagen IV, entactin, and heparin sulfate proteoglycan, and consequently migrate to the lower chamber were measured (Figure 3G). Interestingly, RAGE overexpression had the

highest impact on invasion in MelSTV, which initially showed the lowest invasion capacity based on its melanocytic-like character. Here, the overexpression was accompanied with a three – fold higher number of cells invading through extracellular matrices *in vitro* as quantified by fluorescent staining (**$p < 0.005$). For the melanoma cell lines, this assay revealed an interesting pattern: The A375 cells, which displayed a significantly higher proliferation upon RAGE overexpression, failed to increase their invasion capacity. In contrast, MeWo RAGE OE cells showed only a slightly enhanced proliferation in comparison to control cells, but a significantly higher invasion (*$p < 0.05$).

These experiments demonstrate that overexpression of RAGE significantly changes melanocytic as well as melanoma cell behavior. More specifically, it enhances cell metabolism and proliferation, and influences the invasion capacity in a cell line- or cell stage-dependent manner.

VIII.3. Pro-survival effects of RAGE OE are based on RAGE-mediated inhibition of apoptosis

The high plasticity of melanoma cells enabling them to switch between 'proliferative' and 'invasive' phenotypes complexes the work on these two features [97]. Indeed, the results of the CSFE and the invasion assay might suggest that A375 and MeWo cells represent two different functional states. Here, further studies were focused on the role of RAGE-mediated pro-survival effects, which were consistent in all – melanocytic and melanoma – cell lines.

In order to ensure that observed alterations were RAGE-specific and to exclude overexpression-associated artefacts, RAGE OE cells were additionally transfected with siRNA targeting *AGER* transcripts or correspondent control siRNA, as illustrated in Figure 4A. Noteworthy, the *AGER* siRNA used in these experiments targets besides transcripts encoding for fl-length RAGE also soluble and other truncated RAGE forms comprising RAGE_v1, RAGE_v4, RAGE_v6, RAGE_v8, RAGE_v9, RAGE_v10, and RAGE_v16. The amino acid lengths of these alternative forms range from 342 to 390 aa (more information can be found in Table 16). The interference with the overexpression was successfully verified by determining *AGER* transcript levels *via* qPCR analysis (Figure 4B). In fact, *AGER* siRNA treatment abolished the overexpression in MelSTV and MeWo cells, and led to an approximately six - fold reduction of *AGER* expression in A375 RAGE OE cells. In contrast, treatment with control siRNA showed only slight effects in MelSTV and A375 RAGE OE cells while a greater side effect was observed in MeWo RAGE OE cells. Nevertheless, effects with the control siRNA were markedly lower than with *AGER* siRNA in all RAGE OE cell lines.

Cells of the different conditions were then analyzed for alterations in cell metabolism using the alamarBlue® method. When normalized to control cells (pcDNA3.1.) the RNA

interference partially impaired the cell metabolism-dependent pro-survival effect of the RAGE overexpression in MelSTV, and significantly abolished the effects in A375 and MeWo RAGE OE cells (Figure 4C). A slightly impaired cell metabolism was also found in the RAGE OE cells transfected with control siRNA. Nevertheless, these side-effects were negligible since approaches using *AGER*-specific siRNA were still significantly impaired when compared to the control siRNA-treated cells.

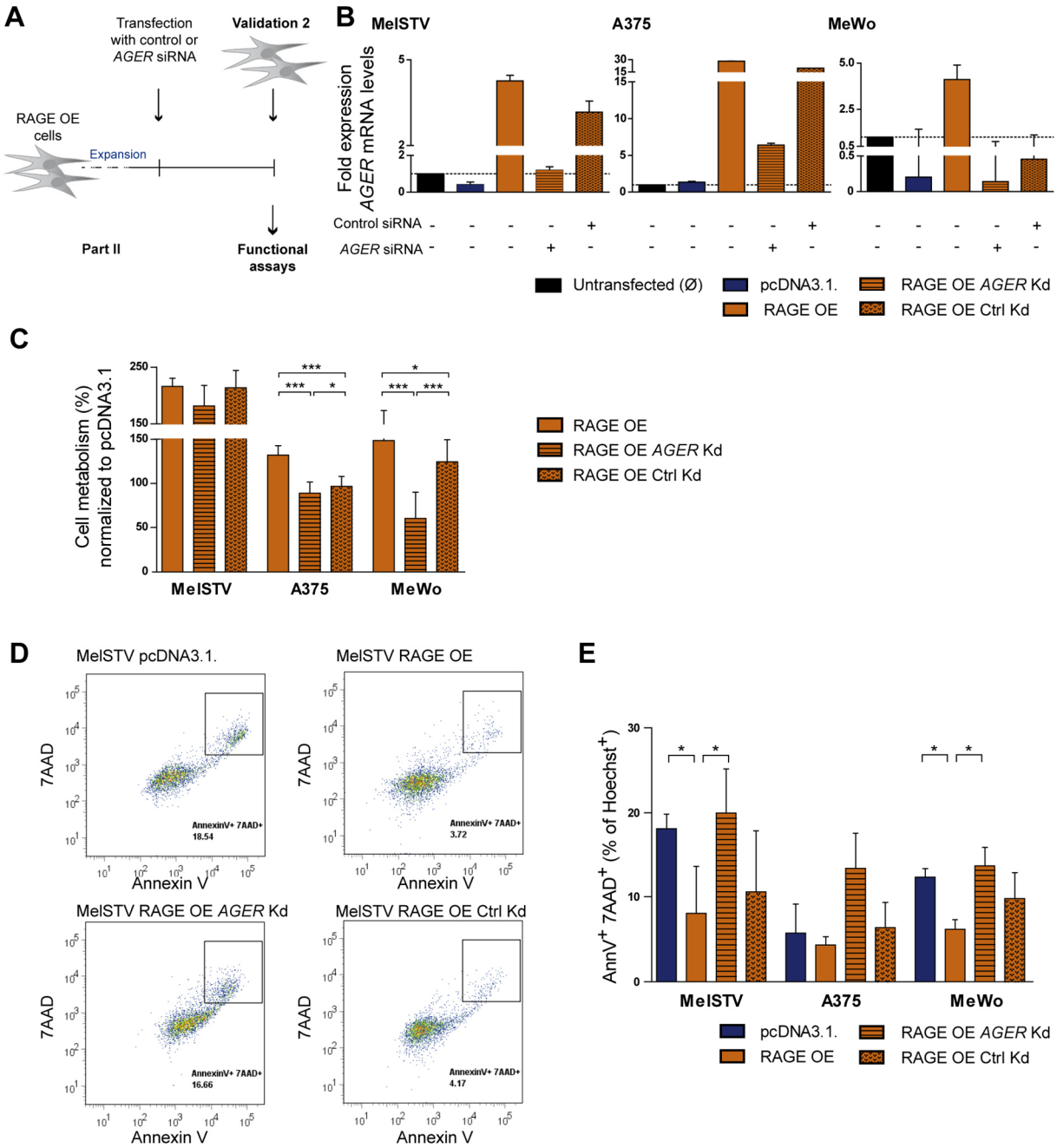

Figure 4 RAGE mediates pro-survival effects by inhibiting apoptosis in human melanocytic and melanoma cell lines. RAGE overexpressing cells were additionally transfected with control siRNA or siRNA targeting *AGER* transcripts to generate a reversion of the overexpression in MelSTV, A375 and MeWo cells (**A**). Knockdown was verified *via* qPCR with *18S* as endogenous control and untransfected cells as reference sample (**B**). Control (pcDNA3.1.), untreated RAGE OE, RAGE OE + *AGER* siRNA, RAGE OE + Ctrl siRNA cells were seeded and analyzed after 72 h for differences in cell health as indicated by cell metabolic changes using alamarBlue®. 2 hours after alamarBlue® administration fluorescence was measured and the mean value for control cells was used for normalization (**C**). At the same time point (72 h after seeding), attached and floating cells of all conditions were harvested and stained with Hoechst, 7AAD, and an Annexin V antibody. Illustration of a flow cytometric analysis of the Annexin V^+ $7AAD^+$ subpopulation (gated on $Hoechst^+$ single cells (FSC-H/FSC-W)) of MelSTV pcDNA3.1., RAGE OE, RAGE OE + *AGER* siRNA, RAGE OE + Ctrl siRNA cells (**D**). Comparison of the revealed percentages for late apoptotic cells for all cell lines and conditions (**E**). Graphs display mean ± SD of three (alamarBlue®) individual experiments with technical triplicates, and three (apoptosis) biological replicates with technical duplicates. (*$p < 0.05$, ***$p < 0.0001$, unpaired student's t-test)

The observed increase in cell metabolic activity strongly suggested an enhanced cell viability of the RAGE OE melanocytic and melanoma cell lines but provided no additional information about the affected aspect influencing cellular health. Therefore, a closer examination on the pro-survival effect of RAGE overexpression was conducted. Control and overexpression cells were stained with Hoechst and the dead cell-dye 7AAD, as well as with antibodies against Annexin V, and analyzed *via* flow cytometry (Figure 4D). The analysis showed that the overexpression of RAGE was accompanied with a decreased number of late apoptotic cells ($Hoechst^+$, $7AAD^+$, Annexin V^+), which was found to be significant for the melanocytic cell line MelSTV and for MeWo (*$p < 0.05$). The siRNA-mediated reversion of the overexpression could significantly abolish this effect in these two cell lines (*$p < 0.05$). The same tendency was also observed for the A375 cell line (Figure 4E).

These results not only verified the pro-survival effect of the RAGE overexpression in melanocytic and melanoma cell lines but rather defined it as an anti-apoptotic effect.

VIII.4. RAGE controls the transcription of DNA damage signaling molecules in human and mouse

As described in section V.1.2, cancer cells, including melanoma, often display impaired apoptosis induction [76, 78]. Since apoptosis represents a possible outcome of DNA damage, one mechanism is circumventing DNA damage signaling [74]. Therefore, in a next step effects on the regulation of the DNA damage repair network in melanoma was investigated.

The highest fold change in *AGER* transcript levels upon overexpression was observed in the A375 cell line. Hence, this cell line was used for studying a potential involvement of RAGE in the regulation of DNA damage repair molecules. Since the applied method necessitated a high sample quality, cDNA of A375 RAGE OE and control cells was tested for fulfilling the

quality recommendations, such as the appropriate 260 nm/ 280 nm and 260 nm/ 230nm ratio, and for a low intersample variance regarding the expression of the endogenous control, here *18S* (Figure 5A).

HMGB1, a ligand of RAGE (described in V.2.2.2.2), has shown to be involved in DNA damage responses upon drug administration [380], therefore consequences of RAGE overexpression on its transcript levels and associated side-effects were ruled out to guarantee optimal requirements for investigating RAGE-dependent regulation mechanisms. In fact, in none of the used cell lines the overexpression of RAGE was accompanied with an upregulation of *HMGB1* transcripts (Figure 5B).

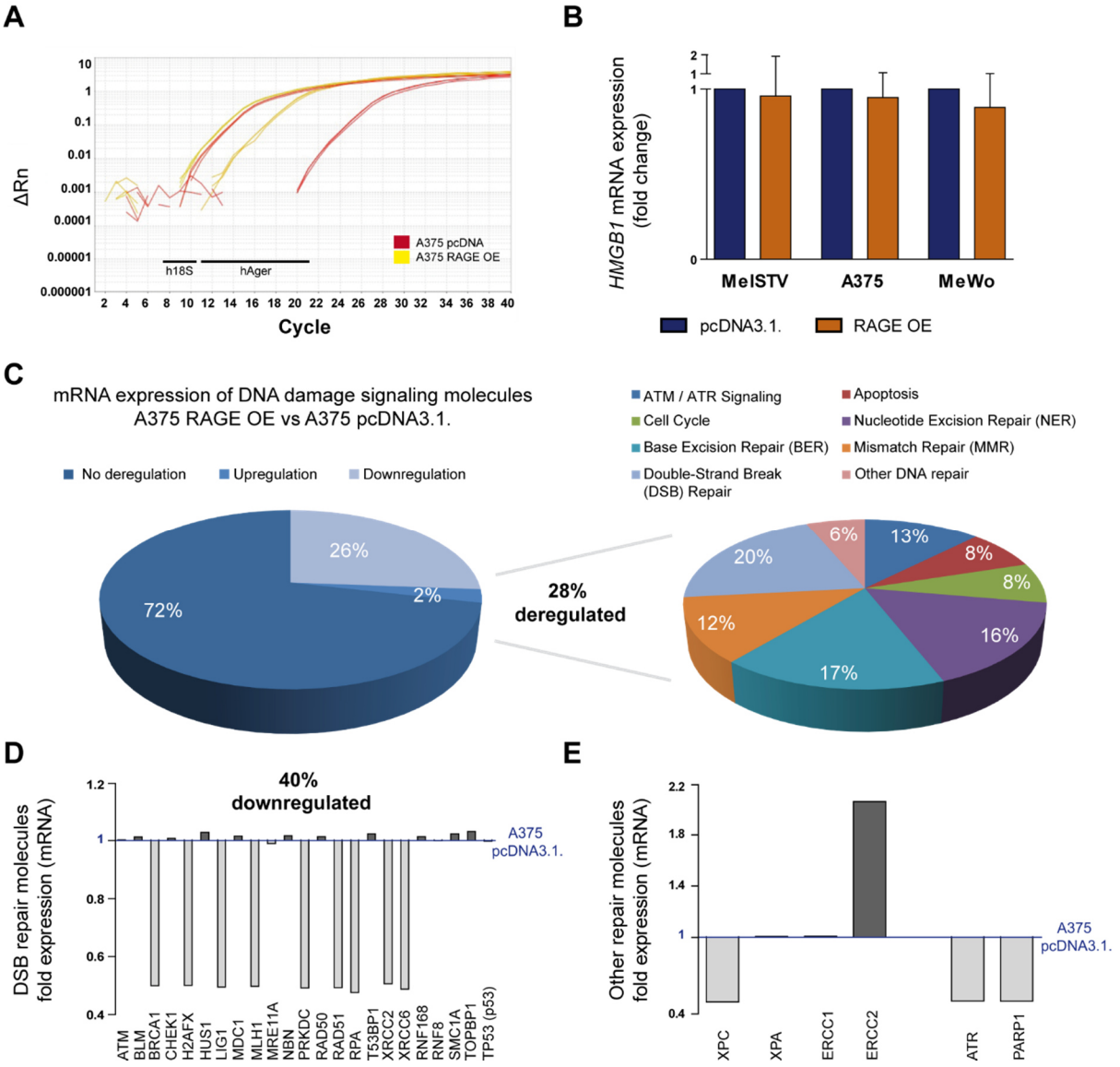

Figure 5 RAGE mediates the downregulation of DNA repair molecules in humans. A375 pcDNA3.1. and RAGE OE cDNAs were validated for low intersample variance of the endogenous control *18S,* as illustrated by a qPCR example analysis (**A**). If *HMGB1* expression was affected by RAGE OE in MelSTV, A375, or MeWo was analyzed by comparing its transcript levels *via* qPCR analysis to the corresponding pcDNA3.1. cells with *18S* as endogenous control (**B**). A375 pcDNA3.1. and RAGE OE cDNAs were analyzed for differentially regulated DNA damage signaling molecules applying RT² Profiler PCR Arrays with normalization to *βACTIN* and *RPLO* transcript levels. 28 % of the monitored genes have found to be deregulated, with 2 % being up- and 26 % being downregulated upon overexpression (A375 RAGE OE vs pcDNA3.1.) (**C**) ***left graph***. The ranking of affected pathways was performed by illustrating the percentage of deregulated genes within the distinct pathways. DSB repair (20 %), BER (17 %), NER (16 %) were identified as most affected pathways (**C**) ***right graph***. Monitored transcript levels of molecules belonging to the DSB repair pathway were illustrated by their fold change to A375 pcDNA3.1. control cells. Transcript levels *BCRA1*, *H2AFX*, *LIG1*, *MLH1*, *PRKDC*, *RAD51*, *RPA*, *XRCC2*, *XRCC6* were found downregulated in A375 RAGE OE cells in comparison to corresponding pcDNA3.1. control (**D**). Expression of genes involved in *xeroderma pigmentosum* such as *XPC*, *XPA*, *ERCC1*, *ERCC2*, and of the two genes *ATR* and *PARP1*, of which alterations have been associated with increased melanoma risk, was investigated (**E**).

All these criteria allowed for the quantitative comparison of DNA damage signaling molecules and predicted a high stringency of the results. The applied 'RT² Profiler™ Human DNA Damage Signaling Pathway PCR Array' enabled the simultaneous monitoring of 79 DNA damage signaling-related genes with an average correlation coefficient higher than 0.99. This ensured a reliable detection of differences in expression between biological samples, here A375 RAGE OE and control cDNA.

Normalizing the different expression values of the investigated DNA repair molecules to the two house-keeping genes *βACTIN* and 50S ribosomal protein L15 (*RPLO*), and consequent comparison of the obtained data sets for A375 RAGE OE and A375 control, revealed a deregulation of 28 % of all analyzed transcripts. Interestingly, only 2 % were upregulated in A375 RAGE OE cells, whereas 26 % were downregulated in comparison to control (pcDNA3.1.) cells (Figure 5C, left pie chart).

The monitored genes were further subgrouped into distinct DNA repair pathways (allocations can be found in Table 13), namely ATM/ATR signaling, nucleotide excision repair (NER), base excision repair (BER), mismatch repair (MMR), double-strand break repair (DSB), other DNA repair genes, apoptosis, and cell cycle. 20 % of the deregulated genes were found within the double-strand break (DSB) repair pathway (Figure 5D, right pie chart). Indeed, 40 % of the genes associated with DSB repair were differentially regulated between A375 RAGE OE and A375 control cells. More specifically, *BRCA1*, *H2AFX*, *LIG1*, *MLH1*, *PRKDC*, *RAD51*, *RPA*, *XRCC2*, and *XRCC6* were found to be downregulated, whereas there was no difference in *ATM*, *BLM*, *CHEK1*, *HUS1*, *MDC1*, *MRE11A*, *NBN*, *RAD50*, *TP53BP1*, *RNF168*, *RNF8*, *SMC1A*, *TOPBP1*, *TP53* transcript levels.

However, also some genes commonly affected in the rare disease *xeroderma pigmentosum* (XP) [59], namely *XPC* and *ERCC2* were found to be deregulated in the melanoma cell line upon RAGE overexpression (Figure 5E). In addition, these data were compared to the study by Zhang and colleagues, who evaluated 1,463 genetic variants across 60 DNA repair–related pathway genes in relation to melanoma risk, thereby identifying SNPs in *ATR* and *PARP1* to correlate significantly with a higher melanoma risk [63]. Interestingly, the expression of these two genes was found to be dysregulated upon RAGE overexpression in this study (Figure 5E).

In order to verify the RAGE-mediated regulatory effect on the expression of molecules within DNA repair pathways, a comparable approach was performed using a completely different model; the murine B16F10 melanoma.

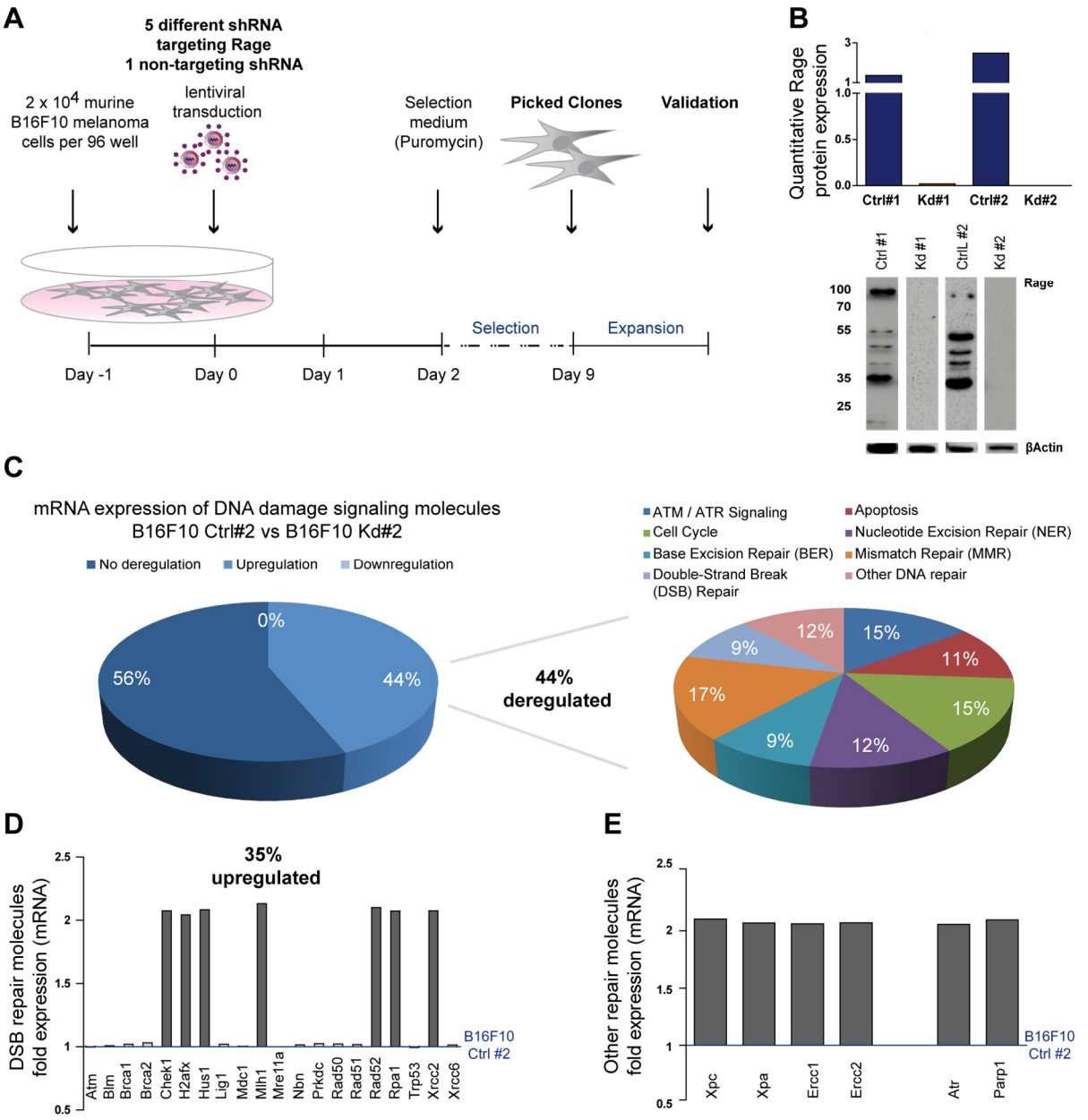

Figure 6 Rage mediates the downregulation of DNA repair molecules in mice. Experimental set up of the stable *Ager* RNA interference (RNAi) in the murine B16F10 melanoma line using shRNA lentivectors (**A**). Knockdown was verified *via* qPCR with *Hprt* and *Gapdh* as endogenous controls and untransfected B16F10 cells as reference sample (**B**, ***upper graph***), and *via* immunoblotting using a rabbit-anti Rage antibody and βActin as loading control (**B**, ***lower graph***). B16F10 control (non-targeting shRNA) and Rage knockdown (*Ager* shRNA) cell cDNAs were analyzed for differentially regulated DNA damage signaling molecules applying RT2 Profiler PCR Arrays with *βActin* and *Hsp90ab1* as endogenous controls. 44 % of the monitored genes have found to be deregulated, with 0 % being down- and 44 % being upregulated upon Rage knockdown (B16F10 Kd#2 vs Ctrl#2, (**C**, ***left graph***). The ranking of affected pathways was performed by illustrating the percentage of deregulated genes within the distinct pathways. MMR repair (20 %), ATM/ATR signaling (17 %), cell cycle (16 %) were identified as most affected pathways. The DSB pathway contained 9 % of all differentially regulated genes (**C, *right graph***). Monitored transcript levels of molecules belonging to the DSB repair pathway were illustrated by their fold change to B16F10 Ctrl#2 cells. About 35 % of the monitored genes showed enhanced expression. *Chek1*, *H2afx*, *Hus1*, *Mlh1*, *Rad52*, *Rpa1*, *Xrcc2* transcripts were found upregulated upon Rage knockdown in B16F10 cells compared to corresponding controls (**D**). Expression of genes involved in *xeroderma pigmentosum* such as *Xpc*, *Xpa*, *Ercc1*, *Ercc2*, and transcript levels of *Atr* and *Parp1* were investigated (**E**).

Since B16F10 cells show comparable features to human melanoma, such as the expression of mouse homologs of melanoma-derived antigens, rapid growth, capacity to form metastases, as well as a low MHC Class I expression, these cells were strongly recommended to represent a reasonable model for human melanoma [381].

In brief, B16F10 melanoma cells were plated and transduced with lentiviral particles as illustrated in Figure 6A. The lentiviral particles contained a puromycin resistance gene, as well as either a non-targeting shRNA or a shRNA targeting *Ager* transcripts. After antibiotic selection of the cells, generated B16F10 clones were validated by qPCR comparing *Ager* transcript levels with *Hprt* and *Gapdh* as endogenous control and untransfected B16F10 cells as reference sample (Figure 6B, upper graph). For conformation of the successful knockdown of Rage, protein levels were determined by immunoblotting using an anti-Rage antibody and βActin as loading control. Indeed, for B16F10 control clones more than one band for Rage were detected; however, all of these bands disappeared or impaired after Rage knockdown, suggesting that the applied shRNA targeted most murine Rage isoforms. Noteworthy, also higher-molecular weight bands were weakened upon knockdown.

With cDNA from a B16F10 control clone and, respectively, cDNA from a Rage knockdown clone two RT² Profiler™ Mouse DNA Damage Signaling Pathway PCR Arrays were performed. Indeed, in this model Rage knockdown was associated with an upregulation of DNA damage signaling molecules. More specifically, when normalized to the two house-keeping genes *βActin* and *Hsp90ab1*, not a single gene was downregulated, but 44 % of all monitored genes showed increased expression (Figure 6C, left pie chart). Beside these consistent findings, differences regarding the affected pathways were observed. For instance, most of the differentially regulated genes were not found within the DSB repair but instead in the mismatch repair (MMR) pathway (Figure 6C, right pie chart).

Nevertheless, since fragmentation, loss, or rearrangement of chromosomes are current events in melanoma, thereby highlighting the importance of DSBs and their repair for its pathogenesis [53], differentially regulated genes within the DSB repair pathway were analyzed next. Indeed, 35 % of the monitored genes were upregulated, namely *Chek1*, *H2afx*, *Hus1*, *Mlh1*, *Rad52*, *Rpa1*, *Xrcc2*. No differences in expression were observed for *Atm*, *Blm*, *Brca1*, *Brca2*, *Lig1*, *Mdc1*, *Mre11a*, *Nbn*, *Prkdc*, *Rad50*, *Rad51*, *Tp53*, and *Xrcc6* (Figure 6D). In line with the data for the human melanoma cell line, Rage interference also exhibited effects on the expression of XP-related genes [59], here *Xpc*, *Xpa*, *Ercc1*, and *Ercc2*, as well as on the genes, for which genetic alterations were associated with a higher risk for melanoma [63], namely *Parp1* and *Atr* (Figure 6E).

These findings suggest a function of the RAGE protein as negative regulator of DNA damage signaling molecules in melanoma. Besides proving that this is true for human and mouse, analyzing transcript levels of genes known to be affected in *xeroderma pigmentosum*, revealed a RAGE-dependent dysregulation of *XPC* and *ERCC2* in the human system, and of *Xpc*, *Xpa*, *Ercc1*, *Ercc2* in the murine B16F10 cell line. Furthermore, four gene homologs involved in DSB repair mechanisms were identified, which are regulated by RAGE in both species: *H2AFX/H2afx*, *MLH1/Mlh1*, *RPA1/Rpa1*, and *XRCC2/Xrcc2*.

VIII.5. RAGE expression enhances cell-intrinsic stress levels and sensitivity of melanocytic and melanoma cells towards DNA damage caused by extrinsic stress

In normal cells, cell metabolism and energetics are proportional to the intracellular ROS levels. However, in cancer cells the relation between ROS homeostasis and energy metabolism is more complex [382].

As demonstrated in section VIII.2, RAGE overexpression was associated with a cell metabolic boost in both, melanocytic and melanoma cell lines (Figure 3). Therefore, alterations in ROS levels associated with RAGE overexpression were determined. In brief, MelSTV, A375, and MeWo control and RAGE OE cells were seeded and stained with the non-fluorescent dye DCFDA. Intracellular ROS levels were monitored by their capacity to oxidize DCFDA to the highly fluorescent compound DCF. Indeed, RAGE overexpression significantly induced DCF and accordingly ROS levels in all of the cell lines (Figure 7A *$p < 0.05$, ***$p < 0.0001$). In terms of numbers, RAGE OE cells showed a 1.2 - to five - fold higher ROS production compared to control cells. Although enhanced ROS levels stand for increased cell-intrinsic oxidative stress, RAGE promoted melanocytic and melanoma cell survival *in vitro* (Figure 4D & E). Therefore, the question raised whether RAGE cannot only

mediate a higher resistance to cell-intrinsic stress but also when facing extrinsic stress signals.

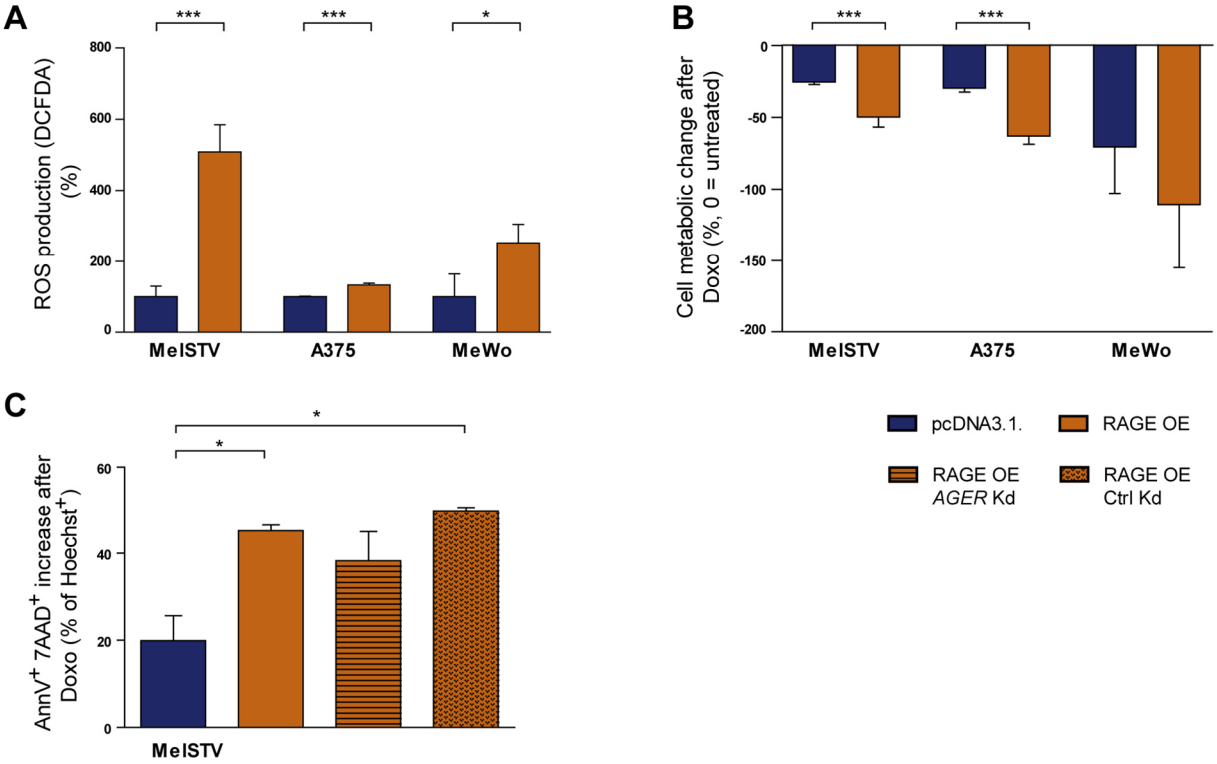

Figure 7 RAGE enhances ROS production and sensitivity towards extrinsic genotoxic stress in human melanocytic and melanoma cell lines. MelSTV, A375, and MeWo control or RAGE OE cells were stained with DCFDA, allowing the measurement of endogenous levels of ROS by detecting its oxidized, and fluorescent state, namely DCF. RFUs of the RAGE OE cells were normalized to the corresponding control (pcDNA3.1.) (**A**). Comparison of changes in cell metabolism after 72 h Doxorubicin (100 nM) treatment between overexpressing and control MelSTV, A375 and MeWo cells. Values generated for the correspondent untreated cells were set as zero (**B**). MelSTV pcDNA3.1. RAGE OE, RAGE OE *AGER* siRNA, RAGE OE control siRNA were cultivated in the presence of 100 nM Doxorubicin and analyzed for apoptotic cells after 72 h using flow cytometry. Illustrated is the amount of Annexin V^+ $7AAD^+$ cells (gated on $Hoechst^+$ single cells (FSC-H/FSC-W)) after subtraction of the monitored frequency for the corresponding untreated cell line (**C**). Graphs display mean ± SD of three (ROS, alamarBlue®) individual experiments with technical triplicates, and three (apoptosis) biological replicates with technical duplicates. (*$p < 0.05$, **$p < 0.005$, ***$p < 0.0001$, unpaired student‘s t-test)

In order to address this question MelSTV, A375, and MeWo control (pcDNA3.1.) and RAGE OE cells were seeded and effects of exogenous genotoxic stress were monitored. More specifically, applying alamarBlue® assays including doxorubicin (Doxo) (100 nM) insults or DMSO treatments as control, cells were analyzed for distinct cell metabolic responses. Doxo is a drug used in cancer chemotherapy, intercalating in DNA molecules and thereby interfering with replication and transcription [383]. Interestingly, increased RAGE levels were associated with a greater cell metabolic collapse induced by doxorubicin in all three cell lines. The increased sensitivity towards genotoxic stress was highly significant for MelSTV and A375 RAGE OE cells (***$p < 0.0001$), and a same tendency was also observed for MeWo

RAGE OE cells (Figure 7B). Furthermore, Doxo treatment of control or RAGE OE MelSTV cells induced apoptosis in cells with elevated RAGE levels to a significantly higher extend compared to control (pcDNA3.1.) cells. More specifically, with 40 % Annexin V^+ $7AAD^+$ cells after Doxo treatment the amount of late apoptotic cells doubled upon RAGE overexpression. This effect was partially abolished using *AGER* siRNA, but not with control siRNA (Figure 7C).

To further evaluate the role of RAGE in mediating drug sensitivity to exogenous DNA damage-inducing agents or factors for its general validity, the effect of UV radiation-induced DNA damage in the murine B16F10 model upon Rage knockdown was investigated.

Two B16F10 Rage knockdown clones, as well as corresponding control clones, were UV-radiated and the effect of the radiation onto the cells was monitored by investigating differences in their cell metabolism as described before. The alamarBlue® assays showed that upon UV radiation a significant drop in cell metabolism could only be observed for the control clones (*$p < 0.05$) but not for the Rage knockdown clones (Figure 8A).

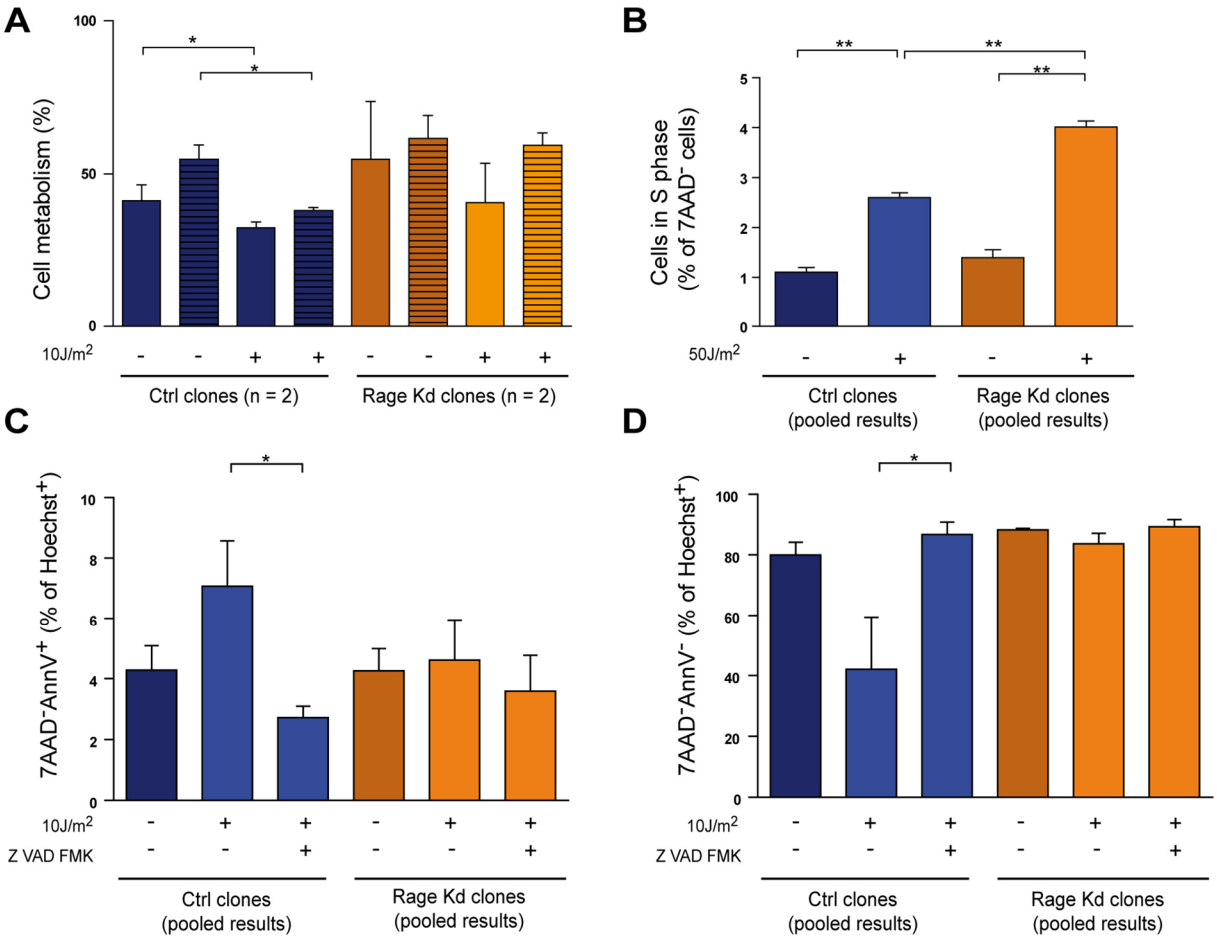

Figure 8 Rage enhances sensitivity towards extrinsic genotoxic stress in murine B16F10 melanoma. B16F10 Rage knockdown (Rage Kd) and control (Ctrl) clones (clone 1 = plain, clone 2 = lined) were UV radiated (10J/m^2) and effects on cell metabolism were monitored using alamarBlue® and normalized to untreated, untransfected B16F10 cells (**A**). Cell cycle analysis with Vybrant DyeCycle Violet stained B16F10 Ctrl and Rage Kd cells before and after UV radiation (50J/m^2) was performed by flow cytometry. Revealed percentages of cells in S phase (gated on single, 7AAD$^-$ cells) were compared (**B**). Using flow cytometry, UV radiation-induced, Rage-dependent effects on apoptosis were investigated with Hoechst, 7AAD and Annexin V antibody-stained B16F10 control and Rage Kd cells. Percentages of early apoptotic (7AAD$^-$, AnnexinV$^+$ (**C**)) and living cells (7AAD$^-$, AnnexinV$^-$ (**D**)) before and after UV radiation were compared. Radiated cells treated with an apoptosis inhibitor Z VAD FMK (20µM) served as control. Graphs display mean ± SD of three (alamarBlue®) with technical triplicates, and two (cell cycle) or three (apoptosis) biological replicates with technical duplicates. (*$p < 0.05$, **$p < 0.005$, unpaired student's t-test)

In order to rule out that potential cell cycle deregulations induced by Rage knockdown were responsible for this effect, cell cycle analysis was performed. Briefly, cells were starved overnight using serum-free MEF medium to ensure cell cycle synchronization, and then stained with Vybrant® DyeCycle™ Violet stain. This dye is a DNA-selective stain, which exhibits emission signals proportional to DNA mass. Since DNA mass is different between the three major phases of cell cycle – G0/G1 phase, S phase, G2/M phase – one can investigate the amount of cells within the different phases using flow cytometry [384]. When comparing the amount of cells in S phase, the most vulnerable phase to DNA damage, no basal difference was observed (Figure 8B). This indicates a normal cell cycle regulation in the absence of extracellular stress induction. When B16F10 cells were radiated, numbers of control and knockdown cells in S phase increased (**$p < 0.005$). However, this radiation effect was significantly higher in RAGE knockdown cells (**$p < 0.005$), suggesting the presence of strengthened cell cycle checkpoints or checkpoint-associated mechanisms leading to accumulations of cells in the S phase.

In order to investigate if these effects also influence the survival of B16F10 melanoma cells, control as well as knockdown clones were stained for apoptotic cells using Hoechst, live/dead stain 7AAD, and an antibody against Annexin V. Flow cytometric analysis revealed a significantly increased amount of early apoptotic cells (7AAD$^-$ AnnexinV$^+$) after radiation of B16F10 control cells when compared to apoptosis inhibitor (Z VAD FMK)-treated cells (Figure 8C, *$p < 0.05$). The *vice versa* effect could be demonstrated for the living population, defined as 7AAD$^-$ AnnexinV$^-$, of the B16F10 control cells (Figure 8D, *$p < 0.05$). However, these effects were not observed for the B16F10 Rage knockdown cells (Figure 8C, D).

Summing up this part, human and murine melanoma cells respond to increased levels of RAGE protein with a higher sensitivity towards extrinsic stress signals. RAGE protein expression is thereby not only linked with positive effects for the cells, such as proliferation and pro-survival benefits (demonstrated in VIII.2 and VIII.3), but also with a higher vulnerability (VIII.5). This strongly suggests a complex regulation network controlling RAGE

function in melanoma. Experiments and results facing this question will be described in the next result sections.

VIII.6. Aberrant localization of RAGE points towards a new control level of RAGE functionality in melanoma

In section VIII.1 the observed overexpression of RAGE in melanoma in comparison to benign nevi was described. Taking a closer look at the TMA slides indicated an additional pattern of RAGE expression.

VIII.6.1. Nuclear RAGE found in benign nevi disappears upon malignant transformation

Analyzing samples of benign nevi, primary melanoma, and melanoma metastases in regard to the subcellular localization of the RAGE protein revealed remarkable differences between the tissues. In total, 13 corresponding benign nevi, 27 primary melanoma as well as 37 associated metastases samples were analyzed in this study by two blinded individuals.

In contrast to benign nevi, which showed a high nuclear localization of RAGE (Figure 9A, lower panel, left picture), melanoma cells of the primary tumor as well as of metastases samples displayed a higher cytoplasmic staining for the protein (Figure 9A, central and right picture). In terms of numbers, 29 % of melanocytes within benign nevi were characterized by pure nuclear RAGE expression, while this value dropped to 8 % for primary melanoma cells, and 2 % for melanoma metastases. Interestingly, the difference was not only significant when both melanoma tissues were compared to benign nevi (***$p < 0.0001$), but also between primary melanoma and metastases samples (*$p < 0.005$), suggesting that the loss of nuclear RAGE is an ongoing process during progression (Figure 9A).

In addition, the percentages of cells with predominant nuclear RAGE expression were also significantly reduced in malignant tissues (***$p < 0.0001$); however, in this case no significant difference between primary melanomas and metastases was noted. In contrast, percentages of cells with predominant cytosolic or pure cytosolic RAGE expression increased upon transformation. More specifically, only 19 % of melanocytic cells in benign nevi showed a pure cytosolic RAGE expression, while primary melanoma (45 %) and metastases (46 %) samples showed significantly higher proportions of these cells (***$p < 0.0001$). The same tendency was observed for predominant cytosolic RAGE expression; however, these differences were not significant.

Furthermore, the analysis of a diverse set of human melanoma cell lines suggested a similar expression pattern of primary melanomas and cultured melanoma cells. Briefly, melanoma

cells were either fixed and permeabilized (Figure 9B, upper panel of illustrative pictures) to allow cytoplasmic as well as nuclear staining, or fixed without subsequent permeabilization as control (Figure 9B, lower panel of illustrative pictures). In all non-permeabilized control cells membrane-bound RAGE was present, while its localization within the membrane was found to be heterogeneous (Figure 9B, illustrative pictures). However, permeabilized as well as non-permeabilized cells of each cell line were subgrouped according to predominant cytoplasmic (Figure 9B, left illustrative pictures) or nuclear staining (Figure 9B, right illustrative picture) and statistically analyzed. To exclude distortions by artefacts counts for nonpermeabilized cells were subtracted from cell numbers achieved for permeabilized samples. Indeed, four out of five cell lines showed a higher cytoplasmic expression of RAGE (Figure 9B), whereas the SKmel23 cell line was hallmarked by a predominant nuclear expression.

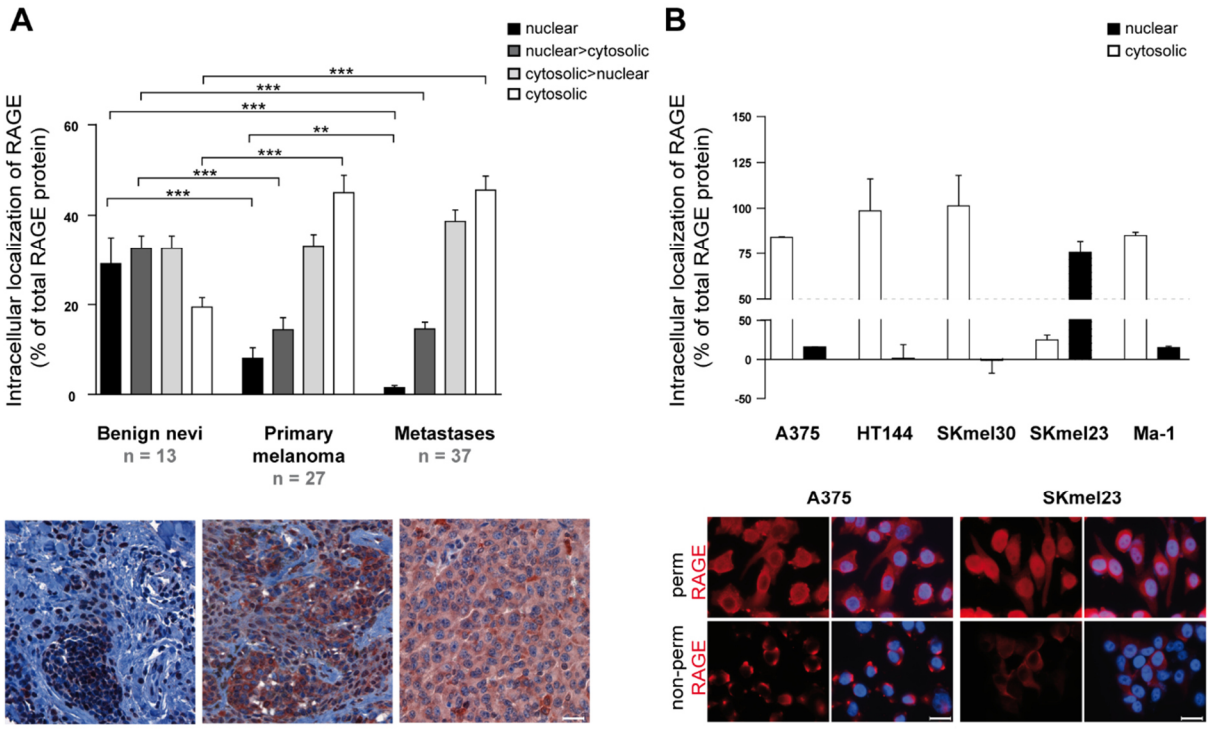

Figure 9 Nuclear RAGE found in benign nevi disappears upon transformation. TMAs containing benign nevi (n = 13), primary melanoma (n = 27) and metastases (n =37) samples were stained with rabbit anti-RAGE antibodies and analyzed for subcellular localization of intracellular RAGE by two blinded individuals. The intracellular distribution of RAGE was illustrated on a percentage basis (black: nuclear, dark grey: nuclear >cytosolic, light grey: cytosolic > nuclear; white: cytosolic, upper panel) and compared between the different tissue types. Illustrative pictures (scale = 25 µm) are displayed in the lower panel (**A**). Cellular localization of RAGE in melanoma cell lines (upper panel: white: cytosolic, black: nuclear; lower panel: illustrative pictures, 1st row: permeabilized; 2nd row: non-permeabilized control, rabbit-anti-RAGE; scale = 25 µm) (**B**). (**p < 0.005, ***p < 0.0001, unpaired student's t-test)

RAGE has been mainly described as receptor present on the cell membrane or as cytosolic molecule; in fact, there is only one publication describing translocation of the cytosolic tail of

RAGE into the nucleus [250]. This raised the question which of the multiple forms of RAGE accumulate in the nucleus of benign nevi and to a significantly lower extend in melanomas. Furthermore, the mechanism behind the translocation was never investigated, although it was demonstrated that the shed cytosolic tail can translocate into the nucleus [250].

VIII.6.2. Subcellular prediction tools revealed a potential role of RAGE as nuclear protein, and predicted NLS and NES as a potential transport mechanism

To address this question, fl-RAGE (Uniprot ID: Q1509-1) as well as described isoforms were characterized *in silico* for features known to be important or obstructive for translocating proteins into the nucleus, such as the presence of a signal peptide, phosphorylation, glycation, and SUMOylation sites, and the existence of nuclear localization (NLS) and export signals (NES) (Table 16).

In 1999, Günter Blobel described the signal peptide as intrinsic signal that governs protein transport and localization in the cell [385]. Its existence potentially enables the protein to translocate to the endoplasmatic reticulum from where it is later passaged to the secretory pathway. *In silico* prediction using the computational online tool Signal P3.0. verified fl-RAGE as well as 15 RAGE isoforms to harbor signal peptides (Table 16). However, not every protein with signal peptide is secreted and *vice versa* its absence does not exclude protein secretion, as one can see in terms of HMGB1 and the S100 proteins [275, 293].

Taking advantage of the classification system CELLO, RAGE variants were assigned to subcellular localizations based on the physico-chemical properties of their amino acids [362]. Indeed, next to predictions of RAGE secretion to the extracellular space, cytosolic and mitochondrial localization, a large amount of isoforms (15/20) was allocated to the nucleus (Table 16).

In addition, potential NLS and NES were detected by two different algorithmic NLS prediction tools (NLStradamus, cNLS Mapper) and by one for NES (NetNES). By applying these tools, five isoforms with potential NLS and 18 with potential NES were identified. Four of the predicted NLS-containing isoforms showed NES with an amino acid (aa) length larger than five aa, namely RAGE_v16 / Q15109-2, RAGE_v6 / Q15109-4, RAGE_v8 / Q15109-8, and Q15109-10 (Table 16). RAGE_v5 / Q15109-6 contained a potential NES of only one amino acid, and was therefore ranked lower.

HUGO nomencl.	Uniprot ID	Length (aa)	Notes	Signal P3.0	CELLO	NLStradamus	cNLS Mapper	NetNES (# of aa)	NLS & NES?	Net-Phos	Net-PhosK	Net-O-Glyc 3.1.	Net-N-Glyc 1.0.	SUMO-sp
RAGE	Q15109-1	404	full-length RAGE	1	Nuc	N	N	1	N	15	PKC	6	2	2
RAGE_v16	**Q15109-2**	342	hRAGEsec	1	Nuc**	Y	N	6	Y	12	PKC	7	2	0
RAGE_v1, RAGE_v10	Q15109-3	347	esRAGE , sRAGE	1	Nuc	N	N	1	N	13	PKC	7	2	2
RAGE_v6	**Q15109-4**	363		1	Nuc	N	Y*	5	Y	15	PKC	7	2	2
RAGE_v12	Q15109-5	121		1	Nuc** Mito*	N	N	1	N	2	PKA	0	2	0
RAGE_v5	**Q15109-6**	420		1	Nuc*	N	Y*	1	Y	15	PKC	8	2	2
RAGE_v4	Q15109-7	390		1	Cyto	N	N	1	N	14	PKC	9	2	2
RAGE_v8	**Q15109-8**	325		1	Nuc* cyto*	Y	N	6	Y	12	PKC	5	2	0
RAGE_v9	Q15109-9	355		1	Nuc**	Y	N	1	N	15	PKC	8	2	0
	Q15109-10	386		1	extracellul	Y	Y	6	Y	17	PKA	6	2	2
RAGE_v2	Q101R2	303	N-truncated (Nt) RAGE	0	Nuc* Cyto	N	N	1	N	13	PKC	9	0	2
RAGE_v3	Q15109	293	Δ8-RAGE	1	Cyto* Nuc	N	N	1	N	14	PKC	7	2	2
RAGE_v7	Q101R5	323		1	Mito* Nuc	N	N	6	N	12	PKC	8	2	0
RAGE_v11	Q3L1R3	36		0	Mito* Nuc*	N	N	1	N	3	PKA	1	0	0
RAGE_v13	Q3L1R2	153		1	extracellul*	N	N	0	N	4	PKA	1	2	0
RAGE_v14	Q71BB6-1	50	sRAGE1	0	extracellul*	N	N	7	N	2	CDK5	1	0	0
RAGE_v15	Q71BB6-2	50	sRAGE3	0	extracellul*	N	N	7	N	2	CDK5	1	0	0
RAGE_v17	E9LVY7	149	NtRAGEΔ	0	Nuc*	N	N	6	N	7	PKC	5	0	0
RAGE_v18	E9LVY6	335	sRAGEΔ	1	Nuc*	N	N	1	N	12	PKA	7	2	2
RAGE_v19	E9LVY5	388	RAGEΔ	1	Nuc*	N	N	1	N	15	PKC	7	2	2

Table 16 *In silico* prediction revealed potential NLS and NES in RAGE isoforms. Full-length RAGE (RAGE) and its isoforms (labeled using HUGO terminology and/or Uniprot ID) were screened for features, predicting their subcellular localization, such as the existence of signal peptides (SignalP3.0), and physico-chemical properties of their aa (CELLO). NLS and NES were predicted using the computational prediction tools NLStradamus; cNLS Mapper (*scores > 8, indicated strong NLS activities), and NetNES (*Y*: Yes, predicted site is present; *N*: No potential site detected; *highlighted (orange)*: isoforms predicted to contain both signals). Posttranslational modifications with potential regulatory effect on subcellular localizations were predicted: Potential phosphorylation sites (NetPhos) and correspondend kinases (PhosK), O- (Net-O-Glyc 3.1) and N- (Net-N-Glyc 1.0) glycosylation sites, SUMOylation sites (SUMO sp). All prediction tools were run using the highest stringency settings.

Furthermore, also potential posttranslational modifications, which might be involved in a regulation of the cytosol/nucleus-shuttling were characterized *in silico*. For instance, a quantitative (amount) and qualitative (highest score) prediction of phosphorylation sites and correspondent kinases was performed. Fl-RAGE showed 15 potential phosphorylation sites, with highest score at aa position 172, which is predicted to be a substrate for PKC. In fact, 13 of the 20 (13/20) analyzed RAGE variants were predicted to be substrates for PKC. Nevertheless, also variants were identified, which were predicted to be phosphorylated by PKA or cyclin-dependent kinase 5 (CDK5). Furthermore, fl-RAGE as well as most other splicing forms were *in silico* predicted to contain O- (19/20) and N-glycosylation (15/20) sites. In contrast, posttranslational modification by SUMOylation was only predicted for half of the splice variants (10/20).

VIII.6.3. Melanoma cells exhibit a unique RAGE splicing factor expression

Showing that structural properties potentially enable some RAGE variants to translocate into the nucleus, did not solve the question, why the nuclear expression was shown to be characteristic for benign nevi but not for melanoma (Figure 9). A possible explanation would be a differential expression of distinct RAGE variants upon malignant transformation. To address this possibility the splicing factors HNRNP A1, HNRNP H, and TRA2-β1, which have been demonstrated not only to favor specific RAGE isoforms but further to be deregulated in diseases such as Alzheimer ’s [240, 241], were analyzed.

Comparative analysis of transcript levels of these splicing factors between normal skin, benign nevi, and melanoma samples was accomplished using microarray data incorporated in the Oncomine database provided by Talantov and colleagues [386]. *HNRNP A1* transcript levels were found to be significantly downregulated in melanoma tissue in comparison to normal skin and benign nevi (Figure 10A, ***$p < 0.0001$). Additionally, melanoma cells displayed a downregulation of *HNRNP H* transcripts when compared to normal skin samples (***$p < 0.0001$). However, these alterations were also found for benign nevi, suggesting a deregulation of HNRNP H as early event in melanocyte transformation (Figure 10B, *$p < 0.05$). In terms of TRA2-β1, transcript levels were found to be significantly downregulated

in melanoma when compared to benign nevi (**p <0.005), but not to normal skin samples (Figure 10C).

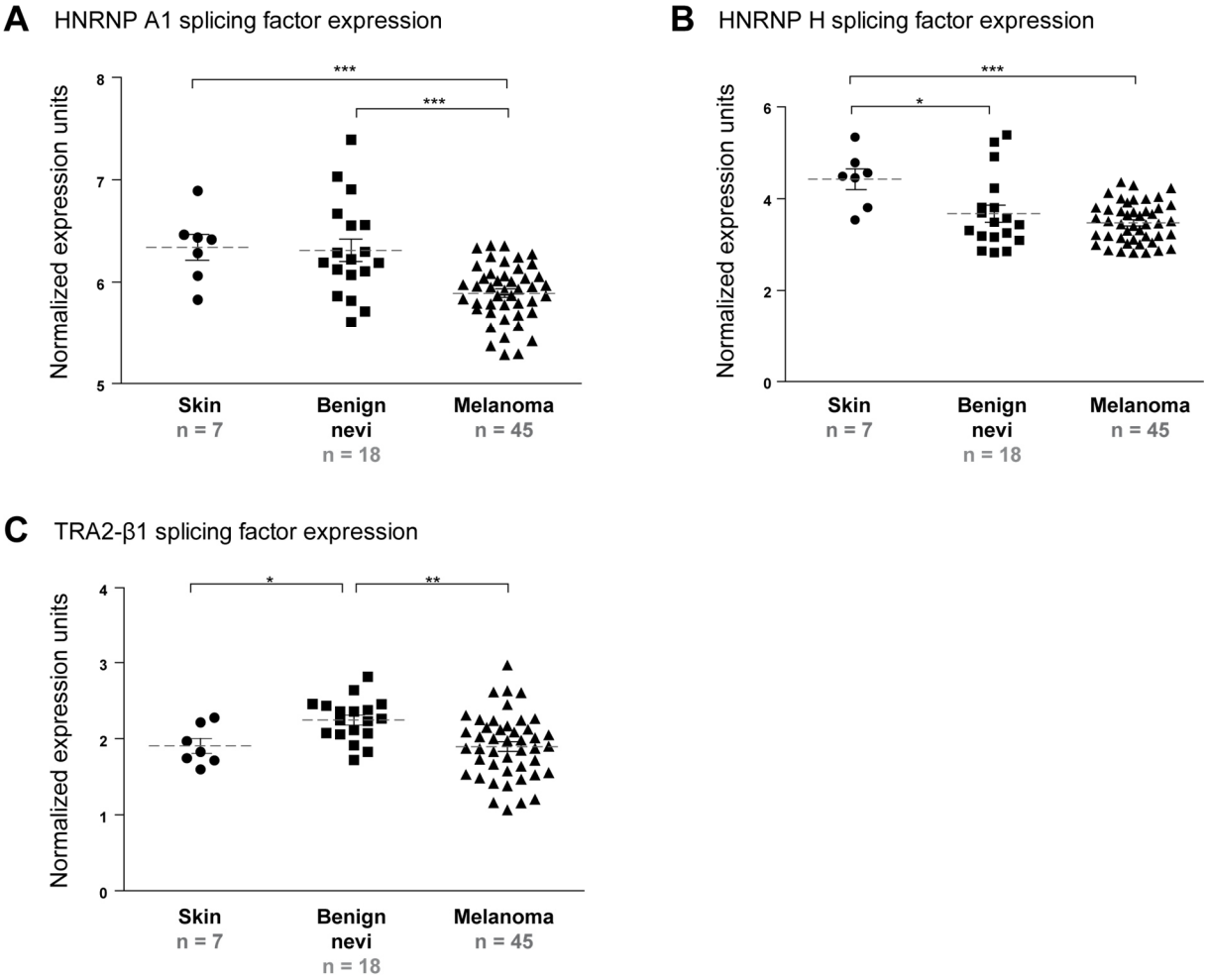

Figure 10 **Melanoma-specific pattern of RAGE splicing factor expression.** Comparative expression analysis of the RAGE splicing factors HNRNP A1, HNRNP H, TRA2-β1 based on data of a human genome U133A array [386] provided by the Oncomine database. Illustrated are the transcript levels of *HNRP A1* (**A**), *HNRNP H* (**B**), *TRA2-β1* (**C**) in control skin (n = 7), benign nevi (n = 18), and melanoma samples (n = 45) in normalized expression units compared to the reporter. (*p < 0.05, **p < 0.005, ***p < 0.0001, unpaired student‘s t-test)

Summing up these results, the comparative analysis of *HNRNP A1*, *HNRNP H*, and *TRA2-β1* revealed a melanoma-specific expression pattern of these factors, strongly recommending a unique RAGE splicing signature in melanoma. Differences in RAGE splicing might therefore represent one factor controlling RAGE protein localization.

VIII.6.4. RAGE isoforms depend (at least partially) on proteins of the import-/export machinery, such as CRM-1

Since the *in silico* characterization of RAGE variants also revealed the existence of potential NLS and NES sites, a deregulated import-/export-machinery might be another factor leading

to aberrant localization of RAGE in malignant melanoma. Indeed, studies claimed an upregulation of proteins controlling the nuclear export in melanoma [387].

Comparative analysis of export machinery proteins, such as CRM-1 and RANBP1, using a human genome array comprising normal skin, benign nevi and melanoma samples, demonstrated a significant upregulation of these molecules in melanoma compared to healthy tissues (Figure 11A, B, *p < 0.05, ***p < 0.0001).

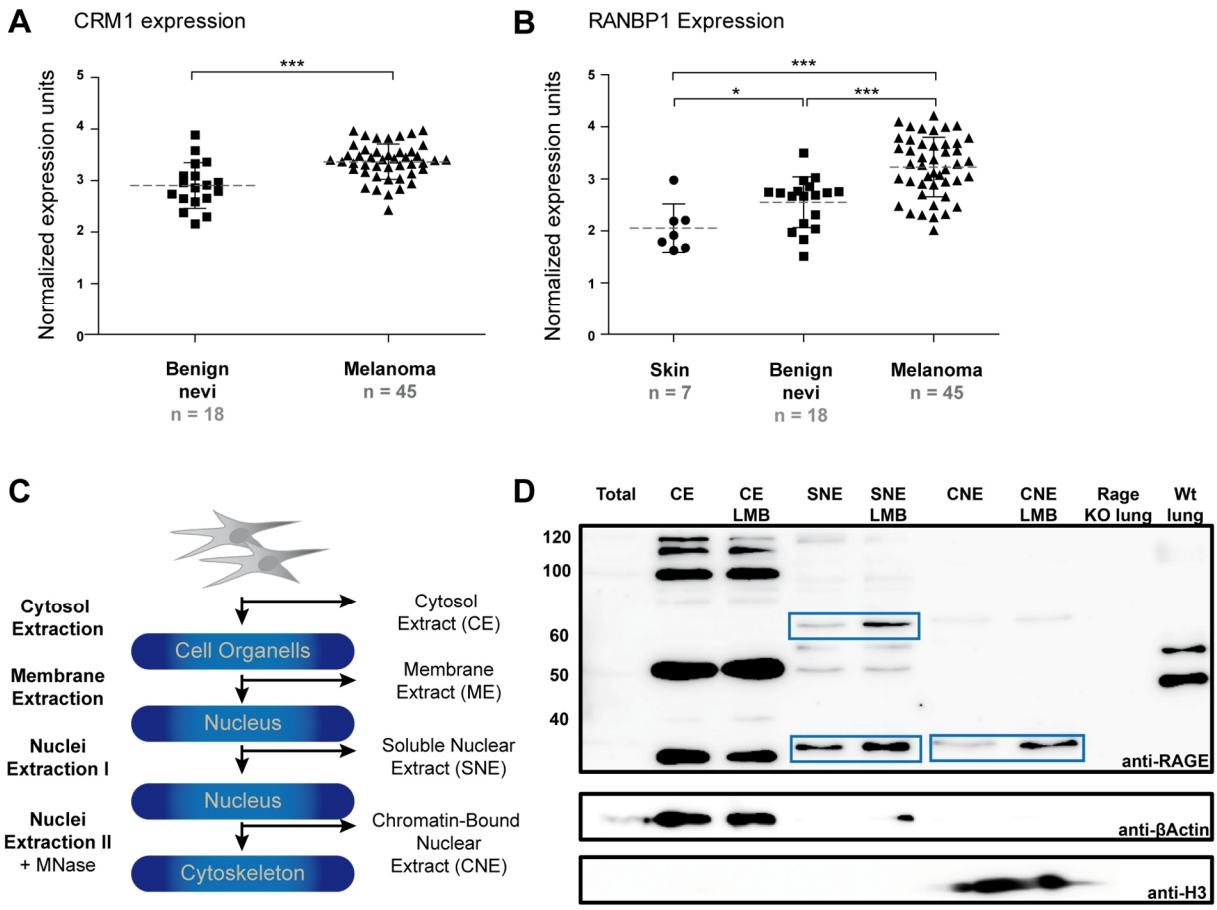

Figure 11 Nuclear/cytosol-shuttling of RAGE depends, at least partially, on NES-mediated export by CRM-1. Comparative expression analysis of the nuclear export proteins CRM-1 and RANBP1 based on data of a human genome U133A array [386] provided by the Oncomine database. Illustrated are the transcript levels of *CRM-1* (**A**), and *RANBP1* (**B**) in normal skin (n = 7), benign nevi (n = 18), and melanoma samples (n = 45) in normalized expression units compared to the reporter. Protein suspensions (30 µg) of cytosol (CE), soluble nuclear (SNE), and chromatin-bound nuclear extract (CNE) from the subcellular protein fractionation of MelSTV cells (method scheme (**C**)) were separated *via* SDS-gel electrophoresis, blotted onto PVDF membranes and incubated with rabbit-anti-RAGE antibodies, while antibodies against histone 3 (H3) and βACTIN served as purification controls (**D**). MelSTV cells used for this experiment were either untreated (DMSO only) or treated with the CRM-1 inhibitor Leptomycin B (LMB, 4nM) prior lysis. Rage$^{-/-}$ and wildtype lung lysates served as internal antibody control. Signals were visualized using ECL™ Western Blotting Detection Reagents and the ImageQuant LAS biomolecular imager. (*p < 0.05, ***p < 0.0001, unpaired student's t-test)

To verify the nuclear expression of RAGE in melanocytic cells and to prove if RAGE translocation is in fact depending on the import-/export-machinery a subcellular fractionation

of the MelSTV cell line was performed. This cell line was not only chosen because it displays best the situation in normal human melanocytes but because the finding that melanoma cells differentially express splicing factors regulating the expression of RAGE isoforms might favor variants lacking NLS and NES.

MelSTV cells were separated in a step-wise manner into cytoplasmic (CE), membrane (ME), nuclear soluble (SNE), chromatin-bound (CNE) and cytoskeletal protein extracts (PE) using special extraction buffers, which address the physical properties of the distinct subcompartments (Figure 11C). In order to test if cytosolic/nuclear-shuttling of RAGE depends on exportins, such as CRM-1, some cells were treated with the CRM-1 inhibitor Leptomycin B (LMB) prior lysis. CE, SNE, and CNE lysates (30 µg) of untreated and LMB-treated MelSTV were then separated *via* SDS-gel electrophoresis and transferred onto PVDF membranes. After blocking, membranes were either incubated with a primary antibody recognizing both, human and murine RAGE, or antibodies against histone 3 (H3) as nuclear and βACTIN as cytosolic loading control. Lysates of murine Rage$^{-/-}$ and wildtype lungs served as control for antibody specificity.

The detection of RAGE isoforms within the SNE and CNE of MelSTV cells (Figure 11D) verified the nuclear appearance of RAGE in melanocytic cells found in the TMA (Figure 9). Interestingly, immunoblotting detected signals in the nuclear fraction, which did not appear in the cytosolic extract, at least with the protein concentration and illumination time used in these experiments. For instance, proteins with a molecular mass of approximately 60 kDa appeared in SNE and CNE, but not in the cytosolic extract. Noteworthy, with 404 aa fl-RAGE is the largest protein of the different variants (Table 16) resulting in a molecular mass of approximately 55 kDa [216]. In the SNE and CNE bands for proteins with approximately 20 to 30 kDa were detected, as well as the aforementioned band with around 60 kDa. Within the SNE additional variants between 50 to 60 kDa, and bands illustrating higher-weight molecules with 80 to 120 kDa were detected (Figure 11D). Noteworthy, bands for 80 to 120 kDa molecules were also detected by blotting immunoprecipitations of RAGE from nuclear lysates (data not shown), and disappeared upon shRNA-mediated knockdown in the B16F10 model (Figure 6B). All these experiments were performed under denaturating conditions. If these higher-order complexes are homo- or heteromultimers with strong disulfide bonds, or posttranslationally modified proteins can only be assumed at this time. Most interestingly, the signals for the 60 kDa band was markedly increased in the SNE, when cells were treated with LMB prior lysis. Furthermore, signals of bands illustrating proteins with a molecular mass of approximately 30 kDa, were also enhanced in SNE and also in CNE after LMB treatment (Figure 11D).

These results strongly recommend an isoform-dependent subcellular localization of RAGE in melanocytic cells. Nuclear expression of the proteins seems to at least partially depend on the import-/export machinery, and thereby on the existence of NLS and NES within RAGE variants.

VIII.6.5. Potential role of RAGE as DNA-binding transcription factor

The nuclear presence of RAGE in melanocytic cells raises questions about the function of nuclear RAGE. Proteins within the nucleus can possess various functions. Besides acting as transcription factor by regulating gene expression, they can also function as so-called 'scaffold' proteins tethering signaling components and localizing those to specific areas within the nucleus. Other functions include packaging of the DNA as well as processing and import or export of RNA molecules or of nuclear proteins.

A first step in elucidating the role of a protein within the nucleus, is to estimate the time the proteins spends there. This indicates if the proteins might be involved in transporting molecules in and out of the nucleus, or if they have a more complex role within the nucleus. Therefore, all isoforms were then analyzed with an *in silico* prediction tool, namely NucPred, which provides information on the time a protein most probably spends in the nucleus (Figure 12A). Interestingly, by comparing these values for isoforms lacking potential NLS and NES (0.1393 ± 0.02069) with isoforms predicted to harbor both (0.2980 ± 0.05678), the latter showed a significantly higher score and were accordingly claimed to spend more time in the nucleus (Figure 12B).

To further approach the nuclear function of RAGE, variants were screened for the existence of potential DNA binding sites by applying algorithms of the BindN tool. These are based on sequence features, such as side chain acidity values, hydrophobicity index, and molecular mass of the respective amino acids [379].

The analysis showed that all isoforms contained potential DNA binding sequences, ranging from one to three alternative motifs within one molecule (Figure 12A). Whereas the observed average number of binding motifs (BM) for RAGE variants without NLS/NES was one to two (1.786 ± 0.2143), molecules with NLS/NES showed between two to three (2.800 ± 0.2000) different BMs (Figure 12C). These observations point towards the existence of structural differences of RAGE variants when compared to fl-RAGE, which is illustrated in Figure 12D.

A

HUGO nomencl.	Uniprot ID	Length (aa)	NLS & NES?	NucPred Score	Binding Motifs (#)
RAGE	Q15109-1	404	N	0,17	2
RAGE_v16	**Q15109-2**	342	Y	0,1	2
RAGE_v1, RAGE_v10	Q15109-3	347	N	0,07	2
RAGE_v6	**Q15109-4**	363	Y	0,26	3
RAGE_v12	Q15109-5	121	N	0,04	1
RAGE_v5	**Q15109-6**	420	Y	0,32	3
RAGE_v4	Q15109-7	390	N	0,18	2
RAGE_v8	**Q15109-8**	325	Y	0,39	3
RAGE_v9	Q15109-9	355	N	0,34	3
	Q15109-10	386	Y	0,42	3
RAGE_v2	Q101R2	303	N	0,21	3
RAGE_v3	Q15109	293	N	0,18	3
RAGE_v7	Q101R5	323	N	0,09	2
RAGE_v11	Q3L1R3	36	N	0,03	1
RAGE_v13	Q3L1R2	153	N	0,14	1
RAGE_v14	Q71BB6-1	50	N	0,16	1
RAGE_v15	Q71BB6-2	50	N	0,16	1
RAGE_v17	E9LVY7	149	N	0,1	1
RAGE_v18	E9LVY6	335	N	0,05	2
RAGE_v19	E9LVY5	388	N	0,17	1

B

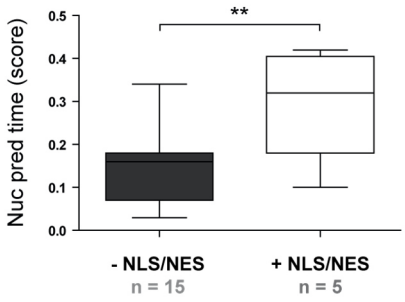

C

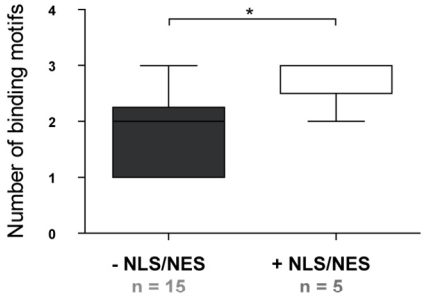

D

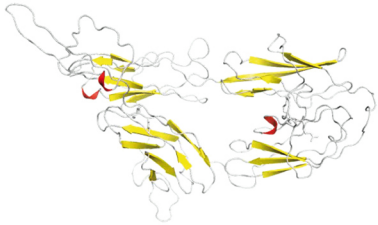

E

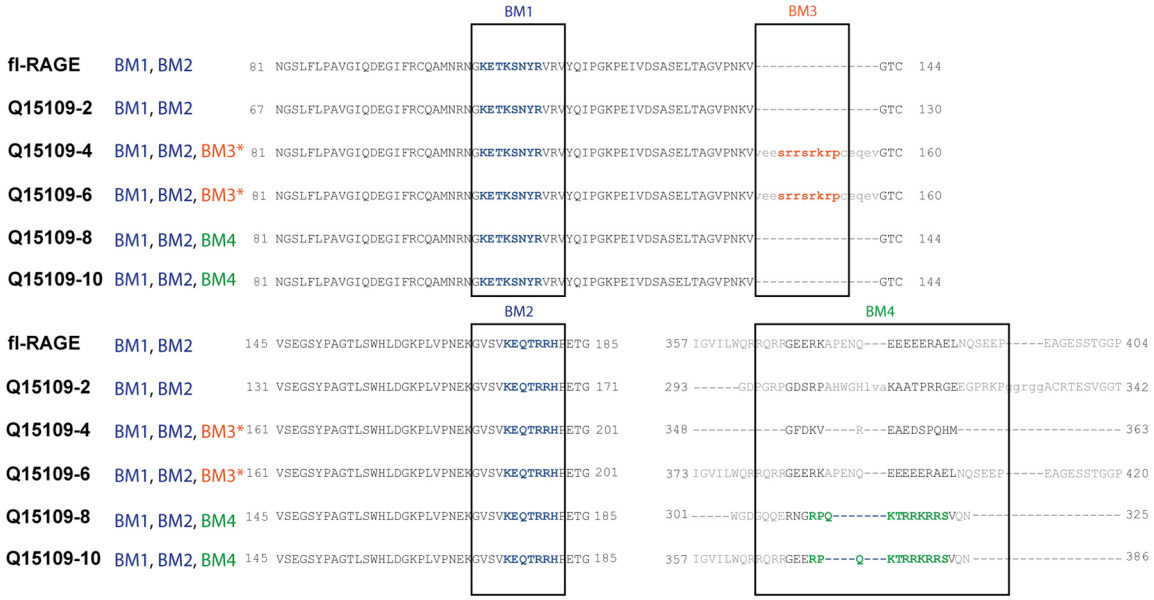

*BM3 is exclusive for NLS/NES containing isoforms and not expressed in any of the other RAGE variants.

Figure 12 Predicted DNA-binding sites within RAGE variants point towards a potential role as transcription factor. Fl-RAGE (RAGE) and its isoforms (labeled using HUGO terminology and/or Uniprot ID) with (highlighted in orange) or without predicted NLS/NES were screened for the time they probably spend in the nucleus (NucPred, scoring range: 0 (short residence) to 1 (long residence)), and for potential DNA binding sites based on their physico-chemical properties (**A**). Number of potential DNA binding sites were predicted using the computational prediction tool BindN. All prediction tools were run using the highest stringency settings. Comparative analysis of nuclear residence (Nuc pred time) (**B**) and numbers of DNA binding sites (**C**) between variants with or without NLS/NES was performed. The mean Nuc pred time of RAGE variants without NLS/NES was calculated as 0.1393 ± 0.02069, and for variants with NLS/NES as 0.2980 ± 0.05678 (**B**). On average, variants lacking NLS/NES showed 1.786 ± 0.2143, and NLS/NES-containing RAGE forms 2.800 ± 0.2000 DNA binding sites (**C**). The structure of fl-RAGE is illustrated in (**D**). Amino acid sequence alignment of RAGE variants with NLS/NES and illustration of identified DNA binding motifs: KETKSYNR (BM1), KEQTRRH (BM2), SRRSRKRP (BM3), KTRRKRRS (BM4) (**E**). BM3 was elusive for two NLS/NES-containing RAGE variants, but not found in RAGE forms without NLS/NES. (*$p < 0.05$, **$p < 0.005$, unpaired student‘s t-test)

Investigating the observed DNA binding motifs in more detail elucidated two general binding sites, from here on referred to as BM1 and BM2, which were found in fl-RAGE as well as in most of the other variants. BM1 composed of the aa sequence KETKSYNR and BM2 of KEQTRRH (Figure 12E). In addition, additional BMs were found for RAGE variants, which were not present in fl-RAGE: SRRSRKRP (BM3), KTRRKRRS (BM4). Whereas the binding motif labeled as BM4 was found in several variants with and without NLS/NES, BM3 was elusively found in two isoforms, both harboring predicted NLS/NES.

To sum up, all this *in silico* predictions strongly recommend distinct nuclear functions of RAGE variants, which might also include direct binding of DNA. However, this needs to be verified in *in vitro* assays comprising methods such as site-directed mutagenesis. For some BMs site-directed mutagenesis was already successfully established, and verified using restriction-digest based methods and sequencing analysis (data not shown). Studies including exogenous expression of these mutants and functional analysis, as well as mass spectrometry for identifying nuclear interaction partners will be essential for further examination of the roles of nuclear RAGE.

Although some *in silico* predictions highlighted RAGE variants with predicted NLS and NES, a contribution of RAGE isoforms lacking these sequences was not excluded, and thereby requires consideration in further examinations.

IX. Discussion

IX.1. RAGE acts on *in trans* control elements thereby driving genomic instability in melanoma

Genomic instability is a hallmark of cancer cells but in particular it is a hallmark for malignant melanoma, where the mutation frequency is even higher compared to most other solid tumors [34]. Genomic aberrations have also been found in benign nevi suggesting an early role for the loss of genomic integrity in melanomagenesis. Furthermore, non-metastatic tumors have been demonstrated to be genomically more stable than metastatic ones, illustrating genomic instability as an ongoing process [51, 53, 54]. Interestingly, *AGER* transcript levels correlate to this pattern: After a first upregulation in benign nevi, they further increased upon transformation to melanoma (Figure 2A).

All cells of our body are perpetually confronted with different types of DNA damage. It has been estimated that cells experience approximately 100,000 spontaneous DNA lesions, daily [388]. Different sources are contributing to DNA damage including exogenous factors, such as UV radiation. However, the majority of this damage is generated endogenously, for instance, by production of ROS [388]. Interestingly, upon RAGE overexpression melanocytic as well as melanoma cells displayed an increased generation of ROS, indicating an elevated cell-intrinsic stress level (Figure 7A). For protecting genome integrity cells developed highly regulated elements, preserving the genome and mediating cellular responses to occurring DNA damage. Among those so-called *in trans* elements involved in replication, cell cycle checkpoints, and DNA damage recognition are listed [389]. However, a complete protection against genomic instability cannot be guaranteed. Occurring mutations are often concentrated to specific instability hotspots, such as fragile sites and highly transcribed DNA sequences, defined as *in cis* elements. Recent studies including whole-exome sequencing data from melanoma tumor/normal pairs revealed great advances in characterizing *in cis*-acting elements in malignant melanoma [10]. Noteworthy, the analysis of a panel of human melanoma cell lines harboring different *in cis* elements, such as *BRAF* and *NRAS* mutations, did not reveal a distinct pattern for RAGE expression in this study (data not shown). The impact of *in trans*-acting elements as well as mechanisms of their regulation or dysregulation in melanoma remain vague. A role for these elements is provided by the fact that patients with *xeroderma pigmentosum* (XP), a rare disease caused by mutations in DNA repair genes, exhibit a 1000 - fold higher frequency combined with early onset of malignant melanoma [59].

In this study, the impact of RAGE overexpression or knockdown on *in trans*-acting elements in the human A375 and the murine B16F10 melanoma cell line was investigated (Figure 5 & 6). More specifically, transcript levels of molecules involved in ATM/ATR signaling, nucleotide excision repair (NER), base excision repair (BER), mismatch repair (MMR), double-strand break repair (DSB), other DNA repair genes, apoptosis, and cell cycle (for complete transcript list, see Table 13) were analyzed. Since the RAGE ligand HMGB1 is a well-known factor for maintenance of genome integrity, an indirect mechanism of action for RAGE was ruled out by demonstrating that RAGE overexpression was not accompanied with upregulated *HMGB1* levels in the tested MelSTV, A375 or MeWo cell lines (Figure 5B).

Instead, experiments performed on human as well as on murine cells consistently identified RAGE as negative regulator of elements involved in DNA repair, cell cycle control, and apoptosis (Figure 5C, 6C). More specifically, gene expression analysis revealed that RAGE overexpression in the human A375 cell line was associated with a downregulation by 26 % (21/79) of the analyzed gene transcripts involved in DNA repair, cell cycle control, and apoptosis (Figure 5C). In the murine system, an even greater effect was recorded: shRNA-mediated Rage knockdown in the B16F10 cell line was accompanied with *vice versa* upregulation by 44 % (35/79) of the gene transcripts (Figure 6C). However, not only differences in the extent of regulatory interference by RAGE were reported, but also affected pathways were found to be species-specific. Major pathways in the human system were DSB repair, BER, and NER, whereas in the murine system the majority of differentially regulated genes were found in ATM/ATR signaling, MMR, and cell cycle.

In 2011, Zhang and colleagues evaluated 1,463 genetic variants across 60 DNA repair–related pathway genes in relation to melanoma risk, thereby identifying SNPs in *ATR* and *PARP1* to correlate most significantly with a higher risk to melanoma [63]. Interestingly, the expression of these two genes was found to be dependent on RAGE in both applied systems, human and mouse (Figure 5E, 6E).

Furthermore, the comparative analysis of transcript levels of genes, known to be affected in XP, revealed a RAGE-dependent dysregulation of *XPC* and *ERCC2* transcription in the human system, and with *Xpc*, *Xpa*, *Ercc1*, *Ercc2* for the murine B16F10 cell line (Figure 5E, 6E). Together, these results clearly demonstrate that RAGE is able to impair genomic integrity in human and murine melanoma cells. For tumors, including melanoma, an achieved genomic instability due to downregulation of DNA repair molecules favors additional acquirement of mutations, thereby allowing the generation of new tumor variants with growth advantages or immunoedited variants [390]. This is also indicated by the finding that the RAGE-dependent downregulation of DNA damage molecules was associated with a better survival *in vitro*, at least under non-toxic conditions (Figure 4D, E).

DSB repair signaling was found to be the major pathway affected upon RAGE overexpression in the human melanoma cell line (Figure 6D). DSBs occur when the phosphate-sugar backbones of both DNA strands are broken at the same position or in close proximity, leading to a physical dissociation. Cancer genome sequencing studies uncovered numerous chromosomal rearrangements harboring pathological DSB repair signatures, thereby demonstrating that not only DSBs themselves but also their misrepair contribute to genomic instability and tumorigenesis. In contrast to single-strand breaks, restoration of DSBs is more problematic, since the genetic information cannot be easily retained from the complementary strand. Therefore, DSBs might lead to fragmentation, loss, or rearrangement of chromosomes [391]. A RAGE/Rage-dependent dysregulation of DSB repair molecules was detected in the human melanoma cell line as well as in the murine B16F10 melanoma (Figure 5C, 6C). The fact that defects in DSB repair also favor melanoma growth *in vivo*, has been demonstrated by the loss of expression of DNA DSB-repair genes in human melanoma. For instance, MLH1 was demonstrated to be lost completely in 60 % of primary melanomas, and also losses of H2AX have been reported [392-394]. Noteworthy, in this study RAGE/Rage was identified as a negative regulator of gene expression for both of these proteins in melanoma (Figure 5D, 6D).

The finding that metastatic tumors are genomically less stable combined with the results of the study from Leclerc and colleagues, demonstrating an upregulation of RAGE protein between stage III and stage IV melanomas, further indicated a correlation of genomic instability and RAGE expression in malignant melanoma [51, 53, 54, 280]. Indeed, in our study the TMA analysis also revealed a higher RAGE expression in metastases compared to primary melanomas (Figure 2B). However, the observed differences were not significant, which may be caused by the small number of samples analyzed.

IX.2. RAGE establishes and drives melanoma hallmarks such as resistance to cell death, proliferative signaling, and enhanced invasion capacity

Cancer cells display common characteristics, so-called cancer hallmarks; however, mechanisms causing these features are divergent between tumors of different localization and type. Elevated *AGER* transcript levels in benign nevi compared to normal skin (Figure 2A) might suggest a role for RAGE in early events during transformation of normal human melanocytes to melanoma.

The basis for all cellular functions of normal or transformed cells is created by an efficient cell metabolism. However, cancer cells seek ways to adapt cell metabolism to suit their altered functional properties, indicating that metabolic reprogramming represents an important

component of malignant transformation [395]. A role for RAGE in regulating cell metabolism was first demonstrated by Kang and colleagues in pancreatic cancer cells [249].

In order to investigate if RAGE might drive transformation of melanocytic and progression of melanoma cell lines by adapting cell metabolic activity, *in vitro* overexpression of RAGE in the melanocytic cell line MelSTV, as well as in two melanoma cell lines, A375 and MeWo, was performed (Figure 3E). Cell metabolism comprises metabolic reactions converting biochemical energy from nutrients into ATP, the so-called 'molecular unit of currency'. The production of ATP is accompanied by the generation of coenzymes like nicotinamide adenine dinucleotide hydride (NADH) or flavin adenine dinucleotide hydroquinone ($FADH_2$). The levels of these coenzymes were measured by the alamarBlue® method and used for illustrating cell metabolic changes in this study [396]. As expected, lowest basal cell metabolic activity was found for the melanocytic MelSTV cell line, whereas highest was exhibited by MeWo (data not shown). Upon RAGE overexpression the basal cell metabolic activity levels in both melanocytic and melanoma cell lines increased by approximately 50 % (Figure 3E).

Kang and colleagues demonstrated that altered cell metabolic activity was caused by cytosolic but not membrane-bound RAGE in a HMGB1-dependent manner [249]. However, since the study was not addressing different RAGE isoforms, their roles in maintaining and regulating tumor cell bioenergetics remain unclear. Reverting RAGE overexpression in the melanoma cell lines using siRNA targeting *AGER* transcripts, did not only significantly return cell metabolic changes to their baseline condition, instead it even seemed to further impair cell metabolism in both melanoma cell lines, although this was not significant (Figure 4C). However, this indicates a potential role for other RAGE isoforms in maintaining and driving tumor cell bioenergetics. In their study, Kang *et al.* were able to demonstrate that HMGB1-induced MEK-ERK-MAPK pathway activation resulted in the phosphorylation of cytosolic RAGE leading to its consequent translocation into the mitochondria, where it induced ATP production [249]. Since the hyperactivation of the MAPK pathway represents a hallmark of melanoma cells, a comparable regulatory function for RAGE might be conceivable.

The fact that melanoma cells display enhanced and deregulated bioenergetics was also supported *in vivo* by the detection of high lactate dehydrogenase (LDH) levels in the blood of melanoma patients. Indeed, melanoma cells seem to deregulate their cell metabolism by favoring glycolysis and impairing citric acid cycle [89-91]. Although glycolysis is in general less efficient compared to the citric acid cycle regarding ATP production, glucose degradation provides cells with intermediates needed for biosynthetic pathways and is also accompanied with higher levels of NADH [395]. Therefore, the elevated coenzyme levels detected by alamarBlue® (Figure 3E, 4C), could not only represent a higher metabolic

activity upon RAGE overexpression, but also a shift of the equilibrium between bioenergetic pathways towards glycolysis. Further investigations including quantitative analysis of mitochondrial RAGE in melanocytes and melanoma, as well as RAGE isoform-specific approaches need to be performed in order to further elucidate the effect of RAGE on cancer cell metabolism.

However, ATP and coenzymes like NADH or $FADH_2$ are not the only molecules generated during cell metabolism. In fact, in normal cells the activity of the mitochondrial electron transport correlates to levels of reactive oxygen species (ROS) [382]. This could not only be verified for the melanocytic cell line MelSTV but also for both melanoma cell lines. More precisely, RAGE overexpression was accompanied with a 1.2- to five-fold higher ROS production compared to control cells (Figure 7A). When generated at low picomolar levels, ROS have been demonstrated to induce tumor cell proliferation, which led to the development of therapeutic strategies targeting tumor proliferation by alleviating intracellular ROS levels [397, 398].

Indeed, upon RAGE overexpression cell proliferation, measured by CSFE dilution, was found to be significantly higher, at least for MelSTV and A375 cells. For MeWo cells the same tendency was observed (Figure 3F). Furthermore, comparative analysis of RAGE overexpressing A375 (A375 RAGE OE) and control cells revealed a dysregulation of 8 % of the cell cycle-associated genes upon overexpression (Figure 5C). As mentioned above, melanoma cells display a high plasticity, and the existence of two distinct cell states. One can distinguish between melanomas and melanoma cell lines with a more ‘proliferative’, or a more ‘invasive’ phenotype. In 2012, Widmer and colleagues generated a systematic classification model in order to distinguish between the two states of melanoma cells by phenotype-specific gene expression mapping. In this study, MeWo cells were characterized as more ‘proliferative’, whereas A375 were defined as an ‘invasive’ melanoma cell line [98]. Indeed, the results for the basal cell metabolic activity (data not shown), with highest values for MeWo cells, verified this finding. A high basal proliferation level might therefore be the reason, why RAGE overexpression did not reveal such a tremendous effect on MeWo cells compared to MelSTV and A375 cells (Figure 3F).

As mentioned before, early melanoma growth often comprises a radial growth phase, characterized by uncontrolled proliferation of melanoma cells, followed by a vertical growth phase, in which the proliferating cells acquire additional features enabling them to invade to new metastatic sites [5, 6]. Upon RAGE overexpression also a significant increase in invasion capacity was demonstrated, this time in MelSTV and MeWo cells, thereby again supporting the hypothesis that A375 and MeWo cell lines present distinct phenotypes (Figure 3G). Indeed, comparing basal invasion levels lowest invasion capacity was found for

MelSTV, and highest for A375 cells. Evidence for a correlation of RAGE expression and invasiveness has been provided for gastric and prostate cancer by the studies of Kuniyasu and colleagues [343, 345]. A possible mechanism explaining the RAGE-dependent increase in invasion capacity, at least for the skin, might be an upregulation of matrix metalloproteinases, such as MMP9, and thereby of the proteolytic activity of skin cells as reported by Zhu and colleagues [399]. Furthermore, a role of RAGE in inducing angiogenesis in melanoma, thereby facilitating metastatic spread, has been suggested; however, studies regarding this topic created conflicting results [356, 357].

In this study, there were neither morphological alterations of melanocytic, nor melanoma cell lines detected upon RAGE overexpression (Figure 3B). Meghnani and colleagues claimed a function of RAGE in EMT-like processes in melanoma, accompanied with the establishment of mesenchymal-like morphologies, higher migration abilities and reduced proliferation properties [358]. In the study presented, the finding that RAGE promotes proliferation as well as invasion in a melanoma cell line-specific manner, provides evidence that its function in melanomagenesis is not favoring one phenotype, instead, it seems to generally enhance melanoma aggressiveness. In addition, the lack of morphological alterations found in this study, also suggests that the findings of Meghnani *et al.* were most likely determined by the phenotype of the used melanoma cell line (WM115), and not melanoma-specific. Indeed, in the study of Widmer and colleagues WM115 showed neither a proliferative, nor an invasive phenotype and thereby does not represent a standard melanoma cell line, at least regarding these features [98]. Upregulated *AGER* transcript levels already found in benign nevi and not solely in melanoma tissue (Figure 2A), as well as the RAGE OE-induced establishment of melanoma cell hallmarks, such as higher cell metabolic activity, increased proliferation, and the capacity to invade, in the melanocytic cell line MelSTV (Figure 3), point towards a driving role of RAGE not only in melanoma progression and metastasis, but also in early events during melanomagenesis.

IX.3. RAGE promotes melanoma growth and survival under non-toxic conditions but sensitizes cells towards exogenous DNA insults

The fact that *AGER* transcripts as well as RAGE protein have been found to be upregulated upon malignant transformation, already indicated a tumor-promoting function of RAGE in malignant melanoma (Figure 2A, B). This was proven by *in vitro* assays, demonstrating that RAGE enables melanocytic and melanoma cells to improve their bioenergetics, thereby achieving an enhanced proliferation and/or invasion capacity, as discussed in the last section (IX.2). Since all these features are indicators for improved cellular health, a contribution of

RAGE-dependent pro-survival effects to tumor promotion was hypothesized. However, the finding that RAGE overexpression was accompanied with an enhanced ROS production (Figure 7A) in the human melanocytic and melanoma cell lines questioned this idea. Normal cells avoid high ROS levels as they are associated with increased cellular stress and potential damage. Indeed, ROS are not only known to oxidize DNA bases, thereby causing DNA base changes, but also to produce mismatches and to enhance DNA deamination [400, 401]. However ROS levels can also provide beneficial effects; for instance, ROS have been demonstrated to induce tumor cell proliferation [397, 398]. The latter results in the finding that tumor cells often acquire different mechanisms, such as impairing apoptosis induction, in order to tolerate higher levels of ROS [398, 402]. To address these questions, RAGE-dependent effects on survival and apoptosis were investigated.

Human melanocytic MelSTV and melanoma cell lines, A375 and MeWo, transfected with the control vector or with the RAGE OE construct, were stained with Hoechst, 7AAD and antibodies against Annexin V to distinguish between living, non-apoptotic cells (Hoechst^{+}, 7AAD^{-}, Annexin V^{-}) and apoptotic cells (Hoechst^{+}, 7AAD$^{+/-}$, AnnexinV^{+}) (Figure 4D, E). Upon RAGE overexpression cells displayed lower numbers of apoptotic cells, when compared to control cells. Furthermore, this effect could be partially reverted by *AGER*-specific RNA interference. These results clearly demonstrate that RAGE provides pro-survival signals or more specifically anti-apoptotic signals to melanocytic and melanoma cell lines.

Different causes could account for the observed alterations in apoptosis. For instance, RAGE overexpression could have led to a deregulated balance between pro- and anti-apoptotic molecules, but also to differences in molecules sensing apoptosis-inducing events. Examples for the latter would be a differential expression of death receptors, such as FAS (first apoptotic signal) or TRAIL (tumor necrosis factor-related apoptosis-inducing ligand), or deregulated DNA lesion sensors and signal transducers. Comparative analysis of transcription levels of molecules covering the potential issues leading to impaired apoptosis of RAGE OE cells, such as ATM/ATR signaling, nucleotide excision repair (NER), base excision repair (BER), mismatch repair (MMR), double-strand break repair (DSB), other DNA repair genes, apoptosis, and cell cycle (for complete transcript list, see Table 13) were investigated in human and mouse.

Indeed, studies on the human A375 and murine B16F10 melanoma cell lines, including RAGE overexpression and Rage knockdown, consistently demonstrated that transcript levels of DNA damage sensors and repair molecules were negatively controlled by RAGE/Rage, and that this was also true at a lower extend for genes encoding for proteins directly involved in the apoptotic cascade (Figure 5C, 6C). More specifically, in the human A375 melanoma cell line the majority of differentially regulated genes upon RAGE overexpression was found

within the DSB repair pathway, while the Rage knockdown in the murine B16F10 cell line was predominantly associated with altered gene expression in ATM/ATR signaling. As mentioned before, the apoptosis pathway was not among the top affected pathways in neither human nor mouse. However, pro- as well as antiapoptotic molecules are often controlled not *via* transcriptional regulation but *via* posttranslational modifications, such as phosphorylation, or direct inhibition [403]. One indication for such mechanism has been provided by the study of Chen and colleagues, demonstrating that in some tissues RAGE also directly interacts with P53, an important tumorsuppressor, known to regulate the expression of pro- and anti-apoptotic molecules [404]. A transcriptional deregulation of P53 could not be observed in this study; however, direct protein-protein interaction of RAGE with apoptotic regulators was not investigated. Therefore, direct RAGE interactions or modulations of activation states cannot be ruled out and need to be further investigated in future studies.

Tumor cells often possess features, which might be unfavorable for a single cell but beneficial for the tumor bulk. For instance, genomic instability can cause cell death on the one hand, and on the other it can lead to the development of new tumor variants, which might be important for immune evasion. Another example is the upregulation of ROS, which enhances cell-intrinsic stress levels but which also promotes tumor proliferation and invasion [397, 398]. This study could demonstrate a role of RAGE in both of these melanoma strategies (Figure 7A). However, the downregulation of molecules involved in DNA repair, and therefore in maintaining genomic integrity might also have disadvantages for melanoma cells under specific conditions.

Indeed, upon RAGE overexpression MelSTV, A375, and MeWo cells were more sensitive towards treatment with doxorubicin, a drug used in cancer chemotherapy, which intercalates in between DNA bases, thereby producing large amounts of DNA double-strand breaks [383]. More specifically, all three overexpression cell lines responded with a greater cell metabolic collapse induced by doxorubicin compared to control cells. This was highly significant for MelSTV and A375 RAGE OE cells, but the same tendency was also observed for the MeWo cell line (Figure 7B). For MelSTV cells this could be further illustrated by following up apoptosis induction upon doxorubicin treatment. Indeed, the amount of late apoptotic cells after doxorubicin treatment doubled upon RAGE overexpression. This effect was partially abolished using *AGER* siRNA, but not by control siRNA (Figure 7C). For A375 and MeWo comparable effects have been observed in one experiment; however, repetitions failed to generate consistent results. This might have different reasons; for instance, the high plasticity combined with the capacity of melanoma cells to circumvent apoptosis in various ways might dampen either doxorubicin sensitivity or doxorubicin-induced responses.

Furthermore, since excessive DNA damage also results in cellular necrosis, future experiments should include TUNEL assay and electron microscopy to distinguish between active and passive cell death. However, the finding that RAGE promotes sensitivity to DNA damage-inducing factors was verified using the murine B16F10 model. There, the Rage knockdown was associated with a lower sensitivity towards UV radiation. More specifically, UV radiation led to a significant cell metabolic collapse in control but not in Rage knockdown cells (Figure 8A). Additionally, control cells showed a significantly induced apoptosis (Figure 8C), and a consequent reduction in the living cell population (Figure 8D); both features were not found for Rage knockdown cells upon radiation. Kang and colleagues demonstrated that RAGE is able to protect pancreatic tumor cells from ROS-induced cell damage, as well as from cell damage by chemotherapy-induced genotoxic stress. For melanoma cells, RAGE overexpression was associated with a higher ROS production (Figure 7A) but also with increased survival (Figure 4C, D), thereby proving that this finding is also true for the role of RAGE in malignant melanoma. However, the published finding, that RAGE protects pancreatic cancer cells from death induced by anticancer treatment could not be transferred to melanoma. A possible explanation might be different mechanisms of action of the anticancer drugs used. Indeed, while the latter study used alkylating agents (oxaliplatin, melphalan) and antimetabolites (gemcitabine), genotoxic insults in the here presented study were triggered using the anthracycline doxorubicin. Nevertheless, Kang and colleagues also verified their results using UV radiation, therefore suggesting that rather tissue-specific differences regarding RAGE modulators and isoform expression, as well as a distinct subcellular localization as described in section IX.4 might account for the observed differences.

Interestingly, Rage knockdown in B16F10 melanoma was also accompanied with altered expression of genes classified as cell cycle pathway genes (Figure 6D). It has been demonstrated that cells within the S phase are most vulnerable towards genotoxic stress. Therefore, a dysregulation of the cell cycle leading to decreased basal numbers of cells within the S phase would also result in a lower sensitivity of Rage knockdown cells towards UV radiation. This was addressed by staining B16F10 control and Rage knockdown cells with Vybrant® DyeCycle™ Violet, a dye exhibiting emission signals proportional to DNA mass. Basal levels of S phase cells between control and Rage knockdown cells were compared and no difference was observed (Figure 8B). This illustrates that the RAGE/Rage-dependent sensitivity of melanoma cells is not due to differences in cell cycle, but might be explained by altered expression of DNA damage signaling molecules (Figure 5C, 6C). For a close relative of Rage, the PRR Tlr4, a role in the repair of UV radiation-induced cutaneous DNA damage has already been proposed [405]. More specifically, Ahmad and colleagues investigated efficacy of DNA damage repair upon local UV exposure in Tlr4$^{-/-}$ and wildtype

mice. They found DNA damage repair being more efficiently repaired in the skin of Tlr4$^{-/-}$ mice as compared to the wildtype situation, and claimed that this was due to the higher expression of *Xpa* observed in the Tlr4$^{-/-}$ mice after UV exposure. A follow-up study provided evidence that the Tlr4-deficiency-dependent resistance to UV radiation was mediated by the protein Myd88 [406]. As mentioned before, Myd88 has also been described as adaptor protein for phosphorylated RAGE [300]. The same study showed that Myd88-deficiency led to a decreased caspase-mediated cleavage of Parp, a DNA repair molecule sensing DNA lesions, for which allelic variants have been described to confer higher risk for melanoma [63, 406]. In fact, in the here-presented study *Xpa* as well as *Parp1* transcript levels were demonstrated to be upregulated in murine Rage knockdown cells compared to control B16F10 melanoma cells (Figure 6E). This strongly recommends that the reduced response of the Rage knockdown cells to UV radiation is caused by impaired activation of downstream effectors, potentially shared with Tlr4 signaling, leading to an enhanced repair of DNA UV damage. Furthermore, upon UV radiation a significantly higher number of S phase cells was observed in Rage knockdown as compared to B16F10 control cells (Figure 8B). This points towards two things: First, cell cycle checkpoints in general seem to be still functional. Second, upon radiation Rage knockdown cells halt cell cycle in S phase, supporting the idea of an enhanced DNA damage sensing or DNA repair.

Since doxorubicin and UV radiation predominantly induce double-strand breaks, genes involved in the DSB repair pathway and altered upon RAGE overexpression in the human A375 melanoma cell line or, respectively, upon Rage knockdown in murine B16F10 melanoma cells, were investigated. Indeed, four gene homologs involved in DSB repair mechanisms were identified, which are regulated by RAGE/Rage in both species: *H2AFX/H2afx*, *MLH1/Mlh1*, *RPA1/Rpa1*, and *XRCC2/Xrcc2* (Figure 5D, 6D).

H2AFX encodes for the histone H2A variant X (H2AX) that constitutes 2 to 25 % of mammalian histone H2A depending on organism and cell type [407]. The structure of H2AX is highly similar to other H2A variants except for its C-terminal tail, which becomes rapidly phosphorylated to form γH2AX upon induction of DSBs. It was shown to play an important role in early responses to DNA damage by regulating the recruitment and accumulation of DNA repair proteins to sites of DSB [408]. Interestingly, mice lacking H2AX were shown to be more sensitive to radiation and more prone to cancer development in a p53 null background [409]. This is in line with the data presented here, showing that Rage knockdown in murine B16F10 melanoma is accompanied with upregulation of *H2ax* (Figure 6D) resulting in increased UV radiation resistance (Figure 8A,C,D). This indicates that H2AX functions as a genome damage sensitizer. Losses of H2AX protein have been demonstrated in melanoma [394], however, the remaining H2AX has been reported to be phosphorylated to a

significantly higher extend as compared to benign nevi [410], illustrating higher amounts of unrepaired DNA damage in melanoma.

The replication protein A (RPA) is a highly conserved heterotrimeric protein involved in maintaining genomic integrity by binding single- and double-stranded DNA breaks and recruiting other DNA repair molecules, such as ATR. Furthermore, RPA has also been demonstrated to colocalize with RAD51 upon UV radiation of mouse fibroblasts [411, 412]. Interestingly, altered RAGE/Rage expression was not only accompanied by differential expression of *RPA*, but also of *RAD51* (Figure 5D, 6D), and of *ATR* (Figure 5E, 6E) in both, human and mouse. A role for RPA in the S phase cell cycle checkpoint was demonstrated; more specifically, when bound to DNA RPA was shown to halt cell cycle progression until DNA repair is completed [413]. This fact and the observed upregulation of *Rpa* upon Rage knockdown might explain the increased number of cells in S phase after UV irradiation in B16F10 Rage knockdown compared to B16F10 control cells (Figure 8B).

While the aforementioned downregulation of *RAD51* upon RAGE overexpression in human melanoma could not be verified in the murine B16F10 model (Figure 5D, 6D), its importance was illustrated by another differentially regulated gene; *XRRC2* (X-ray repair complementing defective repair in Chinese hamster cells 2). Its expression was found to negatively correlate with RAGE/Rage in human and mouse. Previous studies demonstrated that XRCC2 enhances the activity of RAD51 and, consequently, that a loss of *XRCC2* results in a delay of the early DNA damage response mediated by RAD51 [414]. This strongly indicates that the observed downregulation of both, *RAD51* and *XRCC2*, in the human melanoma cell line A375 (Figure 5D) was accompanied with delayed and impaired DNA repair. Other studies reported that Xrcc2 knockout fibroblasts were hypersensitive to various anticancer drugs [415], thereby supporting the here presented finding that RAGE/Rage expression correlates with higher sensitivity to genotoxic insults in human and mouse (Figure 7B, C, Figure 8A,C,D) by negatively influencing DNA damage repair genes like XRCC2/Xrcc2 (Figure 5D, 6D).

Another DSB repair gene deregulated upon altered RAGE/Rage expression, was encoding for the MUTL homolog1 (MLH1) protein (Figure 5D, 6E). MLH1 is a multifunctional protein with important roles in MMR but also reported to have tremendous importance in controlling DSB repair [416]. As aforementioned, MLH1 expression was found to be decreased in malignant melanoma [392, 393]. Within this study elevated RAGE levels were directly linked with impaired *MLH1* gene expression (Figure 5D). The hypothesis of an inverse correlation of the genes is supported by studies in colorectal cancer, where a similar expression pattern of RAGE and MLH1 was observed but never connected [342, 417]. Instead, an association of BRAFV600E mutations with increased hypermethylation of the MLH1 gene was postulated

[417]. However, in the here presented study no effect of *in cis* elements, such as BRAFV600E, on RAGE expression could be observed (data not shown). Nevertheless, future studies with larger cohorts might give a better measure of a potential correlation of BRAFV600E mutation and RAGE, as well as of a possible involvement of RAGE in DNA methylation.

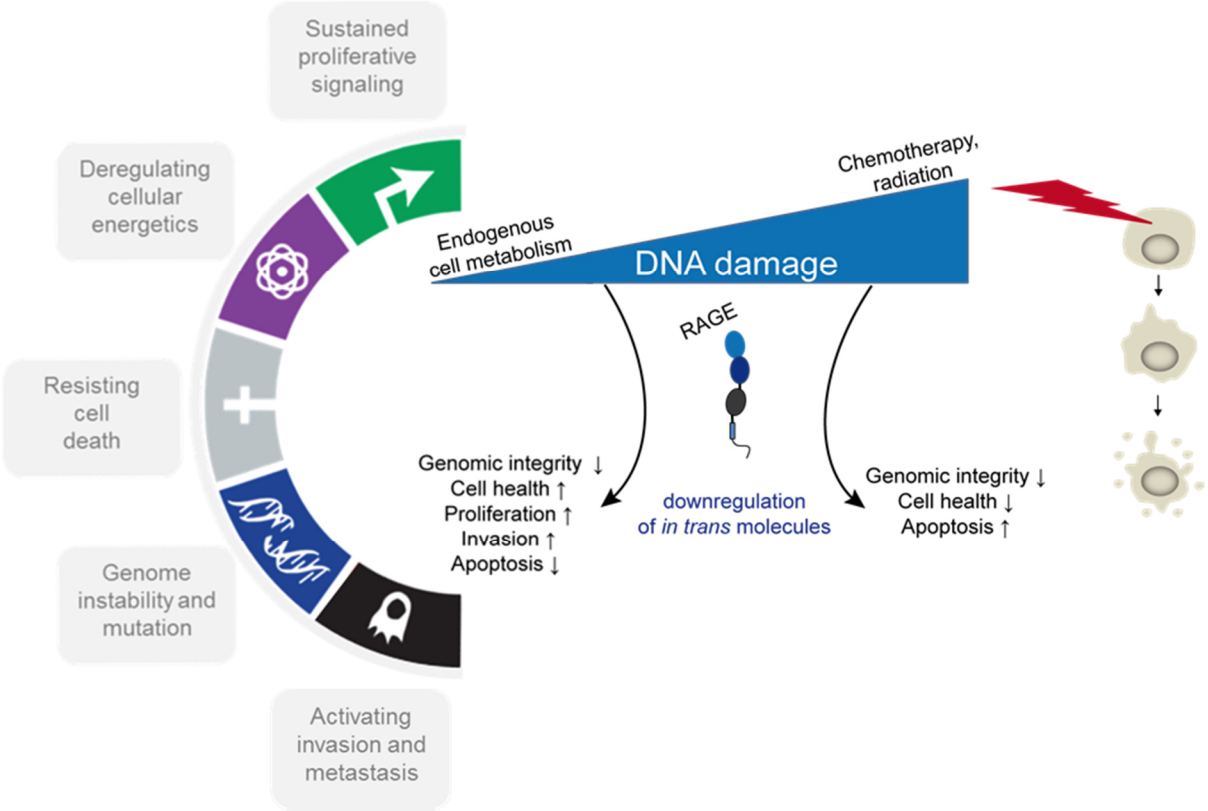

Figure 13 Ambivalent role of RAGE in melanomagenesis. Dependent on the level of DNA damage RAGE either mediates tumor-promoting features by driving characteristic melanoma hallmarks (left side) or induces cell death (right side).

As illustrated in Figure 13, these results demonstrate the benefits of high RAGE expression in leading to enhanced survival (Figure 4C, D) and higher aggressiveness of melanoma cells (Figure 3), and their association with negative effects such as a higher vulnerability to exogenous genotoxic stress (Figure 7B, C; Figure 8A,C,D). These findings as well as the characteristic of melanoma cells to rapidly establish resistance to chemotherapies indicate that melanoma cells possess strategies to regulate RAGE functionality, and these might not only comprise the control of gene expression but also alternative splicing and subcellular translocation as discussed in section IX.4. However, the ambivalent character of RAGE also raises questions regarding its potential as a novel target for therapeutic approaches. *In vitro* generation of isogenic, anticancer drug-resistant melanoma cell lines with concomitant analysis of RAGE/Rage expression would provide first insights. Furthermore, xenograft transplantations of control and RAGE overexpressing melanoma cell lines into

immunodeficient mouse strains, and/or B16F10 Rage knockdown or control injections into immunocompetent mice, with or without administration of anticancer drugs or UV radiation, would shed light onto the behavior of these cells under treatment.

IX.4. Subcellular localization of RAGE: An important level of control in melanoma?

Immunohistochemical analysis of TMA containing samples of benign nevi, primary melanoma and metastases did not only reveal a significantly higher expression of RAGE in non-metastatic and metastatic melanoma samples compared to benign nevi, but also a predominant nuclear RAGE staining for the latter (Figure 2B, C, Figure 9A). This aroused great interest, since RAGE was mainly described as cell-surface receptor, and as secreted or cytosolic molecule. Interestingly, the percentage of cells with exclusive nuclear RAGE expression was not only significantly decreased in all melanoma cells in comparison to melanocytes, but a reduction was additionally observed comparing metastases to primary melanomas. This supports the notion that loss of nuclear RAGE is a relevant feature during process of progression (Figure 9A). However, potential effects mediated by the observed compartmental shift does not necessarily need to come along with loss of nuclear functions but also with a gain of toxic cytosolic functions of RAGE. In fact, while only 19 % of melanocytic cells in benign nevi showed a pure cytosolic RAGE expression, this value was found to be significantly higher in primary melanoma (45 %) and metastases (46 %) samples.

The subcellular localization is a major characteristic of molecules since it has important impacts on the activation state, interaction network, and biological function [418]. Therefore, profiling the position of proteins within a cell is a mandatory task that can be achieved by screening proteins of interest for localization-specific features. Since fl-RAGE contains such a feature, namely a signal peptide indicating a potential secretion of the protein, RAGE variants were first screened for this motif [216]. In terms of numbers, 15 from the 20 analyzed RAGE variants contained such a secretion signal (Table 16). However, an existing secretion signal does not necessarily cause a secretion of the protein. The best example is fl-RAGE itself; due to its structure the protein cannot be secreted without further posttranslational modifications although exhibiting the signal for secretion. To date, only two studies indicated that RAGE might also possess functions in different cellular compartments, such as the mitochondria and the nucleus. One study demonstrated that a phosphorylation of RAGE by MAP kinases such as ERK1/2 initiated by HMGB1-dependent signaling enables RAGE to translocate into the mitochondria, where it is involved in the regulation of cellular bioenergetics [248, 249]. Since a hyperactivation of the MAPK pathways is a characteristic of melanoma cells, an aberrant intracellular distribution of RAGE might be due to a differential posttranslational modification state of the protein [94]. A study by Galichet and coworkers

provided evidence that upon MMP9-, ADAM10- or γ-secretase-induced proteolysis of membrane-bound RAGE its C-terminal fragment is not only found in the cytoplasm but has also been transported into the nucleus [250].

In order to investigate if the nuclear staining in benign nevi might result from enhanced RAGE shedding TMA samples and human melanoma cell lines were stained with multiple antibodies targeting different epitopes of the RAGE molecule (data not shown). The data indicated, that nuclear RAGE not only consists of the C-terminal fragment but instead comprises at least one additional RAGE variant. The cell fractionation of the human melanocytic MelSTV cell line, followed by the detection of RAGE within the cytosolic extract, as well as soluble nuclear and chromatin-bound nuclear fraction *via* Western Blot (Figure 11C, D), verified the existence of more than one RAGE form. In the soluble nuclear (SNE) and the chromatin-bound (CNE) nuclear extract bands for proteins with approximately 20 to 30 kDa were detected, as well as a band around 60 kDa. Within the SNE additional variants between 50 to 60 kDa, and bands illustrating higher-weight molecules with 80 to 120 kDa were stained (Figure 11D). Noteworthy, bands for 80 to 120 kDa molecules were also detected by blotting immunoprecipitations of RAGE from nuclear lysates (data not shown) as well as in the murine B16F10 protein lysate, where they disappeared upon Rage knockdown (Figure 6B). Fl-RAGE consists of 404 amino acids (aa) resulting in a molecular mass of 55 kDa. Shed or alternatively spliced RAGE variants range from 36 to 404 amino acids (Table 16). Without consideration of multimeric aggregates or posttranslational modifications, estimation of the isoform weights according to the mass of full-length RAGE, reveals a molecular weight between 5 to 55 kDa. The 60 kDa band could arise from posttranslation modifications, such as phosphorylation, glycosylation, and SUMOylation. Since fluorescence resonance energy transfer (FRET) showed that RAGE molecules can form homodimers, as well as homooligomers and heterodimers with HSPGs and TLRs [244], the observed higher-molecular weight molecules could illustrate multimers formed by strong disulfide bonds, which were not denaturated under the described conditions. In combination these findings reveal that RAGE isoforms, and maybe also fl-RAGE, might be able to translocate into the nucleus under certain conditions; these conditions seem to be present in benign nevi but not, or at least to a lower extend, upon transformation to malignant melanoma.

Recent studies illustrated the existence of a complex regulatory machinery enabling the selection of alternative *AGER* exons and further correlated differential expression of RAGE isoforms with pathological conditions found in Alzheimer's disease and neurodegeneration [240-242]. The observed aberrant RAGE splicing events were connected to the intracellular concentration or activity of nuclear RNA binding proteins, such as HNRNP H, HNRNP A1, and TRA2-β1 [240, 241]. Comparative analysis of transcript levels of these splicing factors

between normal skin, benign nevi, and melanoma samples identified a significant downregulation of both HNRNP proteins, H and A1, in melanoma tissue in comparison to their expression in normal skin (Figure 10). In terms of HNRNP H, these alterations were also found in benign nevi, thereby providing two indications: First, a deregulation of HNRNP H might be an early event in melanocyte transformation (Figure 10B); second, a deregulation of HNRNP H alone is not sufficient to explain the observation since an aberrant RAGE localization was found by comparing melanoma and benign nevi tissues (Figure 9A). Instead, an additional downregulation of HNRNP A1 upon transformation to melanoma with consequent differential expression of distinct RAGE isoforms seems to be required (Figure 10A). In terms of TRA2-β1, transcript levels were found to be significantly downregulated in melanoma when compared to benign nevi, but not to healthy skin samples (Figure 10C). In total, the comparative analysis of the proteins HNRNP H, HNRNP A1, and TRA2-β1 known to be involved in regulating RAGE splice variant expression, revealed the existence of a melanoma-specific splicing signature. Interestingly, bioinformatics and array data strongly suggest that the alternative splicing process is more prominent among genes playing regulatory functions, thereby underlining the importance of RAGE and the complexity of its regulation [419]. Accordingly, the observed differential expression of the RAGE splicing factors might not only lead to a differential expression of RAGE variants with distinct subcellular localization patterns but also to distinct biological functions. However, the function of many RAGE isoforms is still unknown; indeed, it is difficult to answer what fraction of the huge transcript variation found for RAGE is truly biologically relevant and not only stochastic noise of the splicing process.

Studies dealing with the subcellular localization of RAGE [249, 250] focused on fl-RAGE and its posttranslational modifications but did not take a role of RAGE variants into consideration. Furthermore, no potential mechanism was reported for the observed nuclear localization of the cytoplasmic domain of RAGE. According to the molecular weights of RAGE variants found in SNE and CNE (Figure 11D), a translocation from the cytosol into the nucleus and *vice versa*, cannot be mechanistically explained by pure diffusion. In general, only molecules smaller than 40 kDa can passively diffuse through the nuclear pore complexes (NPCs) while most proteins with functions in the nucleus use active carrier-mediated transport [420]. With this in mind, all described RAGE variants were screened for nuclear localization sequences indicating such an active transport mechanism (Table 16). Alternative splicing processes but also posttranslational modifications can affect – delete or establish – protein target signals as shown for the signal peptide. The computational methods used in this study attempt to predict nuclear localization by applying two different prediction approaches: First, similarity-based models grounded on establishing the similarity of RAGE with already known nuclear proteins; second, NLS-based models detecting target signals and other properties pertinent

to the nuclear import machinery. The best-characterized nuclear target signal is the classical NLS, which is recognized by the protein importin (IMP)-α, leading to the formation of a heterotrimeric cargo complex that is able to enter the nucleus [420]. Indeed, using NLS-based models (NLStradamus, cNLS Mapper, NetNES; Table 16) five of 20 analyzed RAGE variants, namely RAGE_v16 / Q15109-2, RAGE_v6 / Q15109-4, RAGE_v8 / Q15109-8, and Q15109-10, RAGE_v5 / Q15109-6, were identified to contain NLS and NES, whereas full-length RAGE was not found to harbor any of these signals. However, despite the classical pathway several alternative pathways have been characterized lacking these classical localization/export sequences. Noteworthy, cNLS mapper incorporates an additive scoring approach intended to identify classical NLS only [363], whereas NLStradamus represents a probabilistic model allowing screens for classical and non-canonical NLS [369]. Based on these distinct approaches, the different results obtained by the two tools (Table 16) might be explained. Interestingly, the Nuc pred score of NLS/NES-containing RAGE isoforms, essentially corresponding to the statistical probability of nuclear localization, was significantly higher compared to the other RAGE isoforms (Figure 12A, B). Besides structural properties enabling proteins to translocate into the nucleus *via* active transport, molecules were identified, which 'piggyback' into the nucleus by binding to other NLS/NES-containing molecules. Multiple ligands of RAGE, such as HMGB1 and S100 family members [284, 285], are known to translocate into the nucleus, thereby representing a potential alternative mechanism for RAGE molecules without NLS/NES to bypass motif-dependent cargo transport. Therefore, the existence of a NLS and NES strongly recommends a role of those RAGE variants in the nucleus but the absence does not exclude a nuclear function.

Taking advantage of the classification system CELLO, a software tool predicting the subcellular localization of proteins, the position of RAGE variants were modeled based on the physico-chemical properties of their amino acid sequence [362] (Table 16). Indeed, next to predictions of RAGE secretion to the extracellular space, cytosolic and mitochondrial localization, a large amount of isoforms (15/20) were allocated to the nucleus. Since NLS/NES were only present in five of the isoforms, other variants might use different transport mechanisms, or CELLO identified some false-positive nuclear RAGE forms. Interestingly, the RAGE variant Q15109-10 was identified to contain NLS and NES, but was also defined as secretion protein *via* CELLO. This example illustrates that *in silico* predictions may provide important information but need to be interpreted with caution.

When treating the melanocytic MelSTV cells with Leptomycin B, a specific inhibitor of the NES-dependent nuclear export protein CRM-1 (chromosomal maintenance 1) prior to cell lysis, signals for RAGE proteins with approximately 30 and 60 kDa enhanced in the separated nuclear extracts (Figure 11D). On the one hand this verified the results obtained

via in silico prediction that some RAGE variants do contain NES, on the other hand it proved that at least some of these RAGE forms utilize active nuclear transport systems. These findings suggest that alterations in the active cargo transport might also be a potential mechanism controlling subcellular localization of RAGE and might contribute to the aberrant cytosolic localization demonstrated for melanoma (Figure 10A). Indeed, previous studies claimed an upregulation of proteins controlling nuclear export in melanoma [387]. Performing comparative analysis applying a human genome array, which comprises normal skin, benign nevi and melanoma samples, a significant upregulation of the exportins CRM-1 and also RANBP1 could be observed in melanoma when compared to healthy tissues (Figure 11A, B). This indicates that besides a differential RAGE isoform expression, an enhanced nuclear export could also lead to the observed switch from nuclear to cytosolic localization of RAGE proteins in melanoma. Noteworthy, immunofluorescence stainings of human melanoma cell lines for RAGE mainly revealed comparable patterns for its subcellular distribution as obtained by TMA analysis, with the exception of SKmel23 (Figure 9A, B). However, the observation that despite the loss of cell-cell and cell-matrix contacts human melanoma cell lines still display the *in vivo* situation in regards to RAGE localization, as well as the identification of a melanoma cell line showing a different pattern, provides a good starting point for future studies, including expression analyses for distinct RAGE variants.

As mentioned before, posttranslational modifications also represent an important regulatory mechanism of reversible protein translation. A prime example is the phosphorylation-dependent unmasking of the NLS present in the NF-κB transcription factor family. NF-κB activity is regulated by its cytosolic inhibitor IκB. More specifically, IκB binds to NF-κB, thereby masking its NLS and retaining it in the cytoplasm. Signals from extracellular stimuli, such as TNFα but also DNA-damaging agents, induce the phosphorylation and consequent ubiquitination and proteolysis of IκB. Subsequently, the NLS of NF-κB gets unmasked and allows the transcription factor to translocate into the nucleus [421, 422]. Kang and colleagues provided evidence that phosphorylation of RAGE in fact regulates its subcellular localization, i.e. in their settings the translocation into the mitochondria [249]. On average, 11 phosphorylation sites were predicted in RAGE proteins, ranging from two to 15 (Table 16). Most of the analyzed RAGE variants were predicted to be substrates for PKC. Nevertheless, also variants were identified, which were predicted to be phosphorylated by PKA or cyclin-dependent kinase 5 (CDK5). The functional impact of these phosphorylation sites, in other words if these sites are involved in signaling, stability or proteolysis of RAGE variants, or in their subcellular distribution, needs to be further investigated. Furthermore, fl-RAGE as well as most other splicing forms were *in silico* predicted to contain O- (19/20) and N-glycosylation (15/20) sites. Glycosylation-dependent nuclear transport was first supported in 1989 by studies assuming that sugar residues could act as nuclear targeting signals [423]. In

fact, Duverger and colleagues verified this assumption by demonstrating that fluorescein-coupled BSA substituted to sugars could translocate to the nucleus, while unsubstituted could not [424]. Nowadays, a role of glycosylation in regulating subcellular localization of proteins is widely accepted, although it is still under discussion if it functions as nuclear targeting signal or rather as signal for nuclear residence [425]. Posttranslational modification by SUMOylation was only predicted for the half of the splice variants (10/20; Table 16). Nevertheless, SUMOylation was already reported to be involved in the nucleocytoplasmic transport of molecules belonging to the RAGE network. In fact, the mutation of SUMOylation sites within the RAGE ligand S100A4 abolished its ability to translocate into the nucleus [426].

Taken together, these data identified RAGE as a nuclear protein in melanocytes and indicated a loss of nuclear RAGE as characteristic of human malignant melanoma. Furthermore, the translocation of RAGE in the nucleus and *vice versa* has been demonstrated to at least partially depend on classical nuclear targeting sites, and consequently on the active cargo transport proteins, including the exportin CRM-1. The results further indicated possible mechanisms behind the aberrant subcellular localization of RAGE upon malignant transformation, such as a pathological upregulation of nuclear export proteins, and differential expression of splicing factors with subsequently altered frequency pattern of distinct RAGE isoforms. Ongoing experiments, including affinity enrichment/purification strategies coupled with mass spectrometry-based protein analysis, will provide more information on the identity of nuclear RAGE, as well as on potential posttranslational modifications enabling nuclear transport. Furthermore, taking advantage of stable isotope labeling by amino acid in cell culture (SILAC), a quantitative analysis of RAGE and its isoforms between melanocytic and melanoma cells will be achieved.

IX.5. Potential role of nuclear RAGE

In 2013, Sirois and colleagues demonstrated that RAGE functions as atypical nucleic-acid sensing immune receptor on the cell surface. Usually, these receptors are solely expressed in endolysosomal compartments or in the cytosol, thereby limiting receptor engagement by self-nucleic acids present in the extracellular space under homeostatic conditions. More specifically, RAGE was reported to bind to double-stranded DNA *via* interactions with the V1-C1 unit [427]. Many studies proved that RAGE is able to induce the transcription of several genes, including the *AGER* gene itself; however, this was believed to happen elusively in an indirect manner. Since this study was able to demonstrate that RAGE also occurs as nuclear protein (Figure 9), the question rose whether it can also bind to nuclear DNA, and maybe influence gene expression in a direct manner by functioning as transcription factor or in transcription factor complexes. Transcription factors bind to conserved sequence patterns in

promoters of their target genes, nevertheless, also binding to different primary sequence patterns but similar DNA structures has been described. Interaction of RAGE with extracellular DNA has been supposed to occur in a sequence-independent manner *via* binding to the charged sugar-phosphate backbones [427].

When screening RAGE proteins for potential DNA binding sites, fl-RAGE as well as eight other RAGE variants displayed two sites within the C1 domain, hereinafter referred to as binding motif 1 (BM1) and 2 (BM2) (Figure 12A, E). Interestingly, alternative splicing resulted in the generation of additional predicted DNA binding sites, labeled as either BM3 or BM4, in seven of the investigated RAGE isoforms (Figure 12A, E). When comparing the number of the predicted DNA binding sites between the different RAGE variants, the ones harboring potential NLS/NES displayed a significantly increased amount (Figure 12C). Surprisingly, the binding motif BM4 was found in both groups in contrast to BM3, which was elusively predicted in isoforms containing NLS and NES. Also differences regarding their localization were observed: BM3 was localized in the C1 domain while BM4 was found in the cytosolic portion of the RAGE protein (Figure 12E). So far, posttranslational modifications of RAGE isoforms have not been investigated. Nevertheless, Galichet and colleagues demonstrated a translocation of the intracellular domain of RAGE upon proteolytic cleavage into the nucleus [250]. Consequently, it can assumed that modified RAGE variants might also be shed by matrix metalloproteinases, thereby gaining the ability to translocate into the nucleus by pure diffusion. One indication for RAGE as component of transcription factor complexes was given by the results of Chen and colleagues, showing a direct interaction of RAGE and the tumor suppressor p53 in adipocytes [404].

However, all these findings are purely speculative at this stage. Ongoing experiments, combining affinity enrichment and mass spectrometry-based protein analysis of the RAGE protein, will provide more information on a potential nuclear interaction network. Furthermore, electrophoretic mobility shift assay (EMSA) studies with immunoprecipitated nuclear RAGE and genomic DNA will answer the question if RAGE is able to bind not only to extracellular but also to nuclear DNA. These results will shed more light onto the functional consequences of the nucleus-to-cytosol switch observed upon transformation from benign nevi to melanoma. In fact, the compartmental shift does not necessarily need to come along with loss of nuclear functions but also with a gain of toxic cytosolic functions of RAGE.

Taken together this work proposes a beneficial role of RAGE for melanoma development, growth, and progression. RAGE was demonstrated to be involved in the establishment and regulation of characteristic melanoma hallmarks, such as genomic instability and mutation, resisting cell death, deregulating cellular energetics, sustained proliferative signaling, activating invasion and metabolism. Besides highlighting the importance of investigating

RAGE isoforms separately, this study showed for the first time that the subcellular localization of RAGE proteins is deregulated during the process of progression from benign nevi to malignant melanoma and metastasis, at least partly mediated *via* an active cargo transport to the nucleus. However, from a translational point of view the finding that RAGE causes a higher sensitivity of melanoma cells towards UV radiation but also towards anticancer treatment might be of great relevance.

X. References

1. Tsao, H., M.B. Atkins, and A.J. Sober, *Management of cutaneous melanoma.* N Engl J Med, 2004. **351**(10): p. 998-1012.
2. Howlader, N., A.M. Noone, and M. Krapcho. *SEER Cancer Statistics Review 1975-2011*. 2013.
3. Bauer, J. and C. Garbe, *Acquired melanocytic nevi as risk factor for melanoma development. A comprehensive review of epidemiological data.* Pigment Cell Res, 2003. **16**(3): p. 297-306.
4. Skowronek, J., et al., *DNA ploidy in malignant melanoma, skin cancer and pigmented nevi.* Neoplasma, 1997. **44**(5): p. 282-8.
5. de Braud, F., et al., *Malignant melanoma.* Crit Rev Oncol Hematol, 2003. **47**(1): p. 35-63.
6. Miller, A.J. and M.C. Mihm, Jr., *Melanoma.* N Engl J Med, 2006. **355**(1): p. 51-65.
7. Whiteman, D.C., C.A. Whiteman, and A.C. Green, *Childhood sun exposure as a risk factor for melanoma: a systematic review of epidemiologic studies.* Cancer Causes Control, 2001. **12**(1): p. 69-82.
8. Raimondi, S., et al., *MC1R variants, melanoma and red hair color phenotype: a meta-analysis.* Int J Cancer, 2008. **122**(12): p. 2753-60.
9. Gandini, S., et al., *Meta-analysis of risk factors for cutaneous melanoma: II. Sun exposure.* Eur J Cancer, 2005. **41**(1): p. 45-60.
10. Hodis, E., et al., *A landscape of driver mutations in melanoma.* Cell, 2012. **150**(2): p. 251-63.
11. Lucas, R., et al., *Solar ultraviolet radiation: Global burden of disease from solar ultraviolet radiation*. Environmental Burden of Disease. Vol. 13. 2006.
12. Greco, G., et al., *A melanin-inspired pro-oxidant system for dopa(mine) polymerization: mimicking the natural casing process.* Chem Commun (Camb), 2011. **47**(37): p. 10308-10.
13. Greco, G., et al., *The fundamental building blocks of red human hair pheomelanin are isoquinoline-containing dimers.* Pigment Cell Melanoma Res, 2012. **25**(1): p. 110-2.
14. Panzella, L., et al., *Red human hair pheomelanin is a potent pro-oxidant mediating UV-independent contributory mechanisms of melanomagenesis.* Pigment Cell Melanoma Res, 2014. **27**(2): p. 244-52.
15. Napolitano, A., et al., *Pheomelanin-induced oxidative stress: bright and dark chemistry bridging red hair phenotype and melanoma.* Pigment Cell Melanoma Res, 2014. **27**(5): p. 721-33.
16. Green, A.C., et al., *Reduced melanoma after regular sunscreen use: randomized trial follow-up.* J Clin Oncol, 2011. **29**(3): p. 257-63.
17. Mitra, D., et al., *An ultraviolet-radiation-independent pathway to melanoma carcinogenesis in the red hair/fair skin background.* Nature, 2012. **491**(7424): p. 449-53.
18. Gandini, S., et al., *Meta-analysis of risk factors for cutaneous melanoma: I. Common and atypical naevi.* Eur J Cancer, 2005. **41**(1): p. 28-44.

19. Gandini, S., et al., *Meta-analysis of risk factors for cutaneous melanoma: III. Family history, actinic damage and phenotypic factors.* Eur J Cancer, 2005. **41**(14): p. 2040-59.

20. Draper, G.J., B.M. Sanders, and J.E. Kingston, *Second primary neoplasms in patients with retinoblastoma.* Br J Cancer, 1986. **53**(5): p. 661-71.

21. Sanders, B.M., et al., *Non-ocular cancer in relatives of retinoblastoma patients.* Br J Cancer, 1989. **60**(3): p. 358-65.

22. Eng, C., et al., *Mortality from second tumors among long-term survivors of retinoblastoma.* J Natl Cancer Inst, 1993. **85**(14): p. 1121-8.

23. Fletcher, O., et al., *Lifetime risks of common cancers among retinoblastoma survivors.* J Natl Cancer Inst, 2004. **96**(5): p. 357-63.

24. Zuo, L., et al., *Germline mutations in the p16INK4a binding domain of CDK4 in familial melanoma.* Nat Genet, 1996. **12**(1): p. 97-9.

25. Soufir, N., et al., *Prevalence of p16 and CDK4 germline mutations in 48 melanoma-prone families in France. The French Familial Melanoma Study Group.* Hum Mol Genet, 1998. **7**(2): p. 209-16.

26. Molven, A., et al., *A large Norwegian family with inherited malignant melanoma, multiple atypical nevi, and CDK4 mutation.* Genes Chromosomes Cancer, 2005. **44**(1): p. 10-8.

27. Koh, J., et al., *Tumour-derived p16 alleles encoding proteins defective in cell-cycle inhibition.* Nature, 1995. **375**(6531): p. 506-10.

28. Carreira, S., et al., *Mitf cooperates with Rb1 and activates p21Cip1 expression to regulate cell cycle progression.* Nature, 2005. **433**(7027): p. 764-9.

29. Zhang, S., E.S. Ramsay, and B.A. Mock, *Cdkn2a, the cyclin-dependent kinase inhibitor encoding p16INK4a and p19ARF, is a candidate for the plasmacytoma susceptibility locus, Pctr1.* Proc Natl Acad Sci U S A, 1998. **95**(5): p. 2429-34.

30. Wolfel, T., et al., *A p16INK4a-insensitive CDK4 mutant targeted by cytolytic T lymphocytes in a human melanoma.* Science, 1995. **269**(5228): p. 1281-4.

31. Tsao, H., et al., *Novel mutations in the p16/CDKN2A binding region of the cyclin-dependent kinase-4 gene.* Cancer Res, 1998. **58**(1): p. 109-13.

32. Kamijo, T., et al., *Functional and physical interactions of the ARF tumor suppressor with p53 and Mdm2.* Proc Natl Acad Sci U S A, 1998. **95**(14): p. 8292-7.

33. Stott, F.J., et al., *The alternative product from the human CDKN2A locus, p14(ARF), participates in a regulatory feedback loop with p53 and MDM2.* EMBO J, 1998. **17**(17): p. 5001-14.

34. Lawrence, M.S., et al., *Mutational heterogeneity in cancer and the search for new cancer-associated genes.* Nature, 2013. **499**(7457): p. 214-8.

35. Davies, H., et al., *Mutations of the BRAF gene in human cancer.* Nature, 2002. **417**(6892): p. 949-54.

36. Maldonado, J.L., et al., *Mechanisms of cell-cycle arrest in Spitz nevi with constitutive activation of the MAP-kinase pathway.* Am J Pathol, 2004. **164**(5): p. 1783-7.

37. Pollock, P.M., et al., *High frequency of BRAF mutations in nevi.* Nat Genet, 2003. **33**(1): p. 19-20.

38. Yazdi, A.S., et al., *Mutations of the BRAF gene in benign and malignant melanocytic lesions.* J Invest Dermatol, 2003. **121**(5): p. 1160-2.

39. Kumar, R., et al., *BRAF mutations are common somatic events in melanocytic nevi.* J Invest Dermatol, 2004. **122**(2): p. 342-8.

40. Saldanha, G., et al., *High BRAF mutation frequency does not characterize all melanocytic tumor types.* Int J Cancer, 2004. **111**(5): p. 705-10.

41. Michaloglou, C., et al., *BRAFE600-associated senescence-like cell cycle arrest of human naevi.* Nature, 2005. **436**(7051): p. 720-4.

42. Omholt, K., et al., *Screening of N-ras codon 61 mutations in paired primary and metastatic cutaneous melanomas: mutations occur early and persist throughout tumor progression.* Clin Cancer Res, 2002. **8**(11): p. 3468-74.

43. Whitman, M., et al., *Type I phosphatidylinositol kinase makes a novel inositol phospholipid, phosphatidylinositol-3-phosphate.* Nature, 1988. **332**(6165): p. 644-6.

44. Cantley, L.C., *The phosphoinositide 3-kinase pathway.* Science, 2002. **296**(5573): p. 1655-7.

45. Chalhoub, N. and S.J. Baker, *PTEN and the PI3-kinase pathway in cancer.* Annu Rev Pathol, 2009. **4**: p. 127-50.

46. Yang, S.H., A.D. Sharrocks, and A.J. Whitmarsh, *MAP kinase signalling cascades and transcriptional regulation.* Gene, 2013. **513**(1): p. 1-13.

47. Engelman, J.A., *Targeting PI3K signalling in cancer: opportunities, challenges and limitations.* Nat Rev Cancer, 2009. **9**(8): p. 550-62.

48. Lozano, G., *The oncogenic roles of p53 mutants in mouse models.* Curr Opin Genet Dev, 2007. **17**(1): p. 66-70.

49. Hanahan, D. and R.A. Weinberg, *The hallmarks of cancer.* Cell, 2000. **100**(1): p. 57-70.

50. Hanahan, D. and R.A. Weinberg, *Hallmarks of cancer: the next generation.* Cell, 2011. **144**(5): p. 646-74.

51. Bastian, B.C., et al., *Gene amplifications characterize acral melanoma and permit the detection of occult tumor cells in the surrounding skin.* Cancer Res, 2000. **60**(7): p. 1968-73.

52. Grichnik, J.M., *Genomic instability and tumor stem cells.* J Invest Dermatol, 2006. **126**(6): p. 1214-6.

53. Bastian, B.C., *Understanding the progression of melanocytic neoplasia using genomic analysis: from fields to cancer.* Oncogene, 2003. **22**(20): p. 3081-6.

54. Bastian, B.C., et al., *Genetic changes in neoplasms arising in congenital melanocytic nevi: differences between nodular proliferations and melanomas.* Am J Pathol, 2002. **161**(4): p. 1163-9.

55. Wang, E., et al., *Clonal persistence and evolution during a decade of recurrent melanoma.* J Invest Dermatol, 2006. **126**(6): p. 1372-7.

56. Draeger, J., et al., *Chromosome gain and loss in paraffin sections from malignant melanomas of the skin.* Int J Oncol, 1997. **10**(1): p. 89-92.

57. Meyskens, F.L., Jr., et al., *Luminol-enhanced chemiluminescent response of human melanocytes and melanoma cells to hydrogen peroxide stress.* Pigment Cell Res, 1997. **10**(3): p. 184-9.

58. Wondrak, G.T., *Redox-directed cancer therapeutics: molecular mechanisms and opportunities.* Antioxid Redox Signal, 2009. **11**(12): p. 3013-69.

59. Kraemer, K.H., et al., *The role of sunlight and DNA repair in melanoma and nonmelanoma skin cancer. The xeroderma pigmentosum paradigm.* Arch Dermatol, 1994. **130**(8): p. 1018-21.

60. Stefanini, M. and K. Kraemer, *Xeroderma Pigmentosum*, in *Neurocutaneous Diseases*, M. Ruggieri, I. Pascual-Castroviejo, and C. Di Rocco, Editors. 2008. p. 771 - 792.

61. Schiffner, S., et al., *p54nrb is a new regulator of progression of malignant melanoma.* Carcinogenesis, 2011. **32**(8): p. 1176-82.

62. Alfano, L., et al., *NONO regulates the intra-S-phase checkpoint in response to UV radiation.* Oncogene, 2015.

63. Zhang, M., et al., *Genetic variation in DNA repair pathway genes and melanoma risk.* DNA Repair (Amst), 2011. **10**(1): p. 111-6.

64. Muthusamy, V., et al., *Amplification of CDK4 and MDM2 in malignant melanoma.* Genes Chromosomes Cancer, 2006. **45**(5): p. 447-54.

65. Anic, G.M., et al., *Telomere length and risk of melanoma, squamous cell carcinoma, and basal cell carcinoma.* Cancer Epidemiol, 2013. **37**(4): p. 434-9.

66. Harley, C.B., *Telomere loss: mitotic clock or genetic time bomb?* Mutat Res, 1991. **256**(2-6): p. 271-82.

67. Chen, H., Q.Y. Weng, and D.E. Fisher, *UV signaling pathways within the skin.* J Invest Dermatol, 2014. **134**(8): p. 2080-5.

68. Denat, L., et al., *Melanocytes as instigators and victims of oxidative stress.* J Invest Dermatol, 2014. **134**(6): p. 1512-8.

69. Choi, W., et al., *Regulation of human skin pigmentation in situ by repetitive UV exposure: molecular characterization of responses to UVA and/or UVB.* J Invest Dermatol, 2010. **130**(6): p. 1685-96.

70. Haq, R. and D.E. Fisher, *Biology and clinical relevance of the micropthalmia family of transcription factors in human cancer.* J Clin Oncol, 2011. **29**(25): p. 3474-82.

71. McGill, G.G., et al., *Bcl2 regulation by the melanocyte master regulator Mitf modulates lineage survival and melanoma cell viability.* Cell, 2002. **109**(6): p. 707-18.

72. Placzek, W.J., et al., *A survey of the anti-apoptotic Bcl-2 subfamily expression in cancer types provides a platform to predict the efficacy of Bcl-2 antagonists in cancer therapy.* Cell Death Dis, 2010. **1**: p. e40.

73. Haq, R., et al., *BCL2A1 is a lineage-specific antiapoptotic melanoma oncogene that confers resistance to BRAF inhibition.* Proc Natl Acad Sci U S A, 2013. **110**(11): p. 4321-6.

74. Dynek, J.N., et al., *Microphthalmia-associated transcription factor is a critical transcriptional regulator of melanoma inhibitor of apoptosis in melanomas.* Cancer Res, 2008. **68**(9): p. 3124-32.

75. Saladi, S.V., et al., *BRG1 promotes survival of UV-irradiated melanoma cells by cooperating with MITF to activate the melanoma inhibitor of apoptosis gene.* Pigment Cell Melanoma Res, 2013. **26**(3): p. 377-91.

76. Vucic, D., et al., *ML-IAP, a novel inhibitor of apoptosis that is preferentially expressed in human melanomas.* Curr Biol, 2000. **10**(21): p. 1359-66.

77. Lazar, I., et al., *The clinical effect of the inhibitor of apopotosis protein livin in melanoma.* Oncology, 2012. **82**(4): p. 197-204.

78. Soengas, M.S., et al., *Inactivation of the apoptosis effector Apaf-1 in malignant melanoma.* Nature, 2001. **409**(6817): p. 207-11.

79. Koo, H.M., et al., *Apoptosis and melanogenesis in human melanoma cells induced by anthrax lethal factor inactivation of mitogen-activated protein kinase kinase.* Proc Natl Acad Sci U S A, 2002. **99**(5): p. 3052-7.

80. Eisenmann, K.M., et al., *Mitogen-activated protein kinase pathway-dependent tumor-specific survival signaling in melanoma cells through inactivation of the proapoptotic protein bad.* Cancer Res, 2003. **63**(23): p. 8330-7.

81. Ley, R., et al., *Activation of the ERK1/2 signaling pathway promotes phosphorylation and proteasome-dependent degradation of the BH3-only protein, Bim.* J Biol Chem, 2003. **278**(21): p. 18811-6.

82. Harada, H., et al., *Survival factor-induced extracellular signal-regulated kinase phosphorylates BIM, inhibiting its association with BAX and proapoptotic activity.* Proc Natl Acad Sci U S A, 2004. **101**(43): p. 15313-7.

83. Stambolic, V., et al., *Negative regulation of PKB/Akt-dependent cell survival by the tumor suppressor PTEN.* Cell, 1998. **95**(1): p. 29-39.

84. Madhunapantula, S.V., A. Sharma, and G.P. Robertson, *PRAS40 deregulates apoptosis in malignant melanoma.* Cancer Res, 2007. **67**(8): p. 3626-36.

85. Stahl, J.M., et al., *Loss of PTEN promotes tumor development in malignant melanoma.* Cancer Res, 2003. **63**(11): p. 2881-90.

86. Stahl, J.M., et al., *Deregulated Akt3 activity promotes development of malignant melanoma.* Cancer Res, 2004. **64**(19): p. 7002-10.

87. Warburg, O., *On the origin of cancer cells.* Science, 1956. **123**(3191): p. 309-14.

88. Semenza, G.L., *Tumor metabolism: cancer cells give and take lactate.* J Clin Invest, 2008. **118**(12): p. 3835-7.

89. Gatenby, R.A. and R.J. Gillies, *Why do cancers have high aerobic glycolysis?* Nat Rev Cancer, 2004. **4**(11): p. 891-9.

90. Gatenby, R.A., et al., *Acid-mediated tumor invasion: a multidisciplinary study.* Cancer Res, 2006. **66**(10): p. 5216-23.

91. Fantin, V.R., J. St-Pierre, and P. Leder, *Attenuation of LDH-A expression uncovers a link between glycolysis, mitochondrial physiology, and tumor maintenance.* Cancer Cell, 2006. **9**(6): p. 425-34.

92. B.V., N.T.R.C., *Oncoline - Proliferation Assay*.

93. De Luca, M., et al., *Coculture of human keratinocytes and melanocytes: differentiated melanocytes are physiologically organized in the basal layer of the cultured epithelium.* Eur J Cell Biol, 1988. **46**(1): p. 176-80.

94. Dhawan, P., et al., *Constitutive activation of Akt/protein kinase B in melanoma leads to up-regulation of nuclear factor-kappaB and tumor progression.* Cancer Res, 2002. **62**(24): p. 7335-42.

95. Dhawan, P. and A. Richmond, *A novel NF-kappa B-inducing kinase-MAPK signaling pathway up-regulates NF-kappa B activity in melanoma cells.* J Biol Chem, 2002. **277**(10): p. 7920-8.

96. Meier, F., et al., *The RAS/RAF/MEK/ERK and PI3K/AKT signaling pathways present molecular targets for the effective treatment of advanced melanoma.* Front Biosci, 2005. **10**: p. 2986-3001.

97. Hoek, K.S., et al., *In vivo switching of human melanoma cells between proliferative and invasive states.* Cancer Res, 2008. **68**(3): p. 650-6.

98. Widmer, D.S., et al., *Systematic classification of melanoma cells by phenotype-specific gene expression mapping.* Pigment Cell Melanoma Res, 2012. **25**(3): p. 343-53.

99. Zipser, M.C., et al., *A proliferative melanoma cell phenotype is responsive to RAF/MEK inhibition independent of BRAF mutation status.* Pigment Cell Melanoma Res, 2011. **24**(2): p. 326-33.

100. Hoek, K.S., et al., *Metastatic potential of melanomas defined by specific gene expression profiles with no BRAF signature.* Pigment Cell Res, 2006. **19**(4): p. 290-302.

101. Nieto, M.A., *The ins and outs of the epithelial to mesenchymal transition in health and disease.* Annu Rev Cell Dev Biol, 2011. **27**: p. 347-76.

102. Hsu, M.Y., et al., *Shifts in cadherin profiles between human normal melanocytes and melanomas.* J Investig Dermatol Symp Proc, 1996. **1**(2): p. 188-94.

103. Bachmann, I.M., et al., *Importance of P-cadherin, beta-catenin, and Wnt5a/frizzled for progression of melanocytic tumors and prognosis in cutaneous melanoma.* Clin Cancer Res, 2005. **11**(24 Pt 1): p. 8606-14.

104. Hao, L., et al., *Cadherin switch from E- to N-cadherin in melanoma progression is regulated by the PI3K/PTEN pathway through Twist and Snail.* Br J Dermatol, 2012. **166**(6): p. 1184-97.

105. van den Oord, J.J., et al., *Expression of gelatinase B and the extracellular matrix metalloproteinase inducer EMMPRIN in benign and malignant pigment cell lesions of the skin.* Am J Pathol, 1997. **151**(3): p. 665-70.

106. Vaisanen, A., et al., *Prognostic value of MMP-2 immunoreactive protein (72 kD type IV collagenase) in primary skin melanoma.* J Pathol, 1998. **186**(1): p. 51-8.

107. Airola, K., et al., *Expression of collagenases-1 and -3 and their inhibitors TIMP-1 and -3 correlates with the level of invasion in malignant melanomas.* Br J Cancer, 1999. **80**(5-6): p. 733-43.

108. Hofmann, U.B., et al., *Matrix metalloproteinases in human melanoma.* J Invest Dermatol, 2000. **115**(3): p. 337-44.

109. Fidler, I.J., S.J. Kim, and R.R. Langley, *The role of the organ microenvironment in the biology and therapy of cancer metastasis.* J Cell Biochem, 2007. **101**(4): p. 927-36.

110. Barnhill, R.L., et al., *Angiogenesis and tumor progression of melanoma. Quantification of vascularity in melanocytic nevi and cutaneous malignant melanoma.* Lab Invest, 1992. **67**(3): p. 331-7.

111. Schietroma, C., et al., *Vascular endothelial growth factor-C expression correlates with lymph node localization of human melanoma metastases.* Cancer, 2003. **98**(4): p. 789-97.

112. Widmer, D.S., et al., *Hypoxia contributes to melanoma heterogeneity by triggering HIF1alpha-dependent phenotype switching.* J Invest Dermatol, 2013. **133**(10): p. 2436-43.

113. Pierrat, M.J., et al., *Expression of microphthalmia-associated transcription factor (MITF), which is critical for melanoma progression, is inhibited by both transcription factor GLI2 and transforming growth factor-beta.* J Biol Chem, 2012. **287**(22): p. 17996-8004.

114. Pinner, S., et al., *Intravital imaging reveals transient changes in pigment production and Brn2 expression during metastatic melanoma dissemination.* Cancer Res, 2009. **69**(20): p. 7969-77.

115. Kawakami, Y., *New cancer therapy by immunomanipulation: development of immunotherapy for human melanoma as a model system.* Cornea, 2000. **19**(3 Suppl): p. S2-6.

116. Dunn, G.P., L.J. Old, and R.D. Schreiber, *The immunobiology of cancer immunosurveillance and immunoediting.* Immunity, 2004. **21**(2): p. 137-48.

117. Clark, W.H., Jr., et al., *The histogenesis and biologic behavior of primary human malignant melanomas of the skin.* Cancer Res, 1969. **29**(3): p. 705-27.

118. Day, C.L., Jr., et al., *A prognostic model for clinical stage I melanoma of the upper extremity. The importance of anatomic subsites in predicting recurrent disease.* Ann Surg, 1981. **193**(4): p. 436-40.

119. Tuthill, R.J., et al., *Risk assessment in localized primary cutaneous melanoma: a Southwest Oncology Group study evaluating nine factors and a test of the Clark logistic regression prediction model.* Am J Clin Pathol, 2002. **118**(4): p. 504-11.

120. Clemente, C.G., et al., *Prognostic value of tumor infiltrating lymphocytes in the vertical growth phase of primary cutaneous melanoma.* Cancer, 1996. **77**(7): p. 1303-10.

121. Barnhill, R.L., et al., *Predicting five-year outcome for patients with cutaneous melanoma in a population-based study.* Cancer, 1996. **78**(3): p. 427-32.

122. Thorn, M., et al., *Trends in tumour characteristics and survival of malignant melanoma 1960-84: a population-based study in Sweden.* Br J Cancer, 1994. **70**(4): p. 743-8.

123. Larsen, T.E. and T.H. Grude, *A retrospective histological study of 669 cases of primary cutaneous malignant melanoma in clinical stage I. 3. The relation between the tumour-associated lymphocyte infiltration and age and sex, tumour cell type, pigmentation, cellular atypia, mitotic count, depth of invasion, ulceration, tumour type and prognosis.* Acta Pathol Microbiol Scand A, 1978. **86A**(6): p. 523-30.

124. Taylor, R.C., et al., *Tumor-infiltrating lymphocytes predict sentinel lymph node positivity in patients with cutaneous melanoma.* J Clin Oncol, 2007. **25**(7): p. 869-75.

125. Cohen, P.J., et al., *The immunopathology of sequential tumor biopsies in patients treated with interleukin-2. Correlation of response with T-cell infiltration and HLA-DR expression.* Am J Pathol, 1987. **129**(2): p. 208-16.

126. Belldegrun, A., L.M. Muul, and S.A. Rosenberg, *Interleukin 2 expanded tumor-infiltrating lymphocytes in human renal cell cancer: isolation, characterization, and antitumor activity.* Cancer Res, 1988. **48**(1): p. 206-14.

127. Rosenberg, S.A., et al., *Use of tumor-infiltrating lymphocytes and interleukin-2 in the immunotherapy of patients with metastatic melanoma. A preliminary report.* N Engl J Med, 1988. **319**(25): p. 1676-80.

128. Ostrand-Rosenberg, S., *Immune surveillance: a balance between protumor and antitumor immunity.* Curr Opin Genet Dev, 2008. **18**(1): p. 11-8.

129. Zou, W., *Immunosuppressive networks in the tumour environment and their therapeutic relevance.* Nat Rev Cancer, 2005. **5**(4): p. 263-74.

130. Gabrilovich, D.I. and S. Nagaraj, *Myeloid-derived suppressor cells as regulators of the immune system.* Nat Rev Immunol, 2009. **9**(3): p. 162-74.

131. Sica, A., et al., *Macrophage polarization in tumour progression.* Semin Cancer Biol, 2008. **18**(5): p. 349-55.

132. De Palma, M., et al., *Tie2-expressing monocytes: regulation of tumor angiogenesis and therapeutic implications.* Trends Immunol, 2007. **28**(12): p. 519-24.

133. Fridlender, Z.G., et al., *Polarization of tumor-associated neutrophil phenotype by TGF-beta: "N1" versus "N2" TAN.* Cancer Cell, 2009. **16**(3): p. 183-94.

134. Shurin, M.R., et al., *Regulatory dendritic cells: new targets for cancer immunotherapy.* Cancer Biol Ther, 2011. **11**(11): p. 988-92.

135. Viguier, M., et al., *Foxp3 expressing CD4+CD25(high) regulatory T cells are overrepresented in human metastatic melanoma lymph nodes and inhibit the function of infiltrating T cells.* J Immunol, 2004. **173**(2): p. 1444-53.

136. Ghiringhelli, F., et al., *CD4+CD25+ regulatory T cells inhibit natural killer cell functions in a transforming growth factor-beta-dependent manner.* J Exp Med, 2005. **202**(8): p. 1075-85.

137. Ferrone, S. and F.M. Marincola, *Loss of HLA class I antigens by melanoma cells: molecular mechanisms, functional significance and clinical relevance.* Immunol Today, 1995. **16**(10): p. 487-94.

138. Burke, S., et al., *New views on natural killer cell-based immunotherapy for melanoma treatment.* Trends Immunol, 2010. **31**(9): p. 339-45.

139. Kusmartsev, S. and D.I. Gabrilovich, *Effect of tumor-derived cytokines and growth factors on differentiation and immune suppressive features of myeloid cells in cancer.* Cancer Metastasis Rev, 2006. **25**(3): p. 323-31.

140. Dong, Y., et al., *PTEN functions as a melanoma tumor suppressor by promoting host immune response.* Oncogene, 2014. **33**(38): p. 4632-42.

141. Butte, M.J., et al., *Interaction of human PD-L1 and B7-1.* Mol Immunol, 2008. **45**(13): p. 3567-72.

142. Zippelius, A., et al., *Effector function of human tumor-specific CD8 T cells in melanoma lesions: a state of local functional tolerance.* Cancer Res, 2004. **64**(8): p. 2865-73.

143. Sakuishi, K., et al., *Targeting Tim-3 and PD-1 pathways to reverse T cell exhaustion and restore anti-tumor immunity.* J Exp Med, 2010. **207**(10): p. 2187-94.

144. Ahmadzadeh, M., et al., *Tumor antigen-specific CD8 T cells infiltrating the tumor express high levels of PD-1 and are functionally impaired.* Blood, 2009. **114**(8): p. 1537-44.

145. Appay, V., et al., *New generation vaccine induces effective melanoma-specific CD8+ T cells in the circulation but not in the tumor site.* J Immunol, 2006. **177**(3): p. 1670-8.

146. Pikarsky, E., et al., *NF-kappaB functions as a tumour promoter in inflammation-associated cancer.* Nature, 2004. **431**(7007): p. 461-6.

147. Karin, M. and M. Delhase, *The I kappa B kinase (IKK) and NF-kappa B: key elements of proinflammatory signalling.* Semin Immunol, 2000. **12**(1): p. 85-98.

148. McNulty, S.E., et al., *Comparative expression of NFkappaB proteins in melanocytes of normal skin vs. benign intradermal naevus and human metastatic melanoma biopsies.* Pigment Cell Res, 2004. **17**(2): p. 173-80.

149. Yu, H., M. Kortylewski, and D. Pardoll, *Crosstalk between cancer and immune cells: role of STAT3 in the tumour microenvironment.* Nat Rev Immunol, 2007. **7**(1): p. 41-51.

150. Umansky, V. and A. Sevko, *Melanoma-induced immunosuppression and its neutralization.* Semin Cancer Biol, 2012. **22**(4): p. 319-26.

151. Ben-Neriah, Y. and M. Karin, *Inflammation meets cancer, with NF-kappaB as the matchmaker.* Nat Immunol, 2011. **12**(8): p. 715-23.

152. Mantovani, A., C. Garlanda, and P. Allavena, *Molecular pathways and targets in cancer-related inflammation.* Ann Med, 2010. **42**(3): p. 161-70.

153. Mantovani, A., *Molecular pathways linking inflammation and cancer.* Curr Mol Med, 2010. **10**(4): p. 369-73.

154. Grivennikov, S.I., F.R. Greten, and M. Karin, *Immunity, inflammation, and cancer.* Cell, 2010. **140**(6): p. 883-99.

155. Allavena, P., et al., *Chemokines in cancer related inflammation.* Exp Cell Res, 2011. **317**(5): p. 664-73.

156. Boone, B.A. and M.T. Lotze, *Targeting Damage-Associated Molecular Pattern Molecules (DAMPs) and DAMP Receptors in Melanoma*, in *Molecular Diagnostics for Melanoma*, M. Thurin and F.M. Marincola, Editors. 2014, Humana Press. p. 537-552.

157. McGregor, J.M. and C.M. Proby, *The role of papillomaviruses in human non-melanoma skin cancer.* Cancer Surv, 1996. **26**: p. 219-36.

158. Harwood, C.A., et al., *Human papillomavirus and the development of non-melanoma skin cancer.* J Clin Pathol, 1999. **52**(4): p. 249-53.

159. Dreau, D., et al., *Human papilloma virus in melanoma biopsy specimens and its relation to melanoma progression.* Ann Surg, 2000. **231**(5): p. 664-71.

160. Kaskel, P., et al., *S-100 protein in peripheral blood: a marker for melanoma metastases: a prospective 2-center study of 570 patients with melanoma.* J Am Acad Dermatol, 1999. **41**(6): p. 962-9.

161. Helfman, D.M., et al., *The metastasis associated protein S100A4: role in tumour progression and metastasis.* Br J Cancer, 2005. **92**(11): p. 1955-8.

162. Banerjee, S.S. and M. Harris, *Morphological and immunophenotypic variations in malignant melanoma.* Histopathology, 2000. **36**(5): p. 387-402.

163. Shoup, S.A., et al., *A panel of antibodies useful in the cytologic diagnosis of metastatic melanoma.* Acta Cytol, 1990. **34**(3): p. 385-92.

164. Nakajima, T., et al., *An immunoperoxidase study of S-100 protein distribution in normal and neoplastic tissues.* Am J Surg Pathol, 1982. **6**(8): p. 715-27.

165. Shiro, B. and G. Siegal, *S-100 protein*. Monoclonal Antibodies in Diagnostic Immunohistochemistry, ed. M. Wick and G. Siegal. 1988, New York, NY: Marcel Dekker.

166. Sheffield, M.V., et al., *Comparison of five antibodies as markers in the diagnosis of melanoma in cytologic preparations.* Am J Clin Pathol, 2002. **118**(6): p. 930-6.

167. Xu, X., et al., *Immunoprofile of MITF, tyrosinase, melan-A, and MAGE-1 in HMB45-negative melanomas.* Am J Surg Pathol, 2002. **26**(1): p. 82-7.

168. Riddle, N.D. and M.M. Bui, *When melanoma is negative for S100: diagnostic pitfalls.* Arch Pathol Lab Med, 2012. **136**(3): p. 237-9.

169. Breslow, A., *Thickness, cross-sectional areas and depth of invasion in the prognosis of cutaneous melanoma.* Ann Surg, 1970. **172**(5): p. 902-8.

170. Marghoob, A.A., et al., *Breslow thickness and clark level in melanoma: support for including level in pathology reports and in American Joint Committee on Cancer Staging.* Cancer, 2000. **88**(3): p. 589-95.

171. Balch, C.M., et al., *Final version of 2009 AJCC melanoma staging and classification.* J Clin Oncol, 2009. **27**(36): p. 6199-206.

172. Coit, D.G., et al., *Melanoma.* J Natl Compr Canc Netw, 2009. **7**(3): p. 250-75.

173. Garbe, C., et al., *Diagnosis and treatment of melanoma: European consensus-based interdisciplinary guideline.* Eur J Cancer, 2010. **46**(2): p. 270-83.

174. Barth, A., L.A. Wanek, and D.L. Morton, *Prognostic factors in 1,521 melanoma patients with distant metastases.* J Am Coll Surg, 1995. **181**(3): p. 193-201.

175. Serrone, L., et al., *Dacarbazine-based chemotherapy for metastatic melanoma: thirty-year experience overview.* J Exp Clin Cancer Res, 2000. **19**(1): p. 21-34.

176. Eggermont, A.M., A. Spatz, and C. Robert, *Cutaneous melanoma.* Lancet, 2014. **383**(9919): p. 816-27.

177. Eggermont, A.M. and J.M. Kirkwood, *Re-evaluating the role of dacarbazine in metastatic melanoma: what have we learned in 30 years?* Eur J Cancer, 2004. **40**(12): p. 1825-36.

178. Peggs, K.S., et al., *Principles and use of anti-CTLA4 antibody in human cancer immunotherapy.* Curr Opin Immunol, 2006. **18**(2): p. 206-13.

179. Hodi, F.S., et al., *Improved survival with ipilimumab in patients with metastatic melanoma.* N Engl J Med, 2010. **363**(8): p. 711-23.

180. Chapman, P.B., et al., *Improved survival with vemurafenib in melanoma with BRAF V600E mutation.* N Engl J Med, 2011. **364**(26): p. 2507-16.

181. Hauschild, A., et al., *Dabrafenib in BRAF-mutated metastatic melanoma: a multicentre, open-label, phase 3 randomised controlled trial.* Lancet, 2012. **380**(9839): p. 358-65.

182. Flaherty, K.T., et al., *Improved survival with MEK inhibition in BRAF-mutated melanoma.* N Engl J Med, 2012. **367**(2): p. 107-14.

183. Larkin, J., et al., *Combined vemurafenib and cobimetinib in BRAF-mutated melanoma.* N Engl J Med, 2014. **371**(20): p. 1867-76.

184. Ascierto, P.A., et al., *Phase II trial (BREAK-2) of the BRAF inhibitor dabrafenib (GSK2118436) in patients with metastatic melanoma.* J Clin Oncol, 2013. **31**(26): p. 3205-11.

185. Sosman, J.A., et al., *A phase 1b/2 study of LEE011 in combination with binimetinib (MEK162) in patients with NRAS-mutant melanoma: Early encouraging clinical activity*, in *ASCO Annual Meeting 2014*. 2014.

186. Weber, J.S., et al., *Phase I/II study of ipilimumab for patients with metastatic melanoma.* J Clin Oncol, 2008. **26**(36): p. 5950-6.

187. Hamid, O., et al., *Safety and tumor responses with lambrolizumab (anti-PD-1) in melanoma.* N Engl J Med, 2013. **369**(2): p. 134-44.

188. FDA. *FDA approves Keytruda for advanced melanoma: First PD-1 blocking drug to receive agency approval*. 2014 09/10/2014 Available from: http://www.fda.gov/NewsEvents/Newsroom/PressAnnouncements/ucm412802.htm.

189. FDA. *Nivolumab*. 2014 12/23/2014; Available from: http://www.fda.gov/drugs/informationondrugs/approveddrugs/ucm427807.htm.

190. Kirkwood, J.M., et al., *Immunomodulatory effects of high-dose and low-dose interferon alpha2b in patients with high-risk resected melanoma: the E2690 laboratory corollary of intergroup adjuvant trial E1690.* Cancer, 2002. **95**(5): p. 1101-12.

191. Wang, W., et al., *Modulation of signal transducers and activators of transcription 1 and 3 signaling in melanoma by high-dose IFNalpha2b.* Clin Cancer Res, 2007. **13**(5): p. 1523-31.

192. Paquette, R.L., et al., *Interferon-alpha and granulocyte-macrophage colony-stimulating factor differentiate peripheral blood monocytes into potent antigen-presenting cells.* J Leukoc Biol, 1998. **64**(3): p. 358-67.

193. Parlato, S., et al., *Expression of CCR-7, MIP-3beta, and Th-1 chemokines in type I IFN-induced monocyte-derived dendritic cells: importance for the rapid acquisition of potent migratory and functional activities.* Blood, 2001. **98**(10): p. 3022-9.

194. Brinkmann, V., et al., *Interferon alpha increases the frequency of interferon gamma-producing human CD4+ T cells.* J Exp Med, 1993. **178**(5): p. 1655-63.

195. Palmer, K.J., et al., *Interferon-alpha (IFN-alpha) stimulates anti-melanoma cytotoxic T lymphocyte (CTL) generation in mixed lymphocyte tumour cultures (MLTC).* Clin Exp Immunol, 2000. **119**(3): p. 412-8.

196. Rosenberg, S.A., et al., *Treatment of 283 consecutive patients with metastatic melanoma or renal cell cancer using high-dose bolus interleukin 2.* JAMA, 1994. **271**(12): p. 907-13.

197. Rosenberg, S.A., et al., *Durable complete responses in heavily pretreated patients with metastatic melanoma using T-cell transfer immunotherapy.* Clin Cancer Res, 2011. **17**(13): p. 4550-7.

198. Atkins, M.B., et al., *High-dose recombinant interleukin 2 therapy for patients with metastatic melanoma: analysis of 270 patients treated between 1985 and 1993.* J Clin Oncol, 1999. **17**(7): p. 2105-16.

199. Larkin, J., et al., *Vemurafenib in patients with BRAF(V600) mutated metastatic melanoma: an open-label, multicentre, safety study.* Lancet Oncol, 2014. **15**(4): p. 436-44.

200. Anforth, R., P. Fernandez-Penas, and G.V. Long, *Cutaneous toxicities of RAF inhibitors.* Lancet Oncol, 2013. **14**(1): p. e11-8.

201. Boyd, K.P., et al., *Nonmalignant cutaneous findings associated with vemurafenib use in patients with metastatic melanoma.* J Am Acad Dermatol, 2012. **67**(6): p. 1375-9.

202. Lacouture, M.E., et al., *Analysis of dermatologic events in vemurafenib-treated patients with melanoma.* Oncologist, 2013. **18**(3): p. 314-22.

203. Long, G.V., et al., *Combined BRAF and MEK inhibition versus BRAF inhibition alone in melanoma.* N Engl J Med, 2014. **371**(20): p. 1877-88.

204. Montagut, C. and J. Settleman, *Targeting the RAF-MEK-ERK pathway in cancer therapy.* Cancer Lett, 2009. **283**(2): p. 125-34.

205. Villanueva, J., et al., *Acquired resistance to BRAF inhibitors mediated by a RAF kinase switch in melanoma can be overcome by cotargeting MEK and IGF-1R/PI3K.* Cancer Cell, 2010. **18**(6): p. 683-95.

206. Sosman, J.A., et al., *Analysis of molecular mechanisms of response and resistance to vemurafenib (vem) in BRAFV600E melanoma*, in *ASCO Annual Meeting*. 2012.

207. Nazarian, R., et al., *Melanomas acquire resistance to B-RAF(V600E) inhibition by RTK or N-RAS upregulation.* Nature, 2010. **468**(7326): p. 973-7.

208. Aplin, A.E., F.M. Kaplan, and Y. Shao, *Mechanisms of resistance to RAF inhibitors in melanoma.* J Invest Dermatol, 2011. **131**(9): p. 1817-20.

209. Johannessen, C.M., et al., *COT drives resistance to RAF inhibition through MAP kinase pathway reactivation.* Nature, 2010. **468**(7326): p. 968-72.

210. Smalley, K.S., et al., *Increased cyclin D1 expression can mediate BRAF inhibitor resistance in BRAF V600E-mutated melanomas.* Mol Cancer Ther, 2008. **7**(9): p. 2876-83.

211. Sharma, S.V., et al., *A chromatin-mediated reversible drug-tolerant state in cancer cell subpopulations.* Cell, 2010. **141**(1): p. 69-80.

212. Bronstein, Y., et al., *Radiologic manifestations of immune-related adverse events in patients with metastatic melanoma undergoing anti-CTLA-4 antibody therapy.* AJR Am J Roentgenol, 2011. **197**(6): p. W992-W1000.

213. Corp., M.S.D., *Effect of Proactive Management of Side Effects on Treatment Compliance in Malignant Melanoma Patients on High-dose Intron A Therapy (Study P04600)*. 2008 (Updated in 2014).

214. DeVita, V.T., et al., *Interleukin therapy*, in *Cancer: principles and practice of oncologyy*, V.T. DeVita, T.S. Lawrence, and S.A. Rosenberg, Editors. 2008, Lippincott Williams and Wilkins: Philadelphia.

215. DeVita, V.T., et al., *Interleukin-2*, in *Cancer: principles and practice of oncology*, V.T. DeVita, T. Lawrence, and S.A. Rosenberg, Editors. 2005, Lippincott Williams and Wilkins: Philadelphia.

216. Neeper, M., et al., *Cloning and expression of a cell surface receptor for advanced glycosylation end products of proteins.* J Biol Chem, 1992. **267**(21): p. 14998-5004.

217. Ahmed, N., et al., *Protein glycation, oxidation and nitration adduct residues and free adducts of cerebrospinal fluid in Alzheimer's disease and link to cognitive impairment.* J Neurochem, 2005. **92**(2): p. 255-63.

218. Hofmann, M.A., et al., *RAGE mediates a novel proinflammatory axis: a central cell surface receptor for S100/calgranulin polypeptides.* Cell, 1999. **97**(7): p. 889-901.

219. Orlova, V.V., et al., *A novel pathway of HMGB1-mediated inflammatory cell recruitment that requires Mac-1-integrin.* EMBO J, 2007. **26**(4): p. 1129-39.

220. Bierhaus, A. and P.P. Nawroth, *The Alzheimer's disease-diabetes angle: inevitable fate of aging or metabolic imbalance limiting successful aging. Preface.* J Alzheimers Dis, 2009. **16**(4): p. 673-5.

221. Park, L., et al., *Suppression of accelerated diabetic atherosclerosis by the soluble receptor for advanced glycation endproducts.* Nat Med, 1998. **4**(9): p. 1025-31.

222. Taguchi, A., et al., *Blockade of RAGE-amphoterin signalling suppresses tumour growth and metastases.* Nature, 2000. **405**(6784): p. 354-60.

223. Tsuji, A., et al., *Induction of receptor for advanced glycation end products by EBV latent membrane protein 1 and its correlation with angiogenesis and cervical lymph node metastasis in nasopharyngeal carcinoma.* Clin Cancer Res, 2008. **14**(17): p. 5368-75.

224. Pichiule, P., et al., *Hypoxia-inducible factor-1 mediates neuronal expression of the receptor for advanced glycation end products following hypoxia/ischemia.* J Biol Chem, 2007. **282**(50): p. 36330-40.

225. Li, J. and A.M. Schmidt, *Characterization and functional analysis of the promoter of RAGE, the receptor for advanced glycation end products.* J Biol Chem, 1997. **272**(26): p. 16498-506.

226. Reynolds, P.R., et al., *RAGE: developmental expression and positive feedback regulation by Egr-1 during cigarette smoke exposure in pulmonary epithelial cells.* Am J Physiol Lung Cell Mol Physiol, 2008. **294**(6): p. L1094-101.

227. Hudson, B.I., M.H. Stickland, and P.J. Grant, *Identification of polymorphisms in the receptor for advanced glycation end products (RAGE) gene: prevalence in type 2 diabetes and ethnic groups.* Diabetes, 1998. **47**(7): p. 1155-7.

228. Hudson, B.I., et al., *Effects of novel polymorphisms in the RAGE gene on transcriptional regulation and their association with diabetic retinopathy.* Diabetes, 2001. **50**(6): p. 1505-11.

229. Schenk, S., et al., *A novel polymorphism in the promoter of the RAGE gene is associated with non-small cell lung cancer.* Lung Cancer, 2001. **32**(1): p. 7-12.

230. Sullivan, C.M., et al., *RAGE polymorphisms and the heritability of insulin resistance: the Leeds family study.* Diab Vasc Dis Res, 2005. **2**(1): p. 42-4.

231. Pettersson-Fernholm, K., et al., *The functional -374 T/A RAGE gene polymorphism is associated with proteinuria and cardiovascular disease in type 1 diabetic patients.* Diabetes, 2003. **52**(3): p. 891-4.

232. JiXiong, X., et al., *-429T/C and -374T/A polymorphisms of RAGE gene promoter are not associated with diabetic retinopathy in Chinese patients with type 2 diabetes.* Diabetes Care, 2003. **26**(9): p. 2696-7.

233. Hudson, B.I., et al., *Identification, classification, and expression of RAGE gene splice variants.* FASEB J, 2008. **22**(5): p. 1572-80.

234. Malherbe, P., et al., *cDNA cloning of a novel secreted isoform of the human receptor for advanced glycation end products and characterization of cells co-expressing cell-surface scavenger receptors and Swedish mutant amyloid precursor protein.* Brain Res Mol Brain Res, 1999. **71**(2): p. 159-70.

235. Williams, A.F. and A.N. Barclay, *The immunoglobulin superfamily--domains for cell surface recognition.* Annu Rev Immunol, 1988. **6**: p. 381-405.

236. Dattilo, B.M., et al., *The extracellular region of the receptor for advanced glycation end products is composed of two independent structural units.* Biochemistry, 2007. **46**(23): p. 6957-70.

237. Leclerc, E., et al., *Crosstalk between calcium, amyloid beta and the receptor for advanced glycation endproducts in Alzheimer's disease.* Rev Neurosci, 2009. **20**(2): p. 95-110.

238. Fritz, G., *RAGE: a single receptor fits multiple ligands.* Trends Biochem Sci, 2011. **36**(12): p. 625-32.

239. Ishihara, K., et al., *The receptor for advanced glycation end-products (RAGE) directly binds to ERK by a D-domain-like docking site.* FEBS Lett, 2003. **550**(1-3): p. 107-13.

240. Ohe, K., et al., *Regulation of alternative splicing of the receptor for advanced glycation endproducts (RAGE) through G-rich cis-elements and heterogenous nuclear ribonucleoprotein H.* J Biochem, 2010. **147**(5): p. 651-9.

241. Liu, X.Y., et al., *Regulation of RAGE splicing by hnRNP A1 and Tra2beta-1 and its potential role in AD pathogenesis.* J Neurochem, 2015. **133**(2): p. 187-98.

242. Zhu, H. and Q. Ding, *Lower expression level of two RAGE alternative splicing isoforms in Alzheimer's disease.* Neurosci Lett, 2015. **597**: p. 66-70.

243. Wei, W., et al., *Disulfide bonds within the C2 domain of RAGE play key roles in its dimerization and biogenesis.* PLoS One, 2012. **7**(12): p. e50736.

244. Xie, J., et al., *Structural basis for pattern recognition by the receptor for advanced glycation end products (RAGE).* J Biol Chem, 2008. **283**(40): p. 27255-69.

245. Xu, D., et al., *Heparan sulfate is essential for high mobility group protein 1 (HMGB1) signaling by the receptor for advanced glycation end products (RAGE).* J Biol Chem, 2011. **286**(48): p. 41736-44.

246. Xu, D., et al., *Stable RAGE-heparan sulfate complexes are essential for signal transduction.* ACS Chem Biol, 2013. **8**(7): p. 1611-20.

247. Sorci, G., et al., *The danger signal S100B integrates pathogen- and danger-sensing pathways to restrain inflammation.* PLoS Pathog, 2011. **7**(3): p. e1001315.

248. Srikrishna, G., et al., *N -Glycans on the receptor for advanced glycation end products influence amphoterin binding and neurite outgrowth.* J Neurochem, 2002. **80**(6): p. 998-1008.

249. Kang, R., et al., *The HMGB1/RAGE inflammatory pathway promotes pancreatic tumor growth by regulating mitochondrial bioenergetics.* Oncogene, 2014. **33**(5): p. 567-77.

250. Galichet, A., M. Weibel, and C.W. Heizmann, *Calcium-regulated intramembrane proteolysis of the RAGE receptor.* Biochem Biophys Res Commun, 2008. **370**(1): p. 1-5.

251. Raucci, A., et al., *A soluble form of the receptor for advanced glycation endproducts (RAGE) is produced by proteolytic cleavage of the membrane-bound form by the sheddase a disintegrin and metalloprotease 10 (ADAM10).* FASEB J, 2008. **22**(10): p. 3716-27.

252. Zhang, L., et al., *Receptor for advanced glycation end products is subjected to protein ectodomain shedding by metalloproteinases.* J Biol Chem, 2008. **283**(51): p. 35507-16.

253. Garlick, R.L., et al., *Nonenzymatic glycation of human lens crystallin. Effect of aging and diabetes mellitus.* J Clin Invest, 1984. **74**(5): p. 1742-9.

254. Toth, C., et al., *Diabetes, leukoencephalopathy and rage.* Neurobiol Dis, 2006. **23**(2): p. 445-61.

255. Yan, S.F., et al., *Glycation, inflammation, and RAGE: a scaffold for the macrovascular complications of diabetes and beyond.* Circ Res, 2003. **93**(12): p. 1159-69.

256. Sander, C.S., et al., *Oxidative stress in malignant melanoma and non-melanoma skin cancer.* Br J Dermatol, 2003. **148**(5): p. 913-22.

257. Matzinger, P., *The danger model: a renewed sense of self.* Science, 2002. **296**(5566): p. 301-5.

258. Boni, R., et al., *Immunohistochemical localization of the Ca2+ binding S100 proteins in normal human skin and melanocytic lesions.* Br J Dermatol, 1997. **137**(1): p. 39-43.

259. Schmidt, A.M., et al., *RAGE: a multiligand receptor contributing to the cellular response in diabetic vasculopathy and inflammation.* Semin Thromb Hemost, 2000. **26**(5): p. 485-93.

260. Donato, R., *RAGE: a single receptor for several ligands and different cellular responses: the case of certain S100 proteins.* Curr Mol Med, 2007. **7**(8): p. 711-24.

261. Sparvero, L.J., et al., *RAGE (Receptor for Advanced Glycation Endproducts), RAGE ligands, and their role in cancer and inflammation.* J Transl Med, 2009. **7**: p. 17.

262. Poser, I., et al., *Upregulation of HMG1 leads to melanoma inhibitory activity expression in malignant melanoma cells and contributes to their malignancy phenotype.* Mol Cell Biol, 2003. **23**(8): p. 2991-8.

263. Donato, R., *Intracellular and extracellular roles of S100 proteins.* Microsc Res Tech, 2003. **60**(6): p. 540-51.

264. Heizmann, C.W., *The multifunctional S100 protein family.* Methods Mol Biol, 2002. **172**: p. 69-80.

265. Zimmer, D.B., et al., *Evolution of the S100 family of calcium sensor proteins.* Cell Calcium, 2013. **53**(3): p. 170-9.

266. Marenholz, I., R.C. Lovering, and C.W. Heizmann, *An update of the S100 nomenclature.* Biochim Biophys Acta, 2006. **1763**(11): p. 1282-3.

267. Marenholz, I., C.W. Heizmann, and G. Fritz, *S100 proteins in mouse and man: from evolution to function and pathology (including an update of the nomenclature).* Biochem Biophys Res Commun, 2004. **322**(4): p. 1111-22.

268. Heizmann, C.W., G. Fritz, and B.W. Schafer, *S100 proteins: structure, functions and pathology.* Front Biosci, 2002. **7**: p. d1356-68.

269. Lin, J., et al., *The calcium-binding protein S100B down-regulates p53 and apoptosis in malignant melanoma.* J Biol Chem, 2010. **285**(35): p. 27487-98.

270. Mueller, A., et al., *The calcium-binding protein S100A2 interacts with p53 and modulates its transcriptional activity.* J Biol Chem, 2005. **280**(32): p. 29186-93.

271. Ostendorp, T., et al., *Structural and functional insights into RAGE activation by multimeric S100B.* EMBO J, 2007. **26**(16): p. 3868-78.

272. Wang, G., et al., *Heterodimeric interaction and interfaces of S100A1 and S100P.* Biochem J, 2004. **382**(Pt 1): p. 375-83.

273. Leclerc, E. and C.W. Heizmann, *The importance of Ca2+/Zn2+ signaling S100 proteins and RAGE in translational medicine.* Front Biosci (Schol Ed), 2011. **3**: p. 1232-62.

274. Hermann, A., et al., *S100 calcium binding proteins and ion channels.* Front Pharmacol, 2012. **3**: p. 67.

275. Donato, R., et al., *Functions of S100 proteins.* Curr Mol Med, 2013. **13**(1): p. 24-57.

276. Hsieh, H.L., et al., *S100 protein translocation in response to extracellular S100 is mediated by receptor for advanced glycation endproducts in human endothelial cells.* Biochem Biophys Res Commun, 2004. **316**(3): p. 949-59.

277. Perrone, L., G. Peluso, and M.A. Melone, *RAGE recycles at the plasma membrane in S100B secretory vesicles and promotes Schwann cells morphological changes.* J Cell Physiol, 2008. **217**(1): p. 60-71.

278. Glenney, J.R., Jr., M.S. Kindy, and L. Zokas, *Isolation of a new member of the S100 protein family: amino acid sequence, tissue, and subcellular distribution.* J Cell Biol, 1989. **108**(2): p. 569-78.

279. Maelandsmo, G.M., et al., *Differential expression patterns of S100A2, S100A4 and S100A6 during progression of human malignant melanoma.* Int J Cancer, 1997. **74**(4): p. 464-9.

280. Leclerc, E., C.W. Heizmann, and S.W. Vetter, *RAGE and S100 protein transcription levels are highly variable in human melanoma tumors and cells.* Gen Physiol Biophys, 2009. **28** p. F65-75.

281. Andersen, K., et al., *Expression of S100A4 combined with reduced E-cadherin expression predicts patient outcome in malignant melanoma.* Mod Pathol, 2004. **17**(8): p. 990-7.

282. Weterman, M.A., et al., *Expression of calcyclin in human melanocytic lesions.* Cancer Res, 1993. **53**(24): p. 6061-6.

283. Hibino, T., et al., *S100A9 is a novel ligand of EMMPRIN that promotes melanoma metastasis.* Cancer Res, 2013. **73**(1): p. 172-83.

284. Thomas, J.O. and A.A. Travers, *HMG1 and 2, and related 'architectural' DNA-binding proteins.* Trends Biochem Sci, 2001. **26**(3): p. 167-74.

285. Thomas, J.O., *HMG1 and 2: architectural DNA-binding proteins.* Biochem Soc Trans, 2001. **29**(Pt 4): p. 395-401.

286. Rauvala, H. and A. Rouhiainen, *Physiological and pathophysiological outcomes of the interactions of HMGB1 with cell surface receptors.* Biochim Biophys Acta, 2010. **1799**(1-2): p. 164-70.

287. Rauvala, H., et al., *The adhesive and neurite-promoting molecule p30: analysis of the amino-terminal sequence and production of antipeptide antibodies that detect p30 at the surface of neuroblastoma cells and of brain neurons.* J Cell Biol, 1988. **107**(6 Pt 1): p. 2293-305.

288. Merenmies, J., et al., *30-kDa heparin-binding protein of brain (amphoterin) involved in neurite outgrowth. Amino acid sequence and localization in the filopodia of the advancing plasma membrane.* J Biol Chem, 1991. **266**(25): p. 16722-9.

289. Tang, D., et al., *High-mobility group box 1, oxidative stress, and disease.* Antioxid Redox Signal, 2011. **14**(7): p. 1315-35.

290. Ito, I., J. Fukazawa, and M. Yoshida, *Post-translational methylation of high mobility group box 1 (HMGB1) causes its cytoplasmic localization in neutrophils.* J Biol Chem, 2007. **282**(22): p. 16336-44.

291. Bonaldi, T., et al., *Monocytic cells hyperacetylate chromatin protein HMGB1 to redirect it towards secretion.* EMBO J, 2003. **22**(20): p. 5551-60.

292. Youn, J.H. and J.S. Shin, *Nucleocytoplasmic shuttling of HMGB1 is regulated by phosphorylation that redirects it toward secretion.* J Immunol, 2006. **177**(11): p. 7889-97.

293. Gardella, S., et al., *The nuclear protein HMGB1 is secreted by monocytes via a non-classical, vesicle-mediated secretory pathway.* EMBO Rep, 2002. **3**(10): p. 995-1001.

294. Sims, G.P., et al., *HMGB1 and RAGE in inflammation and cancer.* Annu Rev Immunol, 2010. **28**: p. 367-88.

295. Bald, T., et al., *Ultraviolet-radiation-induced inflammation promotes angiotropism and metastasis in melanoma.* Nature, 2014. **507**(7490): p. 109-13.

296. Sasahira, T., et al., *High mobility group box-1-inducible melanoma inhibitory activity is associated with nodal metastasis and lymphangiogenesis in oral squamous cell carcinoma.* Cancer Sci, 2008. **99**(9): p. 1806-12.

297. Koch, M., et al., *Structural basis for ligand recognition and activation of RAGE.* Structure, 2010. **18**(10): p. 1342-52.

298. Leclerc, E., et al., *Binding of S100 proteins to RAGE: an update.* Biochim Biophys Acta, 2009. **1793**(6): p. 993-1007.

299. Hudson, B.I., et al., *Interaction of the RAGE cytoplasmic domain with diaphanous-1 is required for ligand-stimulated cellular migration through activation of Rac1 and Cdc42.* J Biol Chem, 2008. **283**(49): p. 34457-68.

300. Sakaguchi, M., et al., *TIRAP, an adaptor protein for TLR2/4, transduces a signal from RAGE phosphorylated upon ligand binding.* PLoS One, 2011. **6**(8): p. e23132.

301. Lander, H.M., et al., *Activation of the receptor for advanced glycation end products triggers a p21(ras)-dependent mitogen-activated protein kinase pathway regulated by oxidant stress.* J Biol Chem, 1997. **272**(28): p. 17810-4.

302. Huttunen, H.J., C. Fages, and H. Rauvala, *Receptor for advanced glycation end products (RAGE)-mediated neurite outgrowth and activation of NF-kappaB require the cytoplasmic domain of the receptor but different downstream signaling pathways.* J Biol Chem, 1999. **274**(28): p. 19919-24.

303. Toure, F., et al., *Receptor for advanced glycation end-products (RAGE) modulates neutrophil adhesion and migration on glycoxidated extracellular matrix.* Biochem J, 2008. **416**(2): p. 255-61.

304. Tanaka, N., et al., *The receptor for advanced glycation end products is induced by the glycation products themselves and tumor necrosis factor-alpha through nuclear factor-kappa B, and by 17beta-estradiol through Sp-1 in human vascular endothelial cells.* J Biol Chem, 2000. **275**(33): p. 25781-90.

305. Huttunen, H.J., J. Kuja-Panula, and H. Rauvala, *Receptor for advanced glycation end products (RAGE) signaling induces CREB-dependent chromogranin expression during neuronal differentiation.* J Biol Chem, 2002. **277**(41): p. 38635-46.

306. Bianchi, R., I. Giambanco, and R. Donato, *S100B/RAGE-dependent activation of microglia via NF-kappaB and AP-1 Co-regulation of COX-2 expression by S100B, IL-1beta and TNF-alpha.* Neurobiol Aging, 2010. **31**(4): p. 665-77.

307. Perrone, L., et al., *Thioredoxin interacting protein (TXNIP) induces inflammation through chromatin modification in retinal capillary endothelial cells under diabetic conditions.* J Cell Physiol, 2009. **221**(1): p. 262-72.

308. Bierhaus, A., et al., *Understanding RAGE, the receptor for advanced glycation end products.* J Mol Med (Berl), 2005. **83**(11): p. 876-86.

309. Schmidt, A.M., et al., *The biology of the receptor for advanced glycation end products and its ligands.* Biochim Biophys Acta, 2000. **1498**(2-3): p. 99-111.

310. Brett, J., et al., *Survey of the distribution of a newly characterized receptor for advanced glycation end products in tissues.* Am J Pathol, 1993. **143**(6): p. 1699-712.

311. Hanford, L.E., et al., *Regulation of receptor for advanced glycation end products during bleomycin-induced lung injury.* Am J Respir Cell Mol Biol, 2003. **29**(3 Suppl): p. S77-81.

312. Schraml, P., I. Bendik, and C.U. Ludwig, *Differential messenger RNA and protein expression of the receptor for advanced glycosylated end products in normal lung and non-small cell lung carcinoma.* Cancer Res, 1997. **57**(17): p. 3669-71.

313. Bartling, B., et al., *Down-regulation of the receptor for advanced glycation end-products (RAGE) supports non-small cell lung carcinoma.* Carcinogenesis, 2005. **26**(2): p. 293-301.

314. Liliensiek, B., et al., *Receptor for advanced glycation end products (RAGE) regulates sepsis but not the adaptive immune response.* J Clin Invest, 2004. **113**(11): p. 1641-50.

315. Sakatani, S., et al., *Deletion of RAGE causes hyperactivity and increased sensitivity to auditory stimuli in mice.* PLoS One, 2009. **4**(12): p. e8309.

316. Zhou, Z., et al., *Regulation of osteoclast function and bone mass by RAGE.* J Exp Med, 2006. **203**(4): p. 1067-80.

317. Rong, L.L., et al., *RAGE modulates peripheral nerve regeneration via recruitment of both inflammatory and axonal outgrowth pathways.* FASEB J, 2004. **18**(15): p. 1818-25.

318. Rong, L.L., et al., *Antagonism of RAGE suppresses peripheral nerve regeneration.* FASEB J, 2004. **18**(15): p. 1812-7.

319. Galasko, D., et al., *Clinical trial of an inhibitor of RAGE-Abeta interactions in Alzheimer disease.* Neurology, 2014. **82**(17): p. 1536-42.

320. Schmidt, A.M. and D.M. Stern, *Receptor for age (RAGE) is a gene within the major histocompatibility class III region: implications for host response mechanisms in homeostasis and chronic disease.* Front Biosci, 2001. **6**: p. D1151-60.

321. Damasiewicz-Bodzek, A. and T. Wielkoszynski, *Advanced protein glycation in psoriasis.* J Eur Acad Dermatol Venereol, 2012. **26**(2): p. 172-9.

322. Piruzian, E., et al., *Integrated network analysis of transcriptomic and proteomic data in psoriasis.* BMC Syst Biol, 2010. **4**: p. 41.

323. Heo, Y.J., et al., *The expression of the receptor for advanced glycation end-products (RAGE) in RA-FLS is induced by IL-17 via Act-1.* Arthritis Res Ther, 2011. **13**(4): p. R113.

324. Lv, B., et al., *High-mobility group box 1 protein induces tissue factor expression in vascular endothelial cells via activation of NF-kappaB and Egr-1.* Thromb Haemost, 2009. **102**(2): p. 352-9.

325. Schmidt, A.M., S.D. Yan, and D.M. Stern, *The dark side of glucose.* Nat Med, 1995. **1**(10): p. 1002-4.

326. Sternberg, Z., et al., *AGE-RAGE in multiple sclerosis brain.* Immunol Invest, 2011. **40**(2): p. 197-205.

327. Hori, O., et al., *The receptor for advanced glycation end products (RAGE) is a cellular binding site for amphoterin. Mediation of neurite outgrowth and co-expression of rage and amphoterin in the developing nervous system.* J Biol Chem, 1995. **270**(43): p. 25752-61.

328. Falcone, C., et al., *Plasma levels of soluble receptor for advanced glycation end products and coronary atherosclerosis: possible correlation with clinical presentation.* Dis Markers, 2013. **35**(3): p. 135-40.

329. Moss, S.E., R. Klein, and B.E. Klein, *Cause-specific mortality in a population-based study of diabetes.* Am J Public Health, 1991. **81**(9): p. 1158-62.

330. Schmidt, A.M., et al., *Receptor for advanced glycation end products (AGEs) has a central role in vessel wall interactions and gene activation in response to circulating AGE proteins.* Proc Natl Acad Sci U S A, 1994. **91**(19): p. 8807-11.

331. Wautier, J.L., et al., *Receptor-mediated endothelial cell dysfunction in diabetic vasculopathy. Soluble receptor for advanced glycation end products blocks hyperpermeability in diabetic rats.* J Clin Invest, 1996. **97**(1): p. 238-43.

332. Muhammad, S., et al., *The HMGB1 receptor RAGE mediates ischemic brain damage.* J Neurosci, 2008. **28**(46): p. 12023-31.

333. Glenner, G.G. and C.W. Wong, *Alzheimer's disease: initial report of the purification and characterization of a novel cerebrovascular amyloid protein.* Biochem Biophys Res Commun, 1984. **120**(3): p. 885-90.

334. Yan, S.D., et al., *RAGE and amyloid-beta peptide neurotoxicity in Alzheimer's disease.* Nature, 1996. **382**(6593): p. 685-91.

335. Lue, L.F., et al., *Involvement of microglial receptor for advanced glycation endproducts (RAGE) in Alzheimer's disease: identification of a cellular activation mechanism.* Exp Neurol, 2001. **171**(1): p. 29-45.

336. Son, S.M., et al., *Abeta-induced formation of autophagosomes is mediated by RAGE-CaMKKbeta-AMPK signaling.* Neurobiol Aging, 2012. **33**(5): p. 1006 e11-23.

337. Glasnovic, A., et al., *Decreased level of sRAGE in the cerebrospinal fluid of multiple sclerosis patients at clinical onset.* Neuroimmunomodulation, 2014. **21**(5): p. 226-33.

338. Mantovani, A., et al., *Cancer-related inflammation.* Nature, 2008. **454**(7203): p. 436-44.

339. Xia, W., et al., *Association of RAGE polymorphisms and cancer risk: a meta-analysis of 27 studies.* Med Oncol, 2015. **32**(2): p. 442.

340. Su, S., et al., *RAGE gene polymorphism and environmental factor in the risk of oral cancer.* J Dent Res, 2015. **94**(3): p. 403-11.

341. Kostova, N., et al., *The expression of HMGB1 protein and its receptor RAGE in human malignant tumors.* Mol Cell Biochem, 2010. **337**(1-2): p. 251-8.

342. Turovskaya, O., et al., *RAGE, carboxylated glycans and S100A8/A9 play essential roles in colitis-associated carcinogenesis.* Carcinogenesis, 2008. **29**(10): p. 2035-43.

343. Kuniyasu, H., et al., *Expression of receptors for advanced glycation end-products (RAGE) is closely associated with the invasive and metastatic activity of gastric cancer.* J Pathol, 2002. **196**(2): p. 163-70.

344. Schraml, P., et al., *Identification of genes differentially expressed in normal lung and non-small cell lung carcinoma tissue.* Cancer Res, 1994. **54**(19): p. 5236-40.

345. Kuniyasu, H., et al., *Amphoterin induction in prostatic stromal cells by androgen deprivation is associated with metastatic prostate cancer.* Oncol Rep, 2003. **10**(6): p. 1863-8.

346. Sasahira, T., et al., *Receptor for advanced glycation end products (RAGE) is important in the prediction of recurrence in human oral squamous cell carcinoma.* Histopathology, 2007. **51**(2): p. 166-72.

347. Eichmuller, S., et al., *mRNA expression of tumor-associated antigens in melanoma tissues and cell lines.* Exp Dermatol, 2002. **11**(4): p. 292-301.

348. Wang, D., et al., *Overexpression of the Receptor for Advanced Glycation Endproducts (RAGE) Is Associated with Poor Prognosis in Gastric Cancer.* PLoS One, 2015. **10**(4): p. e0122697.

349. Gebhardt, C., et al., *RAGE signaling sustains inflammation and promotes tumor development.* J Exp Med, 2008. **205**(2): p. 275-85.

350. Kang, R., et al., *The expression of the receptor for advanced glycation endproducts (RAGE) is permissive for early pancreatic neoplasia.* Proc Natl Acad Sci U S A, 2012. **109**(18): p. 7031-6.

351. Kang, R., et al., *RAGE regulates autophagy and apoptosis following oxidative injury.* Autophagy, 2011. **7**(4): p. 442-4.

352. Zhang, Q.-Y., et al., *Autophagy-mediated HMGB1 release promotes gastric cancer cell survival via RAGE activation of extracellular signal-regulated kinases 1/2.* Oncology Reports, 2015. **33**(4): p. 1630-1638.

353. Riuzzi, F., G. Sorci, and R. Donato, *RAGE expression in rhabdomyosarcoma cells results in myogenic differentiation and reduced proliferation, migration, invasiveness, and tumor growth.* Am J Pathol, 2007. **171**(3): p. 947-61.

354. Jules, J., D. Maiguel, and B.I. Hudson, *Alternative splicing of the RAGE cytoplasmic domain regulates cell signaling and function.* PLoS One, 2013. **8**(11): p. e78267.

355. Masaki, H., Y. Okano, and H. Sakurai, *Generation of active oxygen species from advanced glycation end-products (AGEs) during ultraviolet light A (UVA) irradiation and a possible mechanism for cell damaging.* Biochim Biophys Acta, 1999. **1428**(1): p. 45-56.

356. Abe, R., et al., *Regulation of human melanoma growth and metastasis by AGE-AGE receptor interactions.* J Invest Dermatol, 2004. **122**(2): p. 461-7.

357. Ojima, A., et al., *DNA aptamer raised against advanced glycation end products (AGEs) improves glycemic control and decreases adipocyte size in fructose-fed rats by suppressing AGE-RAGE axis.* Horm Metab Res, 2015. **47**(4): p. 253-8.

358. Meghnani, V., S.W. Vetter, and E. Leclerc, *RAGE overexpression confers a metastatic phenotype to the WM115 human primary melanoma cell line.* Biochim Biophys Acta, 2014. **1842**(7): p. 1017-27.

359. Meghnani, V., et al., *The receptor for advanced glycation end products influences the expression of its S100 protein ligands in melanoma tumors.* The International Journal of Biochemistry & Cell Biology, 2014. **57**(0): p. 54-62.

360. Popa, I., E. Ganea, and S.M. Petrescu, *Expression and subcellular localization of RAGE in melanoma cells.* Biochem Cell Biol, 2014. **92**(2): p. 127-36.

361. Wagner, N.B., et al., *Diminished levels of the soluble form of RAGE are related to poor survival in malignant melanoma.* Int J Cancer, 2015.

362. Yu, C.S., C.J. Lin, and J.K. Hwang, *Predicting subcellular localization of proteins for Gram-negative bacteria by support vector machines based on n-peptide compositions.* Protein Sci, 2004. **13**(5): p. 1402-6.

363. Kosugi, S., et al., *Six classes of nuclear localization signals specific to different binding grooves of importin alpha.* J Biol Chem, 2009. **284**(1): p. 478-85.

364. la Cour, T., et al., *Analysis and prediction of leucine-rich nuclear export signals.* Protein Eng Des Sel, 2004. **17**(6): p. 527-36.

365. Gupta, R.J., E.; Brunak, S., *Prediction of N-glycosylation sites in human proteins.* In preparation, 2004.

366. Julenius, K., et al., *Prediction, conservation analysis, and structural characterization of mammalian mucin-type O-glycosylation sites.* Glycobiology, 2005. **15**(2): p. 153-64.

367. Blom, N., S. Gammeltoft, and S. Brunak, *Sequence and structure-based prediction of eukaryotic protein phosphorylation sites.* J Mol Biol, 1999. **294**(5): p. 1351-62.

368. Blom, N., et al., *Prediction of post-translational glycosylation and phosphorylation of proteins from the amino acid sequence.* Proteomics, 2004. **4**(6): p. 1633-49.

369. Nguyen Ba, A.N., et al., *NLStradamus: a simple Hidden Markov Model for nuclear localization signal prediction.* BMC Bioinformatics, 2009. **10**: p. 202.

370. Brameier, M., A. Krings, and R.M. MacCallum, *NucPred--predicting nuclear localization of proteins.* Bioinformatics, 2007. **23**(9): p. 1159-60.

371. Bendtsen, J.D., et al., *Improved prediction of signal peptides: SignalP 3.0.* J Mol Biol, 2004. **340**(4): p. 783-95.

372. Tanami, H., et al., *Involvement of overexpressed wild-type BRAF in the growth of malignant melanoma cell lines.* Oncogene, 2004. **23**(54): p. 8796-804.

373. Xing, F., et al., *Concurrent loss of the PTEN and RB1 tumor suppressors attenuates RAF dependence in melanomas harboring (V600E)BRAF.* Oncogene, 2012. **31**(4): p. 446-57.

374. Gao, W., et al., *Novel mode of action of tylophorine analogs as antitumor compounds.* Cancer Res, 2004. **64**(2): p. 678-88.

375. Raj, D., et al., *Survivin repression by p53, Rb and E2F2 in normal human melanocytes.* Carcinogenesis, 2008. **29**(1): p. 194-201.

376. Fidler, I.J., *Biological behavior of malignant melanoma cells correlated to their survival in vivo.* Cancer Res, 1975. **35**(1): p. 218-24.

377. Pfaffl, M.W., *A new mathematical model for relative quantification in real-time RT-PCR.* Nucleic Acids Res, 2001. **29**(9): p. e45.

378. Schnell, U., et al., *Immunolabeling artifacts and the need for live-cell imaging.* Nat Methods, 2012. **9**(2): p. 152-8.

379. Wang, L. and S.J. Brown, *BindN: a web-based tool for efficient prediction of DNA and RNA binding sites in amino acid sequences.* Nucleic Acids Res, 2006. **34**(Web Server issue): p. W243-8.

380. Ohndorf, U.M., et al., *Basis for recognition of cisplatin-modified DNA by high-mobility-group proteins.* Nature, 1999. **399**(6737): p. 708-12.

381. Overwijk, W.W. and N.P. Restifo, *B16 as a mouse model for human melanoma.* Curr Protoc Immunol, 2001: p. Unit 20 1.

382. Kang, S.W., S. Lee, and E.K. Lee, *ROS and energy metabolism in cancer cells: alliance for fast growth.* Arch Pharm Res, 2015. **38**(3): p. 338-45.

383. Oneil, M.J., *The Merck index : an encyclopedia of chemicals, drugs, and biologicals*. 13th ed. 2001.

384. Pozarowski, P. and Z. Darzynkiewicz, *Analysis of cell cycle by flow cytometry.* Methods Mol Biol, 2004. **281**: p. 301-11.

385. Blobel, G. *Physiology or Medicine for 1999 - Press Release*. 1999 29 May 2015 [cited 2014; Available from: http://www.nobelprize.org/nobel_prizes/medicine/laureates/1999/press.html.

386. Talantov, D., et al., *Novel genes associated with malignant melanoma but not benign melanocytic lesions.* Clin Cancer Res, 2005. **11**(20): p. 7234-42.

387. Pathria, G., C. Wagner, and S.N. Wagner, *Inhibition of CRM1-mediated nucleocytoplasmic transport: triggering human melanoma cell apoptosis by perturbing multiple cellular pathways.* J Invest Dermatol, 2012. **132**(12): p. 2780-90.

388. Barnes, D.E. and T. Lindahl, *Repair and genetic consequences of endogenous DNA base damage in mammalian cells.* Annu Rev Genet, 2004. **38**: p. 445-76.

389. Aguilera, A. and B. Gomez-Gonzalez, *Genome instability: a mechanistic view of its causes and consequences.* Nat Rev Genet, 2008. **9**(3): p. 204-17.

390. Cerbinskaite, A., et al., *Defective homologous recombination in human cancers.* Cancer Treat Rev, 2012. **38**(2): p. 89-100.

391. Aparicio, T., R. Baer, and J. Gautier, *DNA double-strand break repair pathway choice and cancer.* DNA Repair (Amst), 2014. **19**: p. 169-75.

392. Korabiowska, M., et al., *Decreased expression of MLH1, MSH2, PMS1 and PMS2 in pigmented lesions indicates accumulation of failed DNA repair along with malignant transformation and tumour progression.* Oncol Rep, 1997. **4**(3): p. 653-5.

393. Korabiowska, M., et al., *Exonic deletions of mismatch repair genes MLH1 and MSH2 correlate with prognosis and protein expression levels in malignant melanomas.* Anticancer Res, 2006. **26**(2A): p. 1231-5.

394. Gao, K., et al., *Genomic analyses identify gene candidates for acquired irinotecan resistance in melanoma cells.* Int J Oncol, 2008. **32**(6): p. 1343-9.

395. DeBerardinis, R.J., et al., *The biology of cancer: metabolic reprogramming fuels cell growth and proliferation.* Cell Metab, 2008. **7**(1): p. 11-20.

396. Rampersad, S.N., *Multiple applications of Alamar Blue as an indicator of metabolic function and cellular health in cell viability bioassays.* Sensors (Basel), 2012. **12**(9): p. 12347-60.

397. Liou, G.Y. and P. Storz, *Reactive oxygen species in cancer.* Free Radic Res, 2010. **44**(5): p. 479-96.

398. Fruehauf, J.P. and F.L. Meyskens, Jr., *Reactive oxygen species: a breath of life or death?* Clin Cancer Res, 2007. **13**(3): p. 789-94.

399. Zhu, P., et al., *Involvement of RAGE, MAPK and NF-kappaB pathways in AGEs-induced MMP-9 activation in HaCaT keratinocytes.* Exp Dermatol, 2012. **21**(2): p. 123-9.

400. Cooke, M.S., et al., *Oxidative DNA damage: mechanisms, mutation, and disease.* FASEB J, 2003. **17**(10): p. 1195-214.

401. Kow, Y.W., *Repair of deaminated bases in DNA.* Free Radic Biol Med, 2002. **33**(7): p. 886-93.

402. Bechtel, W. and G. Bauer, *Catalase protects tumor cells from apoptosis induction by intercellular ROS signaling.* Anticancer Res, 2009. **29**(11): p. 4541-57.

403. Kutuk, O. and A. Letai, *Regulation of Bcl-2 family proteins by posttranslational modifications.* Curr Mol Med, 2008. **8**(2): p. 102-18.

404. Chen, C.Y., et al., *An advanced glycation end product (AGE)-receptor for AGEs (RAGE) axis restores adipogenic potential of senescent preadipocytes through modulation of p53 protein function.* J Biol Chem, 2012. **287**(53): p. 44498-507.

405. Ahmad, I., et al., *Toll-like receptor-4 deficiency enhances repair of UVR-induced cutaneous DNA damage by nucleotide excision repair mechanism.* J Invest Dermatol, 2014. **134**(6): p. 1710-7.

406. Harberts, E., et al., *Ultraviolet radiation signaling through TLR4/MyD88 constrains DNA repair and plays a role in cutaneous immunosuppression.* J Immunol, 2015. **194**(7): p. 3127-35.

407. Redon, C., et al., *Histone H2A variants H2AX and H2AZ.* Curr Opin Genet Dev, 2002. **12**(2): p. 162-9.

408. Fernandez-Capetillo, O., et al., *H2AX: the histone guardian of the genome.* DNA Repair (Amst), 2004. **3**(8-9): p. 959-67.

409. Bassing, C.H., et al., *Increased ionizing radiation sensitivity and genomic instability in the absence of histone H2AX.* Proc Natl Acad Sci U S A, 2002. **99**(12): p. 8173-8.

410. Warters, R.L., et al., *Melanoma cells express elevated levels of phosphorylated histone H2AX foci.* J Invest Dermatol, 2005. **124**(4): p. 807-17.

411. Boichuk, S., et al., *Functional connection between Rad51 and PML in homology-directed repair.* PLoS One, 2011. **6**(10): p. e25814.

412. Zou, Y., et al., *Functions of human replication protein A (RPA): from DNA replication to DNA damage and stress responses.* J Cell Physiol, 2006. **208**(2): p. 267-73.

413. Das-Bradoo, S. and A. Bielinsky, *DNA Replication and Checkpoint Control in S Phase.* Nature Eductation, 2010. **3**(9).

414. Tambini, C.E., et al., *The importance of XRCC2 in RAD51-related DNA damage repair.* DNA Repair (Amst), 2010. **9**(5): p. 517-25.

415. Tsaryk, R., et al., *Xrcc2 deficiency sensitizes cells to apoptosis by MNNG and the alkylating anticancer drugs temozolomide, fotemustine and mafosfamide.* Cancer Lett, 2006. **239**(2): p. 305-13.

416. Bannister, L.A., B.C. Waldman, and A.S. Waldman, *Modulation of error-prone double-strand break repair in mammalian chromosomes by DNA mismatch repair protein Mlh1.* DNA Repair (Amst), 2004. **3**(5): p. 465-74.

417. English, D.R., et al., *Ethnicity and risk for colorectal cancers showing somatic BRAF V600E mutation or CpG island methylator phenotype.* Cancer Epidemiol Biomarkers Prev, 2008. **17**(7): p. 1774-80.

418. Hung, M.C. and W. Link, *Protein localization in disease and therapy.* J Cell Sci, 2011. **124**(Pt 20): p. 3381-92.

419. Blencowe, B.J., *Alternative splicing: new insights from global analyses.* Cell, 2006. **126**(1): p. 37-47.

420. Marfori, M., et al., *Molecular basis for specificity of nuclear import and prediction of nuclear localization.* Biochim Biophys Acta, 2011. **1813**(9): p. 1562-77.

421. Rayet, B. and C. Gelinas, *Aberrant rel/nfkb genes and activity in human cancer.* Oncogene, 1999. **18**(49): p. 6938-47.

422. Hoffmann, A., et al., *The IkappaB-NF-kappaB signaling module: temporal control and selective gene activation.* Science, 2002. **298**(5596): p. 1241-5.

423. Hubert, J., et al., *Are nuclear lectins and nuclear glycoproteins involved in the modulation of nuclear functions?* Cell Differ Dev, 1989. **27**(2): p. 69-81.

424. Duverger, E., et al., *Sugar-dependent nuclear import of glycoconjugates from the cytosol.* Exp Cell Res, 1993. **207**(1): p. 197-201.

425. Guinez, C., et al., *O-GlcNAc glycosylation: a signal for the nuclear transport of cytosolic proteins?* Int J Biochem Cell Biol, 2005. **37**(4): p. 765-74.

426. Miranda, K.J., R.F. Loeser, and R.R. Yammani, *Sumoylation and nuclear translocation of S100A4 regulate IL-1beta-mediated production of matrix metalloproteinase-13.* J Biol Chem, 2010. **285**(41): p. 31517-24.

427. Sirois, C.M., et al., *RAGE is a nucleic acid receptor that promotes inflammatory responses to DNA.* J Exp Med, 2013. **210**(11): p. 2447-63.

XI. Abbreviations

°C	Degree Celsius
%	Percentage
µ	Micro
7-AAD	7-amino-actinomycin

A

A	Alanine
aa	Amino acid
AD	Alzheimer's disease
ADAM10	A disintegrin and metalloproteinase domain-containing protein 10
AEC	3-amino-9-ethylcarbazole
AGE	Advanced glycation end-product
AGER	Advanced Glycosylation End Product-Specific Receptor (Gene name)
AJCC	American Joint Committee on Cancer
AKT/PKB	Protein kinase B
AP1/2	Activator protein 1 / 2
APS	Ammonium persulfate
ARAF	A rapidly accelerated fibrosarcoma
AMM	Amelanotic malignant melanoma
ATM	Ataxia telangiectasia mutated
ATP	Adenosine triphosphate
ATR	Ataxia telangiectasia and Rad3-related protein
Aβ	Amyloid β

B

BAD	Bcl-2-associated death promoter
BCA	Bicinchoninic acid assay
BCL2	B-cell lymphoma 2
BCL2A1	Bcl-2-related protein A1
BER	Base excision repair
bFGF	Basic fibroblast growth factor
BIM	Bcl-2 interacting mediator of cell death
BIRC7	Baculoviral IAP repeat-containing protein 7

(ML-IAP)	
BLM	Bloom's syndrome protein
BM	Binding motif
BME	Basement membrane extract
BRCA1/2	Breast cancer susceptibility gene 1/2
BSA	Bovine serum albumin

C

C	Cysteine
C domain	Constant domain
$CaCl_2$	Calcium chloride
CAM-II	Ca^{2+} /calmodulin-dependent protein kinase II
CDC	Cell division control protein
CDK	Cyclin-dependent kinase
CDKN2A	Cyclin-dependent kinase inhibitor 2A
cDNA	Complementary DNA
CE	Cytosolic extract
CHEK	Checkpoint kinase
CKI	Cyclin-dependent kinase inhibitor
CKII	Casein kinase II
CLP	Cecal ligation and puncture
CNE	Chromatin-bound nuclear extract
CRAF	C rapidly accelerated fibrosarcoma
CREB	cAMP-responsive element binding protein
CRM-1	Chromosomal maintenance 1 (exportin 1)
CSFE	Carboxyfluorescein succinimidyl ester
CTGP	Connective tissue glycoprotein
CTLA-4	Cytotoxic T-lymphocyte-associated protein 4

D

DAMP	Damage-associated molecular patterns
DAPI	4’,6-diamidino-2-phenylindole
DC	Dendritic cells
DCF	Dichlorodihydrofluorescein
DCFDA	2’,7’ –dichlorofluorescin diacetate
DIA-1	Diaphanous-1

DKK1	Dickkopf-related protein 1
DM	Diabetes mellitus
DMBA	7,12-dimethylbenz-[a]-anthracene
DMEM	Dulbecco's Modified Eagle Medium
DMSO	Dimethyl sulfoxide
DNA	Deoxyribonucleic acid
Doxo	Doxorubicin
DSB	Double-strand break
DTH	Delayed type hypersensitivity
E	
ECL	Enhanced chemoluminescence
ECM	Extracellular matrix
EDTA	Ethylene diamine tetraacetic acid
EGF-R	Epidermal growth factor
EGR1	Early growth response protein 1
EMA	European medicines agency
EMT	Epithelial-to-mesenchymal transition
ER	Endoplasmatic reticulum
ERCC1/2	Excision repair cross- complementation group
ERK	Extracellular signal-regulated kinase
ETS1	V-ets avian erythroblastosis virus E26 oncogene homolog 1
F	
FACS	Fluorescence activated cell sorting
$FADH_2$	Flavin adenine dinucleotide hydroquinone
FAS	First apoptotic signal
FCS	Fetal bovine serum
FDA	Food and drug administration
fl-RAGE	Full-length RAGE
FRET	Fluorescence resonance energy transfer
G	
G	Glycine
GalNAc	N-Acetylgalactosamine
GAPDH	Glyceraldehyde 3-phosophate dehydrogenase
GLUT1	Glucose transporter 1
GP100	Glycoprotein 100

GSK-3	Glycogen synthase kinase 3	
h	Hours	H
H2AFX/H2AX	H2A histone family member X	
H3	Histone 3	
HDM2	Human double minute 2	
HEPES	4-(2-hydroxyethyl)-1-piperazineethanesulfonic acid	
Hgf	Hepatocyte growth factor	
HIF1α	Hypoxia-inducible factor 1 α	
HMGB1	High-mobility group box 1	
HMGS	Human melanocyte growth supplement	
HNRNP	Heterogeneous nuclear ribonucleoprotein	
Hs	Homo sapiens	
HS	Heparan sulfate	
HSP	Heat shock protein	
HSPG	Heparan sulfate proteoglycan	
HUGO	Human genome organization	
HUS1	Human cell cycle checkpoint gene 1	
Ig domain	Immunoglobulin domain	I
IL	Interleukin	
IMP-α	Importin-α	
INSR	Insulin receptor	
JARID1A	Jumonji AT-rich interactive domain 1A	J
K	Lysine	K
KCL	Potassium chloride	
KD	Knockdown	
kDa	Kilodalton	
KO	Knockout	
LB	Lysogeny broth	L
LDH	Lactate dehydrogenase	
LIG1	Ligase 1	
LMB	Leptomycin B	
LMM	Lentigo maligna melanoma	

M

m	Meter
m	Milli
MAPK	Mitogen-activated protein kinase
MART1	Melanoma antigen recognized by T-cells
MDC1	Mediator of DNA damage checkpoint protein 1
MDSC	Myeloid-derived suppressor cells
ME	Membrane extract
MEF	Murine embryonic fibroblasts
MEK	Mitogen activated protein kinase 1 (MAP2K1)
MHC	Major histocompatibility complex
MIA	Melanoma inhibitory activity
min	Minutes
MITF	Microphthalima-associated transcription factor
MLH1	MUTL homolog 1
ML-IAP	Melanoma inhibitor of apoptosis
Mm	Mus musculus
mM	Millimolar
MMP-3	Matrix metallo-protease-3
MMR	Mismatch repair
MMTV	Mouse mammary tumor virus
MOI	Multiplicity of infection
MRE11A	Meiotic recombination 11 homolog A
mRNA	Messenger RNA
MTC	Mitomycin C
MyD88	Myeloid differentiation primary response gene 88

N

n	Nano
NaCl	Sodium chloride
NADH	Nicotinamide adenine dinucleotide
NBN	Nibrin
NCT	National center of tumor diseases
NEAA	Non-essential amino acids

NER	Nucleotide excision repair
NES	Nuclear export signal
NF-κB	Nuclear factor kappa B
NHM	Normal human melanocytes
NLS	Nuclear localization signal
NMM	Nodular malignant melanoma
NO	Nitric oxide
NONO	Non-POU domain containing octamer-binding protein
NRAS	Neuroblastoma rat sarcoma oncogene
N-region	Negative-charge regulatory domain
O	
OE	Overexpression
ORF	Open reading frame
OSCC	Oral squamous cell carcinoma
P	
p	Pico
P14ARF	P14 ADP ribosylation factor
P16INK4A	P16 inhibitor of cell cycle kinase 4A
PBS	Phosphate-buffered saline
PCR	Polymerase chain reaction
PD1	Programmed death receptor 1
PD-L1	Programmed death receptor ligand 1
PE	Pellet extract
PFA	Paraformaldehyde
PI3K	Phosphoinositide 3-kinase
PIP_3	Phosphatidylinositol (3,4,5)-trisphosphate
PKA/C/G	Protein kinase A/C/G
PRKDC	Protein kinase, DNA-activated, catalytic polypeptide
PTEN	Phosphatase and tensin homolog
PVDF	Polyvinylidene difluoride
Q	
qPCR	Quantitative real-time polymerase chain reaction
Q	Glutamic acid
R	
R	Arginine
RAC-1	Ras-related C3 botulinum toxin substrate 1

RAD50/51/52	RecA homolog 50/51/52
RAGE	Receptor for advanced glycation end-products
RANBP1	RAN-specific binding protein 1
RB	Retinoblastoma protein
RGP	Radial growth phase
RHO	Ras homologue
RNA	Ribonucleic acid
RNF8/168	Ring finger protein family member 8/168
ROS	Reactive oxygen species
RPA	Replication protein
RPLO	50S ribosomal subunit protein L15
RSK	Ribosomal s6 kinase
RTK	Receptor tyrosine kinase

S

S	Serine
S100B	S100 calcium-binding protein B
SAPK/JNK	Stress-activated protein kinase/c-Jun-NH2-terminal kinase
SDS	Sodium dodecyl sulfate
shRNA	Short-hairpin RNA
SILAC	Stable isotope labeling by/with amino acids in cell cultur
siRNA	Small-interfering RNA
SMC1A	Structural maintenance of chromosomes 1A
SNE	Soluble nuclear extract
SNP	Single nucleotide polymorphism
SP-1	Specificity protein-1
SRC	Proto-oncogene tyrosine-protein kinase Src
SSM	Superficial spreading melanoma
STAT	Signal transducer and activator of transcription
SUMO	Small ubiquitin-related modifier

T

T	Threonine
TAM	Tumor-associated macrophages
TBHP	Tert-Butylhydroperoxid
TBS	Tris-buffered saline

TEMED	Tetramethylenediamine
TGF-β	Transforming growth factor β
TIM-3	T-cell immunoglobulin and mucin domain-containing protein 3
TIRAP	Toll-interleukin 1 receptor (TIR) domain containing adaptor protein
TLR	Toll-like receptor
TMA	Tissue microarray
TNF-α	Tumor necrosis factor α
TOPBP1	DNA topoisomerase 2-beta-binding protein 1
TP53	Tumor protein 53
TP53BP1	TP53 binding protein 1
TPA	12-*O*-tetradecanoylphorbol-13-acetate
TRA-2β1	Transformer 2 β homolog-1
TRAIL	Tumor necrosis factor-related apoptosis-inducing ligand
Tregs	Regulatory T cells
TTF-1	Thyroid transcription factor 1
TUNEL	TdT-mediated dUTP-biotin nick end labeling
TXNIP	Thioredoxin-interacting protein
TYR	Tyrosinase
U	
UV	Ultraviolet
V	
V region/domain	Variable region/domain
VEGF	Vascular-endothelial growth factor
VGP	Vertical growth phase
W	
WNT	Wingless/Integrated
WPRE	Woodchuck hepatitis virus posttranscriptional regulatory element
Wt	Wildtype
X	
XP	Xeroderma pigmentosum
XPA/C	Xeroderma pigmentosum group A/C protein
XRCC2/6	X-ray repair complementing defective repair in Chinese hamster cells 2/6

XII. Acknowledgements

Though only my name appears on the cover of this dissertation, I could have never come so far without the help, support, guidance, and efforts of a lot of people. I owe my gratitude to all those who have made this dissertation possible. First of all, I want to thank **Dr. Christoffer Gebhardt** and **Prof. Dr. Jochen Utikal** for providing me the opportunity to do my PhD thesis at the DKFZ and supporting me throughout the years. Especially, I want to thank **Christoffer** for his infectious enthusiasm, which has been one of the driving forces in the last years, and for giving me the freedom to pursue projects I was interested in.

I also want to thank **Prof. Dr. Viktor Umansky**, who helped and supported me as first referee of my thesis and part of the thesis advisory committee. I am grateful for the time he donated to help me improving my work by providing scientific advices. I want to acknowledge **Prof. Boutros** and **Prof. Dr. Abdollahi** for enrolling as examiners in my disputation.

Furthermore, I will forever be thankful to my former research advisor Prof. **Hermann Eibel**. He always believed in me and supported me without hesitating. This is also true for the whole 'Eibel lab' – I am so grateful for the time I spent with all of you, especially with **Helene**, **Kathrin P.**, and **Anne**. ☺

A big thanks for their help and for sharing their scientific knowledge goes to all of my **lab colleagues**. In particular, I want to thank **Pan**, our lab organizer, for every prank and for his will to push things forward. Most of all, I want to thank **Kathrin T.** and **Mathias** not only for their support and help with proofreading my dissertation, but also for their authenticity, humor, acceptance, and friendship. I'll never forget our coffee/'trigger' breaks.

I also thank my **outside-lab-friends** who kept me (in)sane through all these years and who, literally, accomplished miracles: Besides bringing 'Bali' to Germany, getting Mafia bosses motivated to organize my New Year's Eve, showing me how to eat fruits☻, bringing sun out in London, putting me on a horse, bringing dinosaurs to Heidelberg, taking me on safari, they managed the impossible: Accepting me as I am! A special thanks goes to **Sander** for checking my spelling and ignoring the 'American slang'. ☺

The greatest thanks is addressed to my family. To my **sister**, who interfered, criticized, 'borrowed' clothes, and monopolized the bathroom but was always there when catastrophes striked, defending me against all corners ❤. To my **parents**, who have sacrificed their lives for my sister and myself and have been pillars of support, guidance, and love since the day I was born. Your faith in me means everything to me. I love you ❤!